INTEGRATED SULPHUR, ENERGY AND NUTRIENT RECOVERY FROM TANNERY WASTEWATER: EXPERIMENTAL CALIBRATION AND PLANT-WIDE DYNAMIC MODELLING

D Ikumi, T Harding, J Minnie, A Opus, M Korotsoane, M Tlali, P Ngobeni, W Ayinde, A Rajan, P Welz

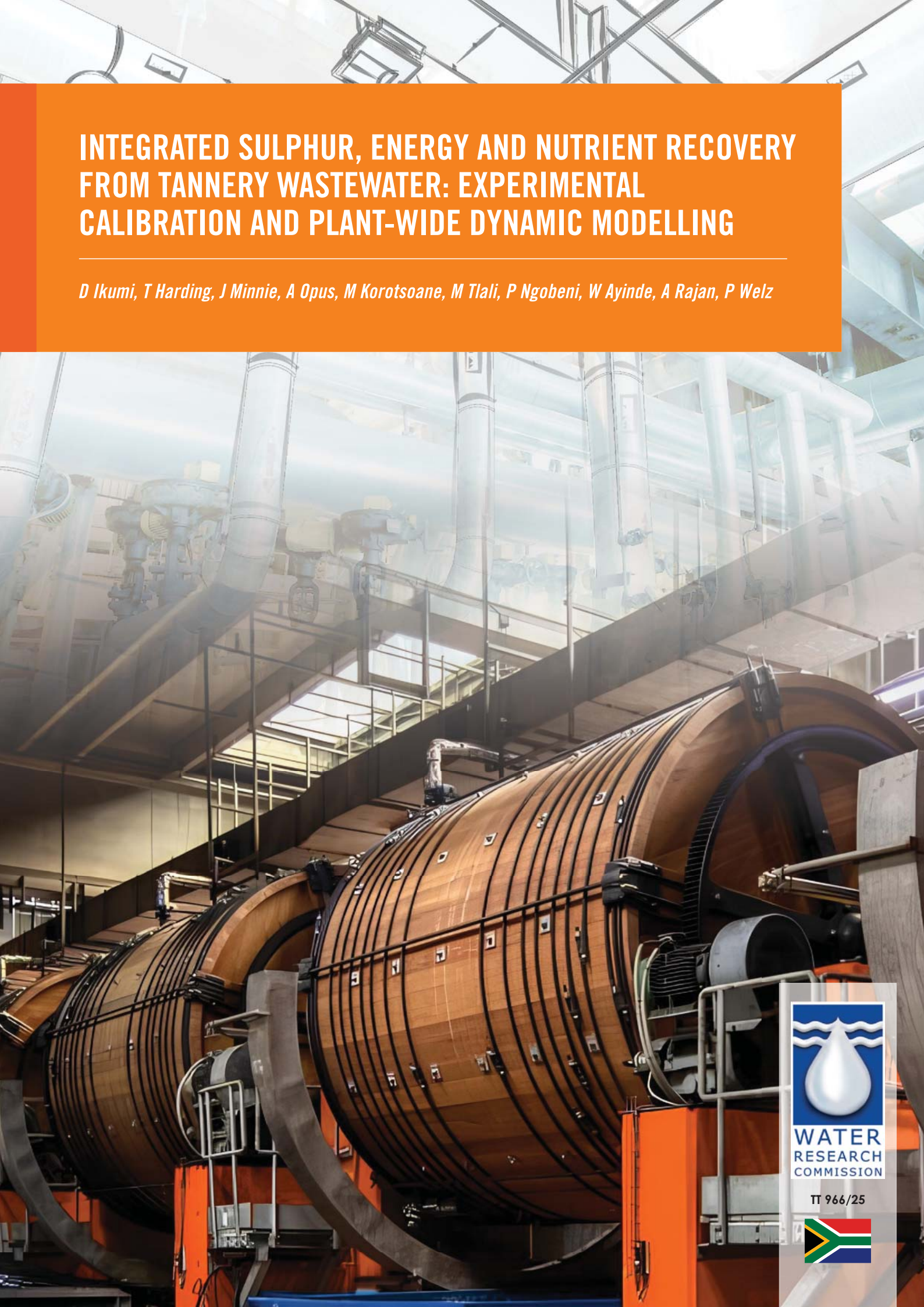

WATER RESEARCH COMMISSION

TT 966/25

INTEGRATED SULPHUR, ENERGY AND NUTRIENT RECOVERY FROM TANNERY WASTEWATER: EXPERIMENTAL CALIBRATION AND PLANT-WIDE DYNAMIC MODELLING

Report

to the Water Research Commission

by

D Ikumi[1], T Harding[1], J Minnie[1], A Opus[1], M Korotsoane[1], M Tlali[1], P Ngobeni[1], W Ayinde[1], A Rajan[2], P Welz[2]

[1] University of Cape Town, South Africa

[2] Cape Peninsula University of Technology, Bellville Campus, South Africa

WRC report no. TT 966/26
ISBN 978-0-6392-0757-5

March 2026

This is the final report of WRC project no. C2022/2023/00923.

DISCLAIMER

This report has been reviewed by the Water Research Commission (WRC) and approved for publication. Approval does not signify that the contents necessarily reflect the views and policies of the WRC, nor does mention of trade names or commercial products constitute endorsement or recommendation for use.

EXECUTIVE SUMMARY

South Africa's tanning sector processes approximately 5.6 million hides per year and generates 4–11 ML d^{-1} of highly saline, sulphate-rich, nitrogen-bearing effluent. Conventional single-process treatments struggle to meet discharge limits or enable water reuse. An integrated, resource-oriented treatment train is therefore required to (i) protect receiving waters, (ii) reduce municipal treatment loads, and (iii) recover valuable resources.

This project demonstrates that tannery wastewater (TWW) can be transformed from a high-risk pollution stream into a source of recoverable water, energy, sulphur, and biomass through an integrated, model-guided treatment platform. The study evaluated and modelled an integrated treatment train capable of achieving regulatory compliance while delivering circular-economy benefits, including water reuse, sulphur and energy recovery, and valorisation of algal biomass.

The treatment train extends prior WRC work (K5/2841/3) by coupling a two-stage hybrid linear flow channel reactor (HLFCR) for sulphate removal and elemental sulphur recovery with anaerobic digestion (AD), followed by tertiary polishing using a microalgal-bacterial (MAB) reactor unit. The model was developed as a plant-wide dynamic platform that extends the existing University of Cape Town (UCT) PWM_SA model implemented in DHI WEST®. This modelling framework supports process design, optimisation, and scale-up of the TWW treatment train.

Accordingly, the project involved the development and testing of the following systems:

- **Two-stage HLFCR:** This system exploits vertical redox stratification. Sulphate-reducing bacteria (SRB) reduce SO_4^{2-} to sulphide, while sulphide-oxidising bacteria (SOB) oxidise sulphide to elemental sulphur (S^0) at the air–liquid interface.
- **Anaerobic digestion (AD):** Treats HLFCR effluent with mitigated sulphide toxicity to maximise methane recovery.
- **Microalgal-bacterial (MAB) polishing process:** Provides tertiary ammonia (NH_4^+) removal with intrinsic oxygen and alkalinity generation, while co-producing protein-rich alga.
- l biomass.
- **Dynamic modelling suite:** Kinetic processes governing sulphur, carbon, and nitrogen transformations were quantified and integrated into a plant-wide dynamic model.

The study approach included operation and testing of (i) bench-scale HLFCRs, (ii) 25 L mesophilic AD batch tests (60 days; 0.25×–2× influent strengths), and (iii) flask and photobioreactor MAB trials. Material mass balances (COD and N) confirmed data reliability. Model parameters were estimated using nonlinear regression and validated through steady-state and dynamic simulations.

Main Technical Findings

HLFCR–AD Pretreatment

1) The HLFCR achieved high sulphate removal with stable S^0 recovery while limiting sulphide toxicity to downstream AD.

2) Stratified modelling incorporating limited mixing and air-interface kinetics accurately reproduced system performance and guided hydraulic retention time (HRT) set-points and reactor geometry selection.

3) Post-HLFCR effluent enabled reliable methane production in AD; sulphate pre-removal proved pivotal for restoring methanogenesis.

AD Kinetics for TWW Treatment

i. Under non-inhibitory conditions, Contois constants of $K_m \approx 15.55$ and $K_s \approx 40.57$ ($R^2 \approx 0.97$) adequately described substrate utilisation.

ii. As influent strength increased (COD:SO_4^{2-} from approximately 0.6 → 0.1), metabolic pathways shifted from methanogenesis to sulphidogenesis, even with H_2S stripping. Substrate-driven inhibition, therefore, predominated at higher loads.

iii. Practical implementation requires monitoring of (i) influent strength to enable staged dilution where necessary, (ii) solids retention time (SRT), and (iii) upstream sulphate/COD ratios.

MAB Tertiary Nitrogen Removal

i. Optimal performance was achieved under intermittent aeration (aerobic during light; anoxic during dark) with sufficient readily biodegradable carbon to complete denitrification.

ii. Microalgae supplied oxygen and alkalinity; autotrophic nitrifiers converted ammonia to nitrate; heterotrophic bacteria denitrified nitrate to nitrogen gas in the presence of biodegradable organics during anoxic periods.

iii. Biomass valorisation is feasible; however, metal stewardship (e.g., chromium) is essential to ensure safe end use.

The integrated modelling of the HLFCR–AD–MAB system provides a robust engineering tool for the design and operation of TWW treatment infrastructure. It reduces scale-up uncertainty, supports investment decision-making, and enables operators to manage performance risks under fluctuating tannery loads.

Project Outcomes

- A validated, plant-wide dynamic model integrating HLFCR, AD, and MAB processes, capturing sulphur, carbon, nitrogen, and fast aqueous chemistry interactions. The model supports design optimisation, scale-up, and cost–performance trade-off analysis.
- Demonstrated resource recovery: elemental sulphur (S^0), methane-rich biogas, and protein-rich algal biomass, with effluents meeting or approaching <10 mg L^{-1} COD and NH_3-N under optimised conditions.
- Actionable design and control guidance:
    i. Pre-remove sulphate in the HLFCR to protect AD; adjust HRT and electron donor dosing as required.
    ii. In AD, limit influent strength or stage feeding to prevent substrate inhibition; maintain COD:SO_4^{2-} ratios favourable to methanogenesis.

iii. In MAB systems, apply time-of-day aeration and moderate carbon dosing to prevent NOx accumulation and manage pH/alkalinity.

The TWW treatment strategy presented in this report offers a replicable pathway for South Africa's leather and hide processing sector to meet tightening discharge standards while transitioning toward resource-efficient, climate-aligned production.

These outcomes have important technical, regulatory, economic, and sustainability implications:

- **Technical:** Stratified bioreactors (HLFCR) combined with mixed-guild polishing (MAB) create plant-wide synergies not achievable through single-unit systems.
- **Regulatory:** Provides a compliance-ready pathway for sulphate, ammonia, and COD removal while reducing the burden on municipal wastewater works.
- **Economic:** Revenue offsets from biogas, elemental sulphur, biomass, and water reuse can significantly improve lifecycle economics. Dynamic modelling further supports optimisation of capital and operating expenditure while reducing scale-up risk.
- **Sustainability:** Aligns with SDG 6.3 and 6.4 by promoting pollution reduction, water reuse, and resource recovery, and supports a just transition of the leather value chain in water-scarce regions.

ACKNOWLEDGEMENTS

The project team thanks the following Reference Group members for their contributions to the project.

Reference Group	Affiliation
Dr John Ngoni Zvimba	Water Research Commission (Chairman)
A/Prof. Sheena Kumari Kuttan Pillai	Durban University of Technology
Mr David Modiri	City of Cape Town Metropolitan Municipality
Dr Pierre Van Zyl	Proxa Water
A/Prof. Lingam Pillay	Stellenbosch University
Dr Clive Jackson-Moss	University of Cape Town
Mr Charl Dupisani	Cape Karoo International
Mr Mluleki Mnguni	Umgeni Water

TABLE OF CONTENTS

LIST OF FIGURES

LIST OF TABLES

CHAPTER 1: INTRODUCTION

1.1 Background

The United Nations Agenda 2030 outlines 17 Sustainable Development Goals (SDGs), which aim to promote global prosperity while safeguarding the environment. Of particular relevance to this study are Goals 6.3 and 6.4, which urge nations to reduce water pollution, eliminate the discharge of untreated hazardous effluents, and promote water recycling and efficient reuse of freshwater resources.

In South Africa, the leather tanning industry remains a significant contributor to the manufacturing sector, serving both domestic and international markets. As highlighted in Natsurv10, 2nd Edition (2017), approximately 35 operational tanneries collectively process around 5.6 million hides annually. This production scale consumes between 4.44 and 11.1 million litres of water per day, equivalent to more than 4 billion litres per year. On average, treating 1 kg of bovine hide can generate up to 15 litres of wastewater with high pollutant concentrations.

Tannery effluent is among the most challenging industrial wastewaters to treat due to its complex composition. It contains both high-strength organic and inorganic pollutants, such as chemical oxygen demand (COD), sulphates (SO_4^{2-}), chlorides, and ammonia, often at concentrations well above regulated discharge limits. For example, typical COD levels may range from 800 to 18,000 mg/L, sulphates from 1,000 to 4,500 mg/L, and ammonia (free and saline) from 100 to 1,400 mg/L. These characteristics pose significant burdens on municipal treatment systems, necessitating robust on-site treatment solutions to protect ecosystems and public health.

In response to these challenges, the Water Research Commission (WRC) of South Africa funded Project K5/2841/3 (Welz *et al.*, 2021), which pioneered the development of a fit-for-purpose integrated TWW treatment system.

The system (see Figure 1.1) combined two main components:

a) A two-stage HLFCR, designed for sulphate removal and elemental sulphur recovery.
b) An anaerobic digester (AD), responsible for further degradation of organics and biogas (methane) production.

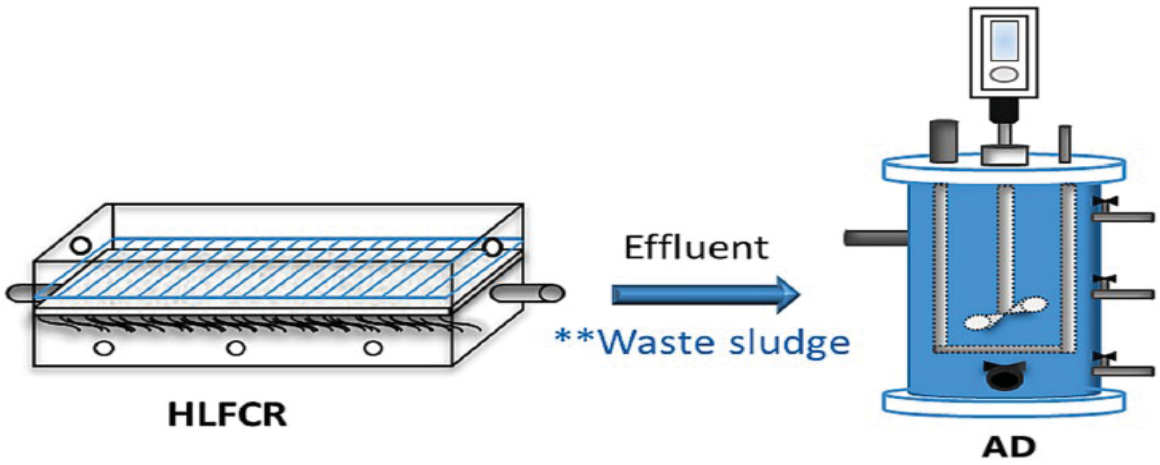

Figure 1.1: Integrated system process layout (Welz *et al.* 2024)

This configuration allowed for the sequential removal of sulphates and organics while limiting sulphide toxicity, which typically inhibits methanogenic activity in anaerobic digesters. The HLFCR significantly reduced sulphate concentrations, achieving removal efficiencies up to 96.6% in bovine/ovine effluents and promoted elemental sulphur recovery. Pre-treated effluent entering the AD unit demonstrated enhanced biodegradability and improved biogas yields, including methane concentrations of up to 52% (Horn *et al.*, 2020).

Studies of the system performance further revealed average COD concentrations of 8,551 mg/L in ostrich tannery effluent (OTE), and up to 28,165 mg/L in bovine/ovine tannery effluent (BOTE), alongside high sulphate loads. Despite these advances, challenges persisted: residual levels of free and saline ammonia (256–593 mgN/L), chlorides (2,050–6,900 mgCl/L), sodium (1,770–2,730 mgNa/L), and calcium (93–465 mgCa/L) often remained above permissible thresholds, indicating a need for further polishing steps.

Moreover, characterisation of the wastewater in terms of its biodegradable and unbiodegradable fractions, both particulate and soluble, is essential for tailoring treatment approaches. Understanding the ratios of Biodegradable Particulate Organics (BPO), Unbiodegradable Particulate Organics (UPO), Biodegradable Soluble Organics (BSO), and Unbiodegradable Soluble Organics (USO) guides process optimisation and reactor design.

Operational insights from Mpofu *et al.* (2020) also highlighted a key finding. During the start-up phase of the AD units, biosulfidogenesis initially outcompeted methanogenesis. However, as operations stabilised, particularly under optimal initial sulphate concentrations, methanogenic activity improved. Notably, visual indicators, such as a white layer forming at the liquid-headspace interface in the reactors, suggested in situ oxidation of sulphide to elemental sulphur.

Building upon the achievements and lessons of WRC Project K5/2841/3, current research aims to evaluate and model an enhanced, integrated treatment system. This includes the incorporation of an algae bioreactor for biological removal of residual ammonia. Figure 1.2 shows the extended integrated system, with references to the sections where the unit processes are discussed in this report.

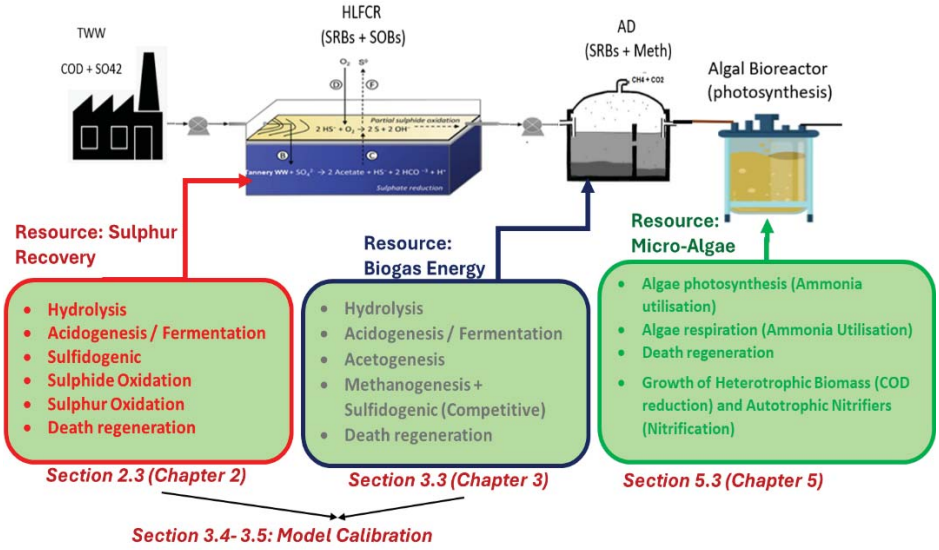

Figure 1.2: Extended integrated system process layout

This study presents a technically robust yet practical solution to one of South Africa's major industrial wastewater challenges, specifically within the tanning industry. It introduces an integrated treatment system that combines biological, anaerobic, and membrane-based processes. Enhanced with advanced polishing units, such as algae bioreactors and membrane bioreactors–activated sludge systems, the proposed approach sets a new standard for the treatment and management of TWW.

A significant advantage of this system is its strong emphasis on resource recovery. Beyond conventional contaminant removal, it enables the extraction of high-value products such as elemental sulphur, methane-rich biogas, and raw materials for producing biofuels and other algae-based bioproducts. This transforms wastewater from a waste burden into a potential resource. In parallel, a virtual modelling component supports the experimental work by using datasets from both the current lab-scale studies and those of the WRC Project No. K5/2841/3.

This component developed a dynamic mathematical model representing the integrated treatment system or its individual unit operations, as illustrated in Figure 1.2. The model will serve as a decision-support tool for evaluating system performance, scaling up designs, and estimating operational and capital costs.

Overall, by integrating these technologies, the study delivers a comprehensive wastewater treatment framework that aligns with national environmental regulations and global sustainability goals.

It promotes circular economy principles via three key outcomes: (1) resource recovery via the generation of valuable by-products, (2) industrial water reuse that reduces dependence on freshwater sources, and (3) improved environmental protection through discharge that meets regulatory standards. Ultimately, this work contributes to the development of cleaner, more sustainable, and economically viable practices for the leather processing sector in South Africa.

1.2 Project Objectives

To address the key challenges identified in this research, the project's aims and objectives are carefully structured to generate targeted insights that support the overall goal. The research is organised into discrete tasks, each with specific objectives, pursued through a combination of bench-scale experiments and simulation-based modelling.

The primary objectives of the project are:

1. **To Determine the Characteristics of Bovine TWW.**
    a. To evaluate the TWW treatability under both biological aerobic, e.g. Activated Sludge, and anaerobic, which includes AD and HLFCR, treatment conditions.
    b. To determine the categories BPO, UPO, BSO and USO.
    c. To extend the characterisation of the feed (substrate) to the framework for standardised notation applied in wastewater treatment modelling (Corominas *et al.*, 2010).
2. **To design, construct, set up, and start up.**
    a. The individual unit operations of the extended integrated system, and

i. IA hybrid linear flow channel reactor coupled to an anaerobic digester (HLFCR-AD)

ii. An Algal bioreactor

b. And develop the mathematical model, presented in a Gujer Matrix, that would allow for the coupling of the individual Unit Operations to the proposed extended integrated system within a virtual environment, using DHI WEST® simulation software.

3. To evaluate the potential for bioremediation of raw and pre-treated TWW using a pre-determined microalgal consortium. (Pre-treated wastewater refers to TWW treated through a two-stage hybrid linear flow channel reactor, coupled to an anaerobic digester (HLFCR-AD) system, as developed in WRC Project No. K5/2841/3.)

4. To characterise the harvested algal biomass from raw TWW and the pre-treated airlift algal bioreactor, assessing its suitability for bioplastics and biofuel production, and to analyse the effluent from the algal bioreactor to determine the organic and nutrient requirements necessary for supplementation via TWW and added process chemicals.

5. To use the datasets generated from the lab-scale experiments to estimate model parameters and to calibrate and validate the mathematical model describing the integrated treatment system.

1.3 Tannery Processes and Primary Wastewater Sources

1.3.1 Overview of Leather Processing

Leather tanning converts raw hides and skins into durable leather products used in upholstery, footwear, handbags, and other consumer leather goods (Swartz *et al.*, 2017). South Africa's leather industry is substantial, with approximately 35 tanneries processing around 5.6 million hides annually, as of 2017. This industrial activity generates significant wastewater volumes, ranging from 4.44 to 11.1 million litres per day, totalling between 1,621 and 4,050 million litres annually (Natsurv10 2nd Edition, 2017).

The bulk of this tannery effluent, estimated at 70–90%, originates from two critical stages of production: beamhouse and Tanyard operations. Figure 1.3 provides an overview of a typical wet blue tannery process flow, outlining the main unit operations, associated by-products, and waste streams. Understanding these stages is essential, as they directly influence the quantity and characteristics of the effluent generated, thereby determining the selection and optimisation of appropriate treatment technologies.

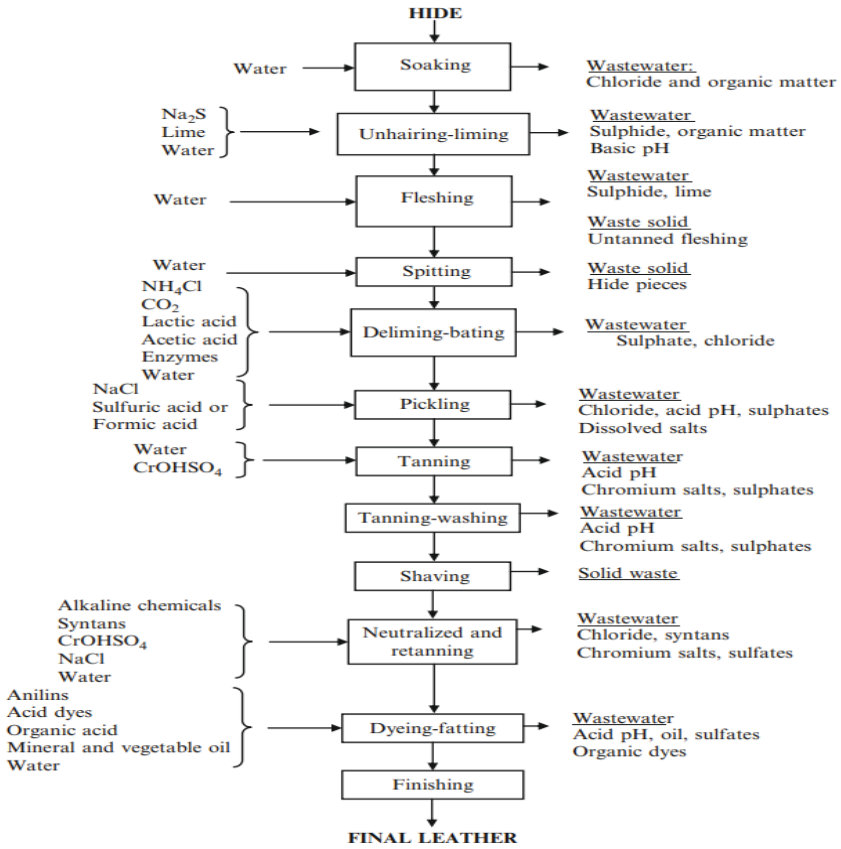

Figure 1.3: Processes, by-products and waste from wet blue tanning (Swartz *et al.*, 2017)

1.3.2 Beamhouse Operations

The beamhouse stage is the first and most pollution-intensive phase of leather processing. It includes soaking, fleshing, unhairing, liming, splitting, deliming, and bating. This stage alone may contribute 60–70% of the total contaminant load in TWW (Wu et al., 2018). Beamhouse wastewater typically contains elevated concentrations of BOD, COD, total dissolved solids (TDS), sulphides, sulphates, chlorides, and sodium. The effluent often appears dark brown and emits strong odours due to its high organic content and the presence of hazardous substances, as well as a range of metallic and non-metallic pollutants. Common constituents include total chromium (TCr), Cr(III) and Cr(VI), chlorides, total Kjeldahl nitrogen (TKN), sulphates (SO_4^{2-}), sulphides (S^{2-}), ammonium nitrogen (NH_4-N), iron, and calcium (Kassim et al., 2022).

1.3.3 Key beamhouse processes

Soaking removes preservatives, blood, manure, urine, and dirt, softening the hide for downstream processing (Thanikaivelan et al., 2004). Fleshing mechanically removes fat and flesh and may occur either before liming (green fleshing) or after liming (lime fleshing). Unhairing and liming are typically performed together using alkaline chemicals such as calcium hydroxide (lime) and sodium sulphide. Splitting may occur at various stages; however, lime splitting is often preferred over post-chromium splitting because it can improve chemical penetration while reducing environmental impact. By the end of beamhouse processing, hides are ready for tanning; however, the wastewater generated is already highly complex and requires robust treatment.

1.3.4 Tanyard Operations

The tanyard stage involves intensive chemical and mechanical processing to improve leather durability and quality. Key processes include degreasing, pickling, and tanning, which prepare hides for subsequent dyeing and finishing.

Degreasing removes fats and oils to support uniform penetration of tanning and dyeing agents. Residual grease may cause dark patches and interfere with chrome tanning, including the formation of insoluble chromium soaps (Covington, 2011). Degreasing can use solvent- or water-based agents, selected based on efficiency and environmental considerations (Kanagaraj et al., 2015). Pickling reduces pH to approximately 2–3 using acids and salts, preventing swelling and improving tanning-agent penetration (Sreeram & Ramasami, 2003). For sheepskins, pickling may also serve as a form of preservation (UNIDO, 2012).

Tanning stabilises collagen fibres and produces leather resistant to decomposition. Chrome tanning, using trivalent chromium (Cr^{3+}), is widely used to produce wet-blue leather due to its efficiency and flexibility (Covington, 2011). Glutaraldehyde tanning provides an alternative to producing wet-white (metal-free) leather, addressing some environmental concerns (Thanikaivelan et al., 2004). Basification is then performed using a mild alkali to bind tanning agents and reduce leaching (Kanth et al., 2009). A final wash removes unbound chemicals (UNIDO, 2012). Tanyard operations are followed by dyehouse and finishing processes. Bovine TWW is therefore a complex mixture of organic and inorganic pollutants generated during hide processing. Its composition depends on the type of raw hide, the tanning method, and the chemicals used. Typical organic constituents include proteins, lipids, carbohydrates, tannins, sulphonated oils, and synthetic organic compounds, which contribute to high BOD and COD.

Inorganic constituents include salts (e.g., sodium chloride, sodium sulphate, and sodium bicarbonate) and heavy metals such as chromium, copper, zinc, and lead. This complexity underscores the need for integrated treatment systems that can simultaneously address organics, salinity, metals, and nutrients while enabling resource recovery.

1.4 Characteristics of Tannery Wastewater (TWW)

Wastewater characterisation is a critical first step in designing effective treatment protocols, particularly for nitrogen (N) and phosphorus (P) removal in wastewater treatment plants (WWTPs) (Rout et al., 2021). Characterisation includes quantifying carbon (C), nitrogen, and phosphorus and classifying them by biodegradability (biodegradable vs non-biodegradable) and physical form (particulate, settleable, non-settleable, and dissolved). Key indicators – such as COD, TKN, free and saline ammonia (FSA), total phosphorus (TP), and orthophosphate (OP) – support qualitative and quantitative assessment (Henze, 2008; Tchobanoglous, Burton & Stensel, 2003).

Mpofu et al. (2020) collected composite (one-month) TWW samples from two South African tannery operations: (1) ostrich and (2) bovine/ovine tanneries. Samples included combined tannery effluent as well as beamhouse and tanyard effluent fractions. These batches were fully characterised and, where necessary, amended to support model development. Samples were frozen during storage and re-characterised before use. The characteristics of bovine/ovine TWW used in WRC Project K5/2841/3 are reported in Mpofu et al. (2020) and summarised in Table 1.1 (beamhouse) and Table 1.2 (tanyard).

Table 1.1: Characteristics of Beamhouse Bovine/Ovine Tannery Effluent (Mpofu *et al.*, 2022)

Parameter	Batch 1	Batch 2	Batch 3	Batch 4	Batch 5	Batch 6	Mean	SD ±
TOC (mg/L)	9250	7240	5160	4710	4220	3540	5687	2150
COD (mg/L)	24650	20350	27725	21675	23180	26200	23963	2776
BOD (mg/L)	7500	6500	5000	6000	6000	7000	6333	876
VOA_t (mg/L AAE)	2637	3109	4173	2674	2007	2691	2882	724
TN (mg/L)	1035	1320	1020	1315	1600	1430	1287	226
TAN (mg/L NH_3-N)	865	96	136	230	176	313	303	286
NO_3 (mg/L)	5.90	4.70	3.15	5.85	5.15	4.10	4.81	1.06
NO_2 (mg/L)	0.30	12.2	10.6	1.10	1.30	1.60	4.5	5.4
TP (mg/L $PO_4^{3-}-P$)	63.2	4.95	5.9	7.5	10.6	40.9	22.2	24.3
SO_4^{2-} (mg/L)	1120	2400	2200	1130	1450	1850	1692	545
HS^- (mg/L)	0.40	476	276	456	1.88	0.60	202	231
Cl (mg/L)	2500	3175	9025	6825	8125	8840	6415	2885
TS (g/L)	31.4	30.5	38.0	46.5	34.0	32.7	35.5	6.01
TVS (g/L)	11.6	9.83	14.4	18.9	10.9	11.8	12.90	3.30
Proteins (mg/L)	1562	2610	2090	3931	4184	2871	2875	1024
K (mg/L)	45.6	78.5	99.6	129	126	ND	95.7	34.8
Na (mg/L)	5552	6446	6058	6820	7184	ND	6412	638
Fe (mg/L)	0.05	0.03	0.08	0.26	0.13	ND	0.111	0.09
Ca (mg/L)	497	254	199	1091	1419	ND	692	539
Mg (mg/L)	375	60.3	151	3.70	11.8	ND	120	154
Zn (µg/L)	169	432	158	739	996	ND	499	366
Cu (µg/L)	21.8	13.8	10.9	26.7	167.9	ND	48.2	67.2
Co (µg/L)	1.79	2.57	2.84	4.36	2.74	ND	2.86	0.93
Cd (µg/L)	0.00	0.00	0.00	0.09	0.32	ND	0.083	0.14
Ni (µg/L)	26.48	30.9	28.9	21.9	25.9	ND	26.8	3.40
Cr (µg/L)	136	62.6	155	66.0	38.8	ND	91.8	50.8
Pb (µg/L)	2.90	2.31	2.15	4.57	8.25	ND	4.04	2.55
Al (µg/L)	42.7	8.51	8.61	52.0	55.5	ND	33.5	23.2
Alk (mg/L $CaCO_3$)	2425	4425	3030	4200	2200	2770	3175	929
EC (mS/cm)	29.8	29.2	33.2	33.1	34.8	ND	32.0	2.16
pH	7.28	10.9	9.56	14.2	14.3	11.2	11.2	2.71
TVS:TS	0.371	0.32	0.38	0.41	0.32	0.36	0.36	0.037
BOD:COD	0.30	0.32	0.18	0.28	0.26	0.27	0.27	0.054
C:N	8.94	5.48	5.06	3.58	2.64	2.48	4.70	2.41
VFA:Alk	1.09	0.70	1.38	0.64	0.91	0.97	0.95	0.30
COD: SO_4^{2-}	22.0	8.5	12.6	19.2	16.0	14.2	15.7	5.30
COD:TVS	2.12	2.07	1.92	1.15	2.13	2.23	1.94	0.40

Table 1.2: Characteristics of Tanyard bovine/ovine tannery effluent (Mpofu et al, 2022)

Parameter	Batch 1	Batch 2	Batch 3	Batch 4	Batch 5	Batch 6	Mean	SD ±
TOC (mg/L)	930	594	1330	875	700	1208	940	285
COD (mg/L)	3880	4625	6570	1725	1955	4795	3925	1842
BOD (mg/L)	1500	1650	2443	900	1200	1800	1575	517
VOA_t (mg/L AAE)	1458	531	1985	1062	167	1102	1051	647
TN (mg/L)	765	580	910	545	595	980	729	185
TAN (mg/LNH_3-N)	760	102	153	315	422	730	414	281
NO_3 (mg/L)	0.70	0.61	0.80	< 0.5	1.10	0.75	0.79	0.19
NO_2 (mg/L)	0.01	5.5	5.65	0.30	0.32	0.34	2.01	2.76
TP (mg/L $PO_4^{3-}-P$)	3.20	5.05	8.05	10.4	7.90	8.60	7.20	2.61
SO_4^{2-} (mg/L)	2740	4200	3400	2310	2090	2450	2865	796
HS^- (mg/L)	0.10	5.70	4.80	0.65	0.68	0.48	2.07	2.57
Cl (mg/L)	7725	7500	9400	2870	4620	7460	6595	2387
TS (g/L)	20.1	16.9	17.5	22.5	12.9	20.1	18.3	3.34
TVS (g/L)	2.34	1.50	2.51	2.02	1.29	1.79	1.91	0.47
Proteins (mg/L)	256	282	204	377	435	560	352	132
K (mg/L)	85.7	ND	80.3	105	130	ND	100	22.5
Na (mg/L)	6235	ND	6072	6664	5928	ND	6225	319
Fe (mg/L)	0.27	ND	0.04	0.34	0.11	ND	0.19	0.14
Ca (mg/L)	198	ND	212	331	183	ND	230	67.6
Mg (mg/L)	218	ND	215	263	186	ND	221	31.9
Zn (µg/L)	110	ND	78.6	189	383	ND	190	137
Cu (µg/L)	20	ND	25.1	22.6	236	ND	75.8	107
Co (µg/L)	0.00	ND	1.36	1.99	4.65	ND	2.00	1.95
Cd (µg/L)	0.00	ND	0.00	0.11	0.06	ND	0.04	0.05
Ni (µg/L)	20	ND	14.6	15.1	15.5	ND	16.3	2.5
Cr (µg/L)	130	ND	119	283	269	ND	200	87.7
Pb (µg/L)	0.00	ND	3.30	3.49	5.64	ND	3.11	2.33
Al (µg/L)	30	ND	15.0	25.3	42.0	ND	28.1	11.2
Alk (mg/L $CaCO_3$)	2010	1730	2705	1960	1590	5420	2569	1449
EC (mS/cm)	31.4	ND	31.1	33.9	29.4	ND	31.5	1.59
pH	8.38	8.80	8.52	8.04	8.48	7.82	8.34	0.35
TVS:TS	0.12	0.09	0.14	0.09	0.10	0.09	0.11	0.02
BOD:COD	0.39	0.36	0.37	0.52	0.61	0.38	0.44	0.11
C:N	1.22	1.02	1.46	1.61	1.18	1.23	1.29	0.21
VFA:Alk	0.73	0.31	0.73	0.54	0.11	0.20	0.44	0.27
COD:SO_4^{2-}	4.17	7.79	4.94	1.97	2.79	3.97	4.27	2.02
COD:TVS	1.66	3.09	2.62	0.85	1.51	2.67	2.07	0.86

Although Mpofu *et al.* (2020) conducted a rigorous characterisation protocol for the TWW, some measurements primarily serve as data for modelling. This is because the most frequently used and universally accepted mathematical models describing wastewater treatment technologies, or integrated plant-wide treatment technologies, are those that comply with the IWA platform,

e.g., ASMs, ADM 1, BSMs, and others following the same IWA framework. These models adhere to a universally recognised standard notation for the variables and parameters used, as reported by Corominas *et al.* (2010) and Guang-Hao Chen (2020), in accordance with the IWA framework.

Domestic, industrial or a mixture of these wastewaters commonly consists of complex organics that can be characterised into biodegradable or unbiodegradable organics. Each of these categories can be further subdivided into soluble and particulate components, i.e., BSO, USO, BPO, and UPO. The soluble organics are usually subdivided further into those that are fermentable (FBSO) and volatile fatty acids (VFAs).

These characterisation categories also apply to the N and P compositions of these organics, and the inorganic ammonia and ortho-phosphates are included in this characterisation (Harding *et al.*, 2009; Ikumi *et al.*, 2013). This characteristic will need to be further characterised to conform to the standardised notation used for wastewater modelling. This influential characteristic is shown in Table 1.3, which refers to the characteristics of wastewater or industrial effluent fed to an anaerobic digester.

Table 1.3: Characteristics of Wastewater Fed to AD or AS Systems (Ikumi et al., 2013)

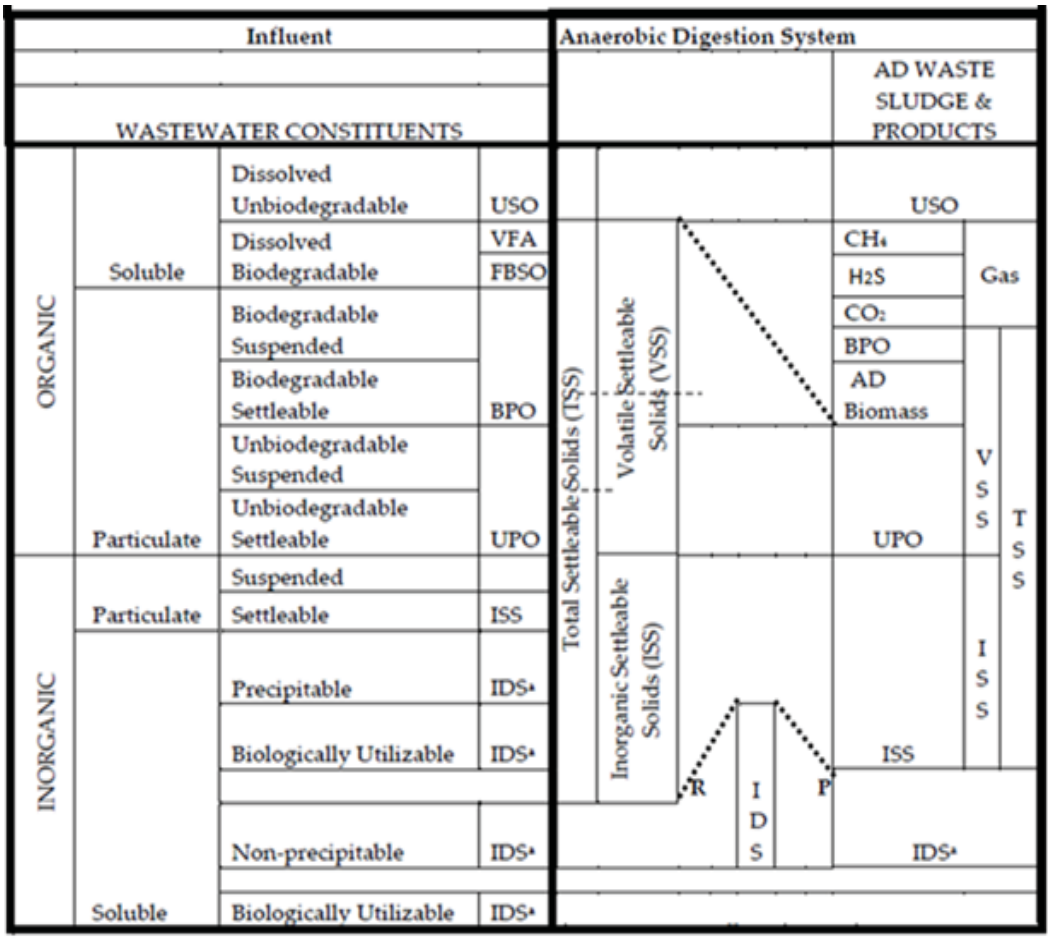

This characterisation procedure continues to present wastewater variables in a format suitable for use as input parameters for mathematical modelling, requiring the BPO, BSO, UPO, USO, VFAs, etc., to be described as the COD, C, H, O, N, P, and S components.

Metals are considered only when metal-based precipitants are included in the model framework. This characterisation framework also enables the auditing of models and meta-datasets to ensure compliance with mass continuity throughout systems and models.

1.5 Overview of Proposed Treatment Technology via an Integrated System Approach

TWW presents a complex treatment challenge due to its high organic load, salinity, nutrients, heavy metals, and recalcitrant compounds. In South Africa, where water scarcity and stringent environmental regulations intersect with the economic imperative to sustain the leather industry, the treatment, recovery, and reuse of TWW have become critical priorities.

However, most existing strategies rely on single-process chemical or biological approaches, which often achieve only partial contaminant removal and rarely address the opportunities for water reuse and resource recovery.

This project directly responds to these gaps by pursuing two interconnected objectives:

A. Developing a robust and scalable treatment system capable of producing regulatory-compliant effluent suitable for safe discharge or industrial reuse, and

B. Transforming wastewater into a resource, recovering energy, nutrients, and value-added by-products to support the principles of the circular economy.

To achieve these objectives, the study proposes a novel integrated treatment framework that strategically combines biological, algal, and advanced sludge processes into a single system. This approach moves beyond conventional “end-of-pipe” treatment by repositioning TWW as a feedstock for resource generation and water recovery.

1.5.1 Integrating Three Complementary Systems

At the core of this research is the development of a novel treatment framework that combines three carefully selected processes:

a. A HLFCR, coupled with an anaerobic digester (AD) – This pairing enhances the breakdown of complex organic matter, enabling both effective contaminant removal and the generation of biogas as an energy-rich byproduct.
b. An Algal Biorefinery System – Leveraging the phycoremediation potential of selected microalgal consortia. This unit supports nutrient removal while producing microalgal biomass rich in pigments and lipids, which can be further processed into bioplastics and biofuels (Natsurv10, 2nd Edition, 2017).
c. A Nitrification–Denitrification Activated Sludge Process – This stage provides advanced nitrogen removal, improving effluent quality and aligning with regulatory discharge standards.

Together, these processes form an integrated treatment train capable of addressing the organic, nutrient, and metal loads characteristic of TWW, while recovering water and generating value-added by-products.

1.5.2 Innovation in Algal Reactor Design

A distinctive feature of this system is the novel algal reactor, which will be evaluated for:

- The growth potential of microalgal consortia in raw and pre-digested tannery effluent,

- The phycoremediation efficiency of selected species,
- The biochemical characteristics of the biomass produced, and
- The potential for pigment and lipid recovery to support downstream valorisation (Bhaskar *et al.*, 2020; Bohra *et al.*, 2022).

This approach extends beyond conventional treatment by transforming wastewater into a feedstock for bioproducts, supporting the principles of the circular economy.

1.5.3 Modelling for System Design and Optimisation

To complement experimental work, the study incorporates dynamic process modelling using the Gujer matrix framework, enabling a detailed representation of biological, physical, and chemical processes occurring within the integrated system.

This includes:

- The development of novel kinetic models for individual unit operations, and
- A system-wide model that facilitates performance evaluation, optimisation, and cost analysis.

Such modelling addresses critical knowledge gaps highlighted by Durai and Rajasimman (2011), who emphasised the need for kinetic studies in TWW treatment. Serdarevic and Dzubur (2016) underscored the value of simulation in advancing treatment design.

1.5.4 Towards a Circular and Sustainable Solution

By merging biological, algal, and sludge-based treatment technologies within a single framework, this project delivers more than compliance-oriented wastewater management. It creates a robust, resource-oriented system that addresses pressing challenges in South Africa's tannery sector, reducing freshwater demand through reuse, mitigating environmental impacts, and generating value-added products from waste streams. This integrated approach advances the discourse on TWW treatment from a purely pollution-control paradigm to one that embodies sustainability, innovation, and circular-economy principles.

1.5.5 Research Scope and Boundaries

The project encompasses both laboratory-scale experimentation and virtual simulation studies:

- Experimental work will focus on the operation of HLFCR - AD and algal bioreactors under varying HRTs and COD concentrations, using a 5×5 matrix design. These operational ranges are based on findings from the WRC Project No. K5/2841/3 for ostrich and bovine/ovine tanneries.
- Virtual experimentation will use DHI WEST® software to simulate and validate system performance, with a 20% relative error tolerance for model validation, as recommended by Brun *et al.* (2002) for moderately defined system parameters.

While this integrated framework is scalable, its model validity will be constrained to the operational ranges defined by the experimental datasets. Any further limitations encountered during experimental or simulation phases will be documented in the final report.

CHAPTER 2: MODELLING THE APPLICATION OF HYBRID LAMINAR FLOW CHANNEL REACTORS FOR TWW TREATMENT

2.1 Introduction

The tanning and leather finishing industries are deeply embedded in South Africa's economy, yet they face a longstanding challenge: the production of large volumes of wastewater that is both highly contaminated and difficult to treat. Tanneries consume significant amounts of water, and their effluents carry high loads of organic matter, sulphates, chlorides, and nitrogen compounds. These characteristics place TWW among the most complex to manage, and conventional treatment systems often fall short, struggling to meet discharge standards and rarely enabling water reuse (Harding *et al.*, 2025).

Within this pollutant mix, sulphates present a particularly pressing concern. Though not directly hazardous in their dissolved form, excessive sulphates destabilise the natural sulphur balance and drive the formation of hydrogen sulphide (H_2S). This byproduct is toxic, corrosive to infrastructure, foul-smelling, and is a precursor to sulphur oxides (SOx), which contribute to air pollution (Serrano *et al.*, 2020).

Beyond these environmental and health impacts, sulphates disrupt downstream biological processes by inhibiting methanogenesis in anaerobic digesters. The result is a significant reduction in methane yields and overall digester performance. For this reason, effective sulphate pretreatment is not merely desirable but essential if TWW treatment is to achieve both compliance and energy-recovery goals.

To move beyond the limitations of conventional systems, researchers and practitioners have increasingly turned to biological processes. Compared to physicochemical methods, biological sulphate reduction (BSR) and sulphide oxidation offer more sustainable, resource-oriented approaches.

Commercial applications, such as THIOPAQ® and Sulfothane™, have demonstrated the feasibility of harnessing microbial consortia for these tasks (Lin *et al.*, 2018), but their high investment and operating costs limit wider adoption. Against this backdrop, the HLFCR has emerged as an innovative alternative.

2.2 The Hybrid Linear Flow Channel Reactor (HLFCR) Technology

The HLFCR was developed under the South African Water Research Commission's Project K5/2841/3 (Welz *et al.*, 2021) as a semi-passive, cost-effective treatment unit designed to address sulphate-rich effluents. Its novelty lies in its ability to create vertically stratified microbial zones within a single reactor. In the oxygen-limited mid and lower regions, SRB dominate, converting sulphates to sulphides.

At the air–liquid interface, limited oxygen penetration sustains sulphide-oxidising bacteria, which transform sulphides into recoverable elemental sulphur. Instead of competing, these processes are choreographed into a complementary sequence, enabling efficient sulphate removal while generating valuable by-products such as elemental sulphur for fertilisers, pesticides, and sulphuric acid production (Chung *et al.*, 2013).

When paired with AD, the benefits of the HLFCR become even clearer. By substantially lowering sulphate concentrations before effluent enters the digester, the system removes the inhibitory barrier to methanogenesis, creating optimal conditions for methane generation. In this way, the HLFCR-AD configuration transforms TWW treatment into a dual-purpose platform that safeguards the environment while enabling the recovery of renewable energy and materials.

Despite its promise, the HLFCR introduces new complexities that challenge existing modelling approaches. Most current models for sulphate reduction and sulphide oxidation are based on simplified frameworks (Ikumi, 2011; Harding *et al.*, 2020) that treat these processes in isolation.

While useful for understanding basic kinetics, they do not capture the defining feature of the HLFCR: its stratified structure, where distinct microbial communities coexist and interact dynamically across redox gradients. Nor do they account for the impacts of operational variables such as HRT, reactor geometry, or fluctuating tannery feed characteristics.

This gap between the HLFCR's innovative design and existing modelling capabilities presents a compelling research opportunity. The development of comprehensive models that can accurately predict the behaviour of these multi-zone systems becomes crucial not only for understanding current performance but also for designing scaled-up installations and optimising operational parameters.

Such models must capture the delicate balance among competing microbial processes, mass transfer limitations that maintain zone separation, and dynamic responses to varying feed conditions that characterise real-world tannery operations. Furthermore, as treatment requirements become increasingly stringent and the demand for resource recovery grows, the HLFCR system itself is evolving.

The integration of additional treatment components, such as algal bioreactors for nutrient recovery and polishing activated sludge systems for final effluent quality assurance, introduces new modelling challenges that extend well beyond the original HLFCR unit. These expanded configurations require modelling frameworks that can describe not only individual unit operations but also their complex interactions within integrated treatment trains.

Current research emerges at the intersection of proven technology and modelling innovation. By building on the established success of HLFCR systems while addressing the limitations of existing modelling approaches, this study seeks to develop the next generation of predictive tools capable of unlocking the full potential of these treatment systems. Its primary objective is to design a dynamic model of a two-stage HLFCR using DHI WEST software, with particular emphasis on optimising HRTs.

The work begins with a thorough understanding of HLFCR processes and the strengths and gaps in current modelling frameworks, before advancing towards more comprehensive solutions that better reflect the complexities of multi-zone microbial interactions. By identifying operational conditions that maximise sulphate removal, enhance elemental sulphur recovery, and produce effluents suitable for efficient anaerobic digestion, this research contributes to both scientific knowledge and the practical deployment of the HLFCR-AD system.

Ultimately, the study aims to position TWW treatment not merely as a matter of regulatory compliance, but as a pathway toward circular resource management, recovering methane as renewable energy and elemental sulphur as an industrial feedstock, while safeguarding environmental and public health.

2.3 State of the Art and Model Description of the Integrated HLFCR-AD System

The HLFCR is a specialised treatment unit designed to address the challenges posed by sulphate-rich wastewater from industries such as tanneries. Its strength lies in creating natural vertical layers, or microenvironments, that allow different microbial processes to occur simultaneously.

In the lower regions, anaerobic conditions favour SRBs, which convert sulphates to sulphides while lowering organic loads, as measured by COD. Near the air–liquid interface, limited oxygen penetration supports SOBs, which transform sulphides into elemental sulphur. This results in a visible floating sulphur layer, sometimes called the 'Flower of Sulphur', a stable and valuable product with industrial applications.

This stratified design is maintained by gentle diffusive mixing rather than mechanical agitation. Avoiding agitation is critical: mixing would introduce oxygen into the anaerobic layers, disrupt microbial balance, and prevent the formation of the floating sulphur layer. By preserving these distinct zones, the HLFCR enables pollutant removal and resource recovery within a single unit.

The reactor's performance depends on factors such as HRT, geometry, scale, and the type of carbon source supplied (Marais *et al.*, 2020b, c). Advances in molecular biology and sequencing technologies (Nielsen *et al.*, 2018; Vasquez *et al.*, 2018) have provided insights into how these conditions shape microbial communities, thus paving the way for more effective optimisation.

Compared with passive systems such as natural or constructed wetlands, which often exhibit slow reaction rates and re-oxidation of sulphur compounds (Rees & Bowell, 2007), the HLFCR provides a far more robust and controllable environment. It enhances sulphate-reducing activity by increasing biomass retention and improving the availability of electron donors, making it a superior option for treating TWW (Marais *et al.*, 2020b).

Recent studies highlight the practical value of HLFCRs. Horn *et al.* (2022) reported that untreated TWW is unsuitable for AD, but pretreatment with HLFCRs enabled high sulphate removal, near-complete sulphide elimination, and a 40% reduction in COD.

These improvements made the wastewater far more amenable to AD, boosting methane production while enabling sulphur recovery. Earlier work by Horn *et al.* (2020) also achieved sulphate removal efficiencies of up to 97%, which was among the highest recorded for this type of system.

When integrated with an anaerobic digester, the benefits are clear. Effluents leaving the HLFCR have reduced sulphate concentrations, thus removing a key barrier to methanogenesis and allowing methanogenic communities to thrive.

This integrated HLFCR-AD system, therefore, not only treats difficult waste streams but also generates renewable energy from methane and recovers elemental sulphur for industrial use, thereby contributing to both environmental protection and resource circularity. Figures 2.1 and 2.2 illustrate the HLFCR design and its visible sulphur layer, highlighting how stratification supports pollutant removal and product recovery.

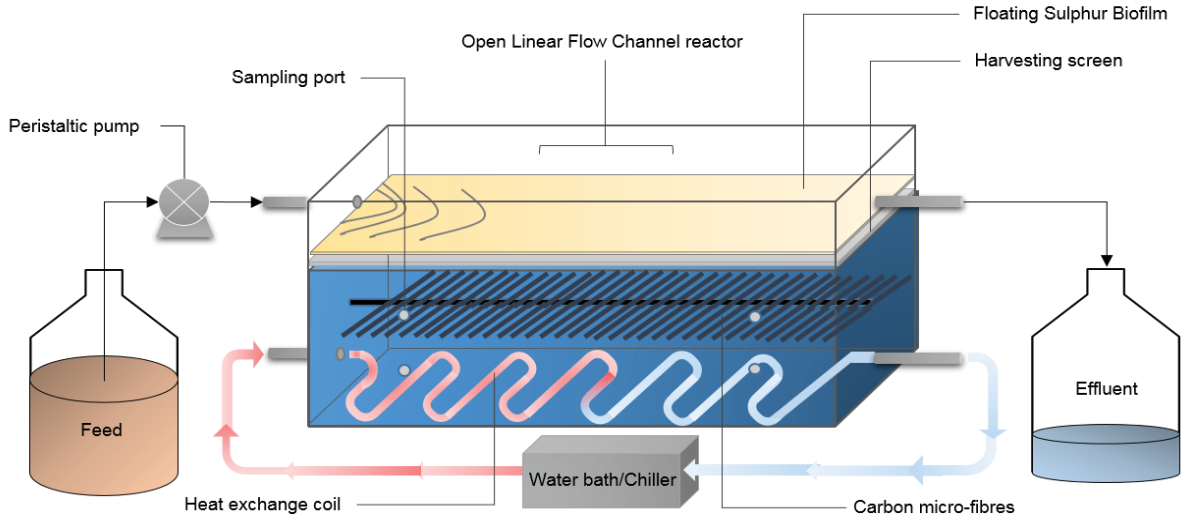

Figure 2.1: Schematic diagram of the reactor setup for an HLFCR

Figure 2.2: Hybrid linear flow channel reactor (HLFCR)

To summarise, the HLFCR-AD system is a state-of-the-art solution for TWW management. It combines efficient sulphate removal, organic matter reduction, and resource recovery into a single treatment train. Yet its stratified design and complex microbial interactions also present challenges for prediction and control. To fully unlock its potential, advanced modelling tools are required to optimise performance, guide scale-up, and ensure reliable operation under real-world conditions. This report addresses these gaps by reviewing current knowledge and developing practical modelling approaches tailored to integrated HLFCR-AD systems.

2.4 Operation and Testing of the HLFCR Unit Process: Experimental Findings

2.4.1 Experimental and virtual approaches

This study employed a dual approach, combining bench-scale experiments with virtual modelling, to evaluate and optimise the HLFCR for treating TWW. The laboratory experiments generated datasets that both characterised system performance and served as input for model calibration and validation. In parallel, the virtual study used the DHI WEST® simulation platform to predict performance and explore operational optimisation under different scenarios. The experimental work was conducted using TWW obtained from the International School of Tanning Technology (ISTT) in Makhanda, South Africa. The wastewater was transported to the

Water Quality Laboratory at the UCT and characterised in terms of soluble and particulate fractions, with measurements of COD, nitrogen, sulphate, and elemental composition. This influential characterisation established the baseline for subsequent analysis.

A two-stage HLFCR at UCT's Water Quality Laboratory was operated on this wastewater under varying HRTs to investigate the kinetics of biological particulate-organics hydrolysis, SRB, and SOB. Samples were taken under steady-state conditions and analysed for COD, sulphate, total suspended solids (TSS), volatile suspended solids (VSS), and inorganic suspended solids (ISS). The data was then evaluated for overall system mass balance. The virtual experimental study was built on this work by developing a dynamic model. Stoichiometric and kinetic equations representing BPO hydrolysis, SRB, and SOB activity were structured using Gujer matrices. Kinetic parameters were estimated through nonlinear regression in MATLAB® (Curve Fitting Toolbox®). The calibrated model was implemented in DHI WEST® software, and steady-state and dynamic simulations were used to validate it against experimental data. Together, these methodologies provided a robust framework for assessing and optimising HLFCR performance.

2.4.2 Collection and handling of TWW: Composition of feed (substrate)

The TWW used in the study represented effluent mixtures from individual tannery unit operations (Figure 2.3), reflecting typical contributions from a conventional bovine-hide processing facility. The effluents produced by various unit operations typically used in the tanning process enable assessment of the impact of each operation's effluent on the overall mixture. The supplier provided standard mixing ratios for the effluent from each unit operation. This guidance ensured a consistent TWW mixture across samples. The mixing ratios are outlined in Table 2.1. The prepared mixture was stored in 600 L tanks at UCT's Water Research Laboratory (Figure 2.3).

Figure 2.3: Components of the TWW based on unit operation origins

Table 2.1: Make-up of conventional TWW mixture

Make-up of Conventional TWW Mixture				
Process		**Per Mass of Hide**	**% of Total**	**Volumes (L)**
1	Dirt Soak	150%	11.1%	17.78
2	Main Soak	150%	11.1%	17.78
3	Liming	130%	9.6%	15.41
4	Wash after liming	150%	11.1%	17.78
5	1st wash before deliming	150%	11.1%	17.78
6	2nd wash before deliming	150%	11.1%	17.78
7	Deliming and bating	100%	7.4%	11.85
8	Wash after bating	150%	11.1%	17.78
9	Basification	70%	5.2%	8.30
10	Final wash	150%	11.1%	17.78
			100.0%	160

Figure 2.4: Holding tank for TWW in cold room at WRG lab

2.4.3 Experimental setup, sampling, and analysis

The HLFCR experimental system consisted of two Perspex reactors (10 L each; 11 mm wall thickness) with internal dimensions of 425 mm (L) × 160 mm (W) × 145 mm (H). Nine front-facing sampling ports enabled monitoring along the reactor length and depth. The design was adapted from the 25 L LFCR described by Van Hille *et al.* (2011), with additions including carbon microfibers as microbial support and a heat exchanger for temperature regulation.

As shown in Figure 2.4, influent was continuously pumped into the first HLFCR via a mid-level inlet port, and effluent was discharged from the opposite side into the second reactor. Final effluent exited from the top right corner of the second unit. Operating conditions included feed sulphate concentrations of 3,000–6,700 mg SO_4^{2-}/L, reactor temperature of 28 °C, and HRTs of 1.5, 2, 5, and 10 days. pH was not controlled.

The microbial cultures were sourced and maintained at UCT. The SRB stock culture was grown in modified Postgate B medium containing 0.46 g/L KH_2PO_4; 1.0g/L NH_4Cl; 2g/L $MgSO_4.7H_2O$; 0.3 $NaSO_4$; 1g/L yeast extract; 0.3g/L sodium citrate ($Na_3C_6H_5O_7$) and 1.6mL of 60% sodium lactate ($NaC_3H_5O_3$). SOB enrichment cultures were developed from SRB reactors using the method of Marais *et al.* (2020b).

Figure 2.5: HLFCR unit based at the WRG lab at UCT. (from L-R, 1st and 2nd reactors)

2.4.4 The Sampling Plan

This section describes the sampling guide employed in the research to generate datasets from the bench-scale experimental system. These datasets were utilised for model component identification, process verification, and validation.

It was crucial to ensure the accuracy and consistency of the sampling and analytical methods to uphold the reliability and quality of the generated datasets. The HLFCR included nine sampling points, and the system was sampled as summarised in Table 2.2.

Table 2.2: Sampling schedule guide

Analytical measurement and information	Sample state	Units	Sample points								
			Inlet			Middle			Outlet		
Flowrate (Volume used)		m//day	P1	P2	P3	P4	P5	P6	P7	P8	P9
COD	Filtered	mgCOD//			■						■
	Unfiltered	mgCOD//	■			■			■		
PH (In situ)											
Aqueous sulphide (H_2S/HS^-)		mg//	■	■	■				■	■	■
Sulphate (SO_4^{2-})		mg//			■						■
Ammonia		mg//			■						■
TSS/VSS/ISS	100°C/550°C	mg//									

■ Sampled port

□ Unsampled port

2.4.5 Analytical Methods

The analytical methods involved COD analysis, pH measurement, dissolved sulphide analysis, sulphate analysis, and determination of TSS, VSS, and ISS. The analysis procedures are detailed in the sections below.

2.4.5.1 Chemical oxygen demand (COD)

COD is a critical parameter in wastewater treatment, representing the amount of a specified oxidant that reacts with a sample under controlled conditions. The quantity of oxidant consumed is expressed in terms of its oxygen equivalence. In COD testing, the dichromate ion ($Cr_2O_7^{2-}$) is the specified oxidant, as it is reduced to the chromic ion (Cr^{3+}) during the analysis process. Both organic and inorganic components of a sample undergo oxidation, though the organic fraction is typically of primary interest. The COD analytical method is crucial, as it provides the foundation for calibrating reaction-rate kinetics related to substrate utilisation. COD also acts as a reference point for other components, helping to determine the feed composition. Therefore, feed COD (S_{ti}) is used as the identifier for the experimental trial runs in this study. The COD method used in this study is the closed reflux titration method, as described in the UCT Water Quality Laboratory Standard Operating Procedure manual.

This method offers several advantages over the open reflux method, including greater reproducibility, reduced sample volume requirements, and lower generation of hazardous

waste. Farina *et al.* (2004) reported that this closed-reflux COD method yields results with significantly lower error rates than the open-reflux COD method when analysing VFAs. These were key considerations for selecting this method for COD analysis.

The analysis was conducted using a reflux apparatus that included COD digestion tubes, a 500 mm condenser, and a COD digestion block with sufficient power to ensure complete digestion. The reagents used included 0.25N potassium dichromate ($K_2Cr_2O_7$), Sulphuric acid (H_2SO_4), 0.05N ferrous ammonium sulphate [$Fe(NH_4)_2(SO_4)_2$], ferroin indicator, and mercuric sulphate ($HgSO_4$) powder.

A defined amount of mercuric sulphate (0.04 g) was added to each digestion tube, along with 10 mL of the sample (or distilled water for blanks), followed by 5 mL of potassium dichromate solution. To ensure efficient oxidation, 15 mL of Sulphuric acid solution was carefully added to the tubes, ensuring that no vapour escaped.

After digestion at 150°C for two hours, the samples were cooled while the condensers remained in place. To wash the inner surfaces of the tubes, approximately 80 ml of distilled water was added before transferring the samples to 250 ml Erlenmeyer flasks. Two drops of the ferroin indicator were added, and the solution was titrated with ferrous ammonium sulphate until a single drop produced a reddish-brown colour change. The final COD concentrations were determined using the Equation 2.1 below.

$$g/lCOD = \frac{(a-b)\times N\times 8000}{ml\ sample} \qquad \textbf{Equation 2.1}$$

Where a = average ml $Fe(NH_4)_2(SO_4)^2$ used to titrate blank

b = average ml $Fe(NH_4)_2(SO_4)^2$ used to titrate sample

N = normality of $Fe(NH_4)_2(SO_4)^2$.

Given that TWW exhibited COD values exceeding 1000 mg COD/L, appropriate dilution factors (40 for unfiltered samples and 10 for filtered samples) were used. The augmented COD analysis, as reported by Ekama (2009b), was used to measure the filtered organic COD in the presence of sulphide for the BSR mixed liquor samples. This method removes the interference of dissolved sulphide in the sample's COD analysis. The augmented COD analysis includes the addition of zinc sulphate ($ZnSO_4$) to the BSR sample. The resulting zinc sulphide precipitate is removed by filtration through a 0.45 µm Millipore filter. The filtered soluble COD represents the organic COD, specifically the VFAs, in this case.

2.4.5.2 Total Kjeldahl Nitrogen (TKN) and Free and Saline Ammonia (FSA)

The TKN and FSA concentrations were measured by microdistillation. The TKN is the combination of organic nitrogen (Org-N) and FSA. In the TKN test, the sample was digested with a sulphuric acid solution containing potassium sulphate ($K_2SO_4^{2-}$), using mercuric sulphate as a catalyst. Digestion converts all nitrogen-containing compounds, such as proteins and peptides, into ammonia.

The sample was then steam distilled using a microdistillation apparatus with sodium hydroxide and sodium thiosulfate. As the ammonia is removed from the sample as a gas, it is condensed and dissolved in a boric acid solution, causing the sample to change colour from purple to green. The sample is then titrated with a standard sulphuric acid solution of normality 0.001 until it regains its purple colour, and the volume of acid titrated is taken to be proportional to the TKN

concentration. For FSA concentration measurement, the sample is not digested; instead, it is steam distilled. The difference between the TKN and FSA values represents the organically bound N (Org-N).

2.4.5.3 pH (in Situ Measurement)

The pH measurements were conducted using a Metrohm 691 pH metre. Before carrying out measurements, the pH metre was calibrated using standard buffer solutions of pH 2,7 and 9. To ensure accuracy, the pH probe was thoroughly rinsed before and after each use. When not in use, the probe was stored in a container containing either a 3M KCl solution or a pH 4 buffer.

2.4.5.4 Dissolved Sulphide Assay (H2S and HS-)

The total dissolved sulphide or free and saline sulphide (FSS), i.e., H_2S, HS^- and S^{2-}, was measured using the method reported by Cline et. al. (1968). This is a colourimetric method in which a Thermo Scientific Helios Alpha® spectrophotometer, set at 670nm, was used to estimate the TS concentration.

The colour development of this method depends on the formation of methylene blue from the reaction of dissolved FFS with the colourimetric reagent N,N-dimethyl-p-phenylenediamine sulphate in an acidic medium (hydrochloric acid). The reaction is catalysed by ferric chloride.

A sample of 20-100µl was added to 200µl of a 1% zinc acetate solution to ensure that the sulphide does not escape the sample and is trapped as ZnS. However, ZnS is soluble in 500µl of N,N-dimethyl-p-phenylenediamine sulphate in a 6N HCl acidic solution, to which is added 500µl of Ferric Chloride in 6N HCl acidic solution, resulting in methylene blue (thiazine dye). A sodium sulphide standard was prepared at known sulphide concentrations to develop a standards plot, which was used to determine the sample concentrations (Harding, 2020).

2.4.5.5 Sulphate Analysis

Sulphate concentration was measured using the Gallery® Discrete Analyser (Thermo Fisher Scientific), a fully automated photometric analyser designed for precise and efficient analysis of various environmental and water-quality parameters. This analyser employs a barium chloride precipitation method, as specified in SM 4500-SO_4^{2-} E, ISBN 0117533406, EPA 375.4, DIN 38405-D, and ISO 15923-1, ensuring standardised and reproducible results.

The Gallery® Discrete Analyser provides multiple calibration options, including factor, bias, linear, logit-log, spline, second order, and point-to-point calibrations. In this study, a second-order calibration curve was utilised to enhance the accuracy of sulphate quantification.

This approach is particularly beneficial for complex sample matrices, as it accommodates nonlinear response patterns and minimises measurement errors. By utilising discrete analysis technology, the system enables simultaneous processing of multiple samples without cross-contamination.

The analyser features a built-in quality control programme that follows Westgard rules, thereby ensuring high precision and reliability, with automatic flagging of out-of-specification results. The choice of the Gallery® Discrete Analyser was based on its high throughput (up to 200 tests per hour), low sample volume requirements (2-120 µL), and automated reagent handling, making it an efficient and accurate tool for sulphate measurement in this study.

2.4.5.6 Total Suspended Solids (TSS), Volatile Suspended Solids (VSS) and Inorganic Suspended Solids (ISS)

The analytical methods for TSS, VSS, and ISS were performed in accordance with the American Public Health Association (APHA) Standard Methods 2540 (2012). To measure TSS, reactor mixed liquor samples were collected into 50 mL centrifuge tubes and then centrifuged for 10 minutes using a Centurion Scientific centrifuge. The supernatant was carefully decanted, ensuring that no accumulated solids were lost. The solids were then washed into a crucible of known mass and dried in a Memmert incubator oven at 105 °C for 24 hours, until only the dried solids remained. The dried sample was cooled in a desiccator, and its mass was measured using an Optika weigher; the mass was recorded as the TSS value. The dried TSS was then incinerated in a Labofurn incinerator at 550 °C for 20 minutes, leaving behind an ash residue. The mass of the remaining ash was measured using the Optika weigher, and the mass was recorded as the ISS. The VSS mass was determined as the difference between the TSS and ISS.

CHAPTER 3: ANAEROBIC DIGESTION OF TANNERY WASTEWATER AND SYSTEM INTEGRATION

3.1 Introduction

In line with the UN SDGs 2030, industries are encouraged to adopt wastewater treatment methods that promote water reuse, resource recovery, and reduced reliance on freshwater. AD has gained global recognition as a cost-effective and environmentally friendly solution for managing organic wastes. It not only reduces pollutant loads but also produces renewable energy in the form of methane, offering particular value for developing regions (Priebe *et al.*, 2016).

AD is a biological process in which microorganisms decompose organic matter in the absence of oxygen. Compared with aerobic treatment, it generates substantially less sludge and can be applied to a wide range of waste streams.

The process is driven by distinct microbial communities that operate sequentially to degrade complex organic matter into simpler compounds and ultimately methane (Sötemann *et al.*, 2005). As a next step in this report, a review of anaerobic digestion literature is presented to support understanding of the individual processes and their relevance to the HLFCR-AD system. This review also provides the foundation for mathematical modelling, particularly the stoichiometry and kinetic rates of the microbial groups involved in this specialised type of AD system.

3.2 Stages of Anaerobic Digestion

The AD of complex organic matter proceeds through a series of interconnected steps: hydrolysis, acidogenesis (fermentation), acetogenesis, and either methanogenesis or sulfidogenesis (sulphate reduction). These processes are illustrated in Figure 3.1.

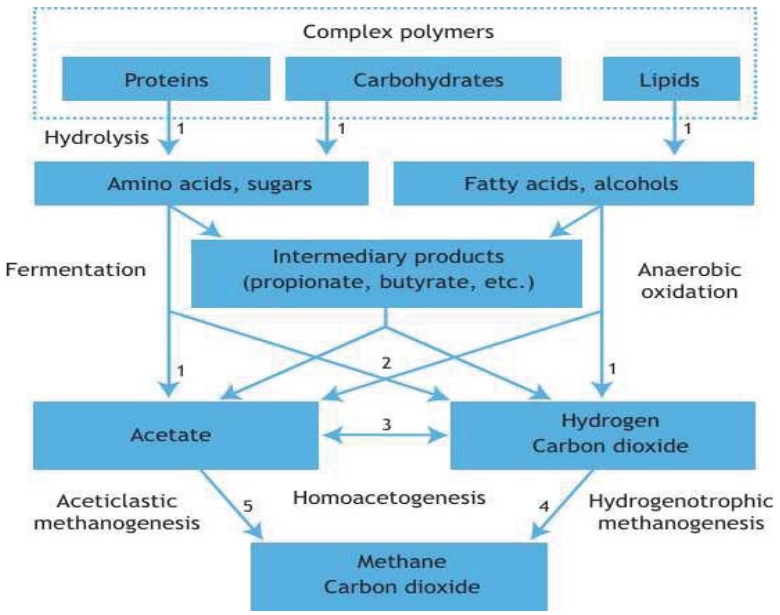

Figure 3.1: Conceptual diagram of sulphate reduction and other biological anaerobic processes

- **Hydrolysis**

Hydrolysis is the first and often rate-limiting stage of AD, especially under high organic loading. Complex organic substrates, such as proteins, carbohydrates, and lipids, are degraded into simpler molecules, including amino acids and sugars. This step is mediated by extracellular enzymes released by anaerobic microbes, which remain attached to the cells within a protective layer of extracellular polymeric substances (EPS). Microorganisms readily absorb the breakdown products for subsequent steps. Hydrolytic and fermentative microbes typically thrive at slightly acidic pH levels (6.5–7.5) (Menzel *et al.*, 2020).

- **Acidogenesis**

In acidogenesis, the hydrolysis products undergo fermentation and anaerobic oxidation, producing VFAs, alcohols, hydrogen, and carbon dioxide. This step is carried out by a broad range of acidogenic bacteria (Chen *et al.*, 2020; Patel *et al.*, 2017). Acidogenesis occurs more rapidly than other AD stages, with bacterial regeneration times of less than 36 hours (Meegoda *et al.*, 2018). However, excessive accumulation of VFAs can reduce pH and destabilise the digester, making this stage a common cause of process failure.

- **Acetogenesis**

VFAs produced during acidogenesis are further converted by acetogenic bacteria into acetate, hydrogen, and carbon dioxide (Chen *et al.*, 2020). Approximately 70% of methane in AD is derived from acetate, with the remainder coming from hydrogen and carbon dioxide through syntrophic interactions with methanogens. Acetoclastic methanogens, which consume acetate, are highly pH-sensitive: they are inhibited below pH 6 and above pH 7.5 (Batstone *et al.*, 2002; Patel *et al.*, 2017). Thus, maintaining a stable pH is critical at this stage.

- **Methanogenesis**

The final step involves methanogenic archaea, which convert acetate into methane and carbon dioxide (Acetoclastic methanogenesis) or reduce carbon dioxide with hydrogen to methane (hydrogenotrophic methanogenesis). Approximately 70% of methane is produced via acetate conversion, whereas hydrogen accounts for about 30% (Chen *et al.*, 2020). Hydrogenotrophic methanogens play a key role in maintaining low hydrogen concentrations, which supports acetogenic processes. Although Acetoclastic methanogens are particularly pH-sensitive, hydrogenotrophic methanogens remain functional until pH drops below 6 (Batstone *et al.*, 2002). Through these steps, influent COD is progressively converted into biogas (predominantly methane), leaving a stabilised digestate.

3.3 Challenges in AD Modelling for TWW

While AD is widely applied to stabilise sludge and recover energy, modelling its behaviour remains challenging. Most models have been developed and calibrated for sewage sludge under steady-state conditions, with limited application to complex industrial effluents such as TWW. TWW contains high sulphate concentrations, which introduce competition between SRB and methanogens for common substrates. This interaction can significantly influence methane yields and system stability. However, existing models often lack accurate calibration of intermediate processes such as hydrolysis and acetogenesis, particularly under dynamic conditions. Consequently, they cannot reliably simulate digester start-up, predict failure scenarios, or quantify the influence of SRB activity on methane production. The IWA AD Model

No. 1 (ADM1) provides a framework using Monod-type kinetics to describe hydrolysis, acidogenesis, acetogenesis, and methanogenesis. Yet, extending this model to tannery wastewater requires careful recalibration with experimental datasets that capture the unique characteristics of TWW, including high COD, nitrogen, and sulphur loads. Addressing these gaps is essential to developing robust AD models that support the optimisation and scale-up of integrated systems for treating tannery effluents.

3.4 Experimental Findings from AD Batch Tests Fed TWW

This section details the experimental setup for the study. It covers the operations and sampling methods utilised, including the collection and storage of TWW, as well as the procedures for conducting the experimental batch tests. The section also presents the analytical methods used to test wastewater parameters. It further describes the estimation of kinetic parameters and the determination of volumetric and substrate-specific utilisation rates. Finally, the final section discusses the use of the MATLAB Curve Fitting Toolbox to fit kinetic equations and estimate kinetic parameters.

3.4.1 Experimental Design

Two identical batched methane and sulphide potential ADs, each having a volume of 25L, were used (see Figure 3.2). The operational volume of 25 L comprised 20 L of TWW feed and 5 L of AD seed. The conditions in the anaerobic digester were maintained at a mesophilic temperature of 36 °C and a pH of 7-8. A mechanical stirrer was used to mix within the AD. The AD was operated for 60 days with various initial feed concentrations. The assumption was that the concentration of TWW at full strength was approximately 18,000 mg COD/L. Therefore, the AD was operated at 0.25, 0.5, 1, 0.75, and twice the full loading rate of raw TWW. Each anaerobic digester was bubbled with nitrogen from a cylinder for 10 minutes to remove sulphide that accumulated during the process. Then, immediately, a rubber stopper was used to seal the digesters.

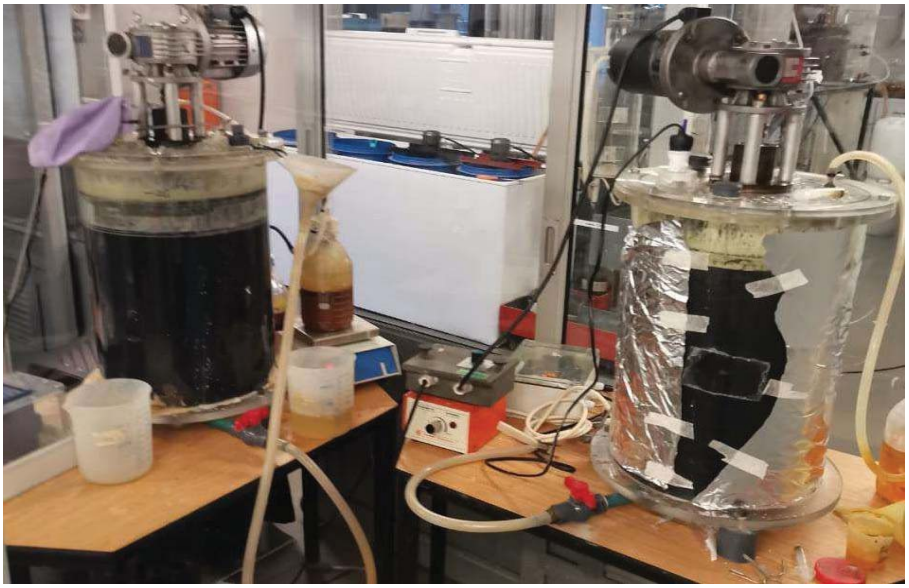

Figure 3.2: Anaerobic digesters (AD1 and AD2)

3.4.2 Operation and sampling of anaerobic digestion system

This section describes the collection and preparation of TWW, the operation of batch AD tests, and the sampling and analysis procedures applied. These steps were essential for generating datasets used in modelling the kinetics of methane-producing and sulphate-reducing microorganisms under high-salinity conditions.

3.4.3 Wastewater Collection and Storage

TWW was sourced from a pilot plant at the ISTT in Makhanda, Eastern Cape, South Africa. Ten-unit operations covering the Tanyard and beam house processes were sampled using 25 L containers. The collected wastewater was transported to the UCT Water Quality Laboratory within two days and stored in a stainless-steel tank at 4 °C. Initial characterisation included measurements of COD (filtered and unfiltered), TKN, FSA, chloride (Cl^-), sulphate (SO_4^{2-}), and sodium (Na^+). Results are presented in Table 3.1 and Table 3.2 below.

Table 3.1: Mixture of conversional TWW

Mixture of Conversional TWW				
	Process	% mass of Hide	% of Total	Volume (L)
1	Dirt Soak	150%	11.1%	17.78
2	Main Soak –150%	150%	11.1%	17.78
3	Liming –130%	130%	9.6%	15.41
4	Wash after liming	150%	11.1%	17.78
5	1st wash before deliming	150%	11.1%	17.78
6	2nd wash before deliming	150%	11.1%	17.78
7	Deliming and bating	100%	7.4%	11.85
8	Wash after bathing	150%	11.1%	17.78
9	Basification	70%	5.2%	8.30
10	Final wash	150%	11.1%	17.78
			100%	160

Table 3.2: Characterisation of raw TWW

Characterisation of the raw TWW		
Total COD	mg/L as COD	14295.7
USO	mg/L as COD	1551.1
UPO	mg/L as COD	4234.0
BPO	mg/L as COD	5210.5
BSO	mg/L as COD	3300.0
TKN	mg/L as N	1829.8
FSA	mg/L as N	775.2
Org-N	mg/L as N	1054.6
So_4^{2-}	mg/ L as SO_4^{2-}	4953.3
Cl^-	mg/L	5473.1
Na^+	mg/L	4932.6

3.4.4 Experimental Batch Test Operation

Two laboratory-scale anaerobic digesters were operated under mesophilic conditions (36°C) for 60 days. Five feed concentrations were tested: 0.25×, 0.5×, 1×, 1.5×, and 2× full strength TWW (assumed COD ≈ 18,000 mg/L). Feed preparation was adjusted by settling raw TWW for 24 hours and decanting varying volumes to manipulate the ratio of particulate to soluble COD:

- 2× strength: COD 38,000–44,000 mg/L, prepared by decanting half the supernatant after settling.
- 1× strength: unmodified raw TWW (≈18,000 mg/L COD).
- 0.25× strength: COD diluted by decanting 75% of supernatant after settling.
- 0.75× and 1.5× strengths: prepared by decanting 25% and 50% of settled supernatant, respectively.

Digester pH was maintained between 7.0 and 8.0, with $CaCO_3$ added when the pH fell below 7.0. To control hydrogen sulphide (H_2S), which inhibits methanogens, nitrogen or carbon dioxide was periodically bubbled through the digesters, depending on pH.

3.4.5 Sampling and Monitoring

Samples were collected every three days over the 60-day run. From each digester, 100 mL samples were collected: half was centrifuged at 6,000 rpm for 10 minutes to separate solids, and the remainder was reserved for pH and conductivity analysis. Supernatant was filtered (0.45 µm) and analysed for COD, TKN, FSA, sulphate, and ammonia. Solids were dried and weighed to determine TSS, VSS, and ISS. Continuous monitoring ensured sufficient SRT for microbial activity and effective removal of inhibitory H_2S. Figure 3.3 shows a schematic representation of the samples and tests performed on the AD systems.

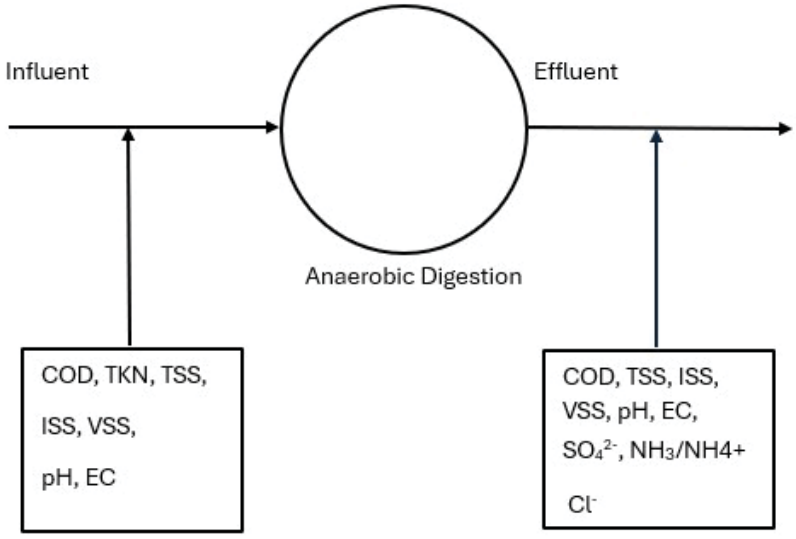

Figure 3.1: Schematic presentation of an anaerobic digester

3.4.6 Analytical Methods

The following steps were conducted to fulfil the requirements of the analytical methods:

- TSS, VSS, ISS: Determined gravimetrically after centrifugation, oven drying (105 °C, 24 h), and incineration (600 °C, 20 min). VSS = TSS – ISS.

- COD: Measured using Standard Method 5220B (open reflux with potassium dichromate and mercury sulphate).

$$\boldsymbol{COD} = \frac{(\boldsymbol{Blank - Titration\ Volume}) \times \boldsymbol{FAS} \times \mathbf{8000}}{\boldsymbol{Sample\ Size}} \times \boldsymbol{Dilution\ Factor} \quad \text{Equation 3.1}$$

- TKN and Organic N: Measured by micro-Kjeldahl digestion, distillation, and titration.

$$\boldsymbol{TKN} = \frac{\boldsymbol{Titration\ Volume} \times \boldsymbol{H_2SO_4} \times \mathbf{14000}}{\boldsymbol{Sample\ Size}} \times \boldsymbol{Dilution\ factor} \quad \text{Equation 3.2}$$

$$\mathbf{Org\ N} = \mathbf{TKN} - \mathbf{FSA} \quad \text{Equation 3.3}$$

- Conductivity: Measured using a Jenway Model 4510 conductivity metre (calibrated with 1413 µS standard).
- pH: Monitored with an Accsen pH Metre, Model pH 8, calibrated with standard buffers (pH 4.01 and 7.01).

3.4.7 Kinetic Parameter Estimation

Substrate utilisation rates were calculated using effluent COD and VFAs. Volumetric rates were converted to specific substrate utilisation rates using the methods of Ikumi (2011). Nonlinear least-squares regression was applied to fit the Contois kinetic model, yielding estimates of microbial kinetic constants.

3.4.8 Determining volumetric and specific substrate utilisation rates

As highlighted by Sötemann *et al.* (2005), determining kinetic constants (Km, Ks) in anaerobic systems is challenging. Traditional linearisation methods (Lineweaver–Burk, Eadie–Hofstee, inversion) often yield inconsistent results. Recent advances in computational tools now allow more accurate nonlinear regression approaches. This study applied the MATLAB® Curve Fitting Toolbox, which employs nonlinear least-squares regression, to estimate maximum substrate consumption rates (Km) and half-saturation constants (Ks) for the Contois model. The procedure followed by Harding *et al.* (2020) focused on the relationships between specific substrate utilisation rates and reactor substrate concentrations.

3.4.9 Application of MATLAB® curve fitting toolbox

The experimental data obtained in Section 3.3.4 were analysed using the MATLAB® Curve Fitting Toolbox to estimate kinetic parameters for the Contois rate equation under different TWW conditions. Nonlinear least-squares regression was applied to identify the best-fit between the observed data and the model, ensuring that the rate equation accurately represented the microbial processes involved. Using this procedure, the key kinetic constants, the maximum substrate consumption rate (Km) and the half-saturation constant (Ks), were determined. These parameters underpin the description of substrate utilisation rates in the AD of high-strength, sulphate-rich wastewaters such as TWW and are essential for reliable model calibration and simulation.

3.5 Results and Discussion

This chapter presents the results and discussion of the experimental investigations, following the methodology outlined earlier. The analyses focus on evaluating the performance of AD systems treating TWW and on developing kinetic models describing substrate degradation,

biomass dynamics, and competition among microbial groups. Section 3.4.1 evaluates the reliability of the experimental data by performing material mass-balance calculations. Section 3.4.2 discusses feed biodegradability characterisation, a key research objective, by partitioning COD and nitrogen into biodegradable and unbiodegradable fractions. Subsequent sections address system performance, biomass evaluation, and microbial competition, while Section 3.5 presents kinetic modelling, parameter estimation using MATLAB®, and comparison with the literature. The chapter concludes with an analysis of factors that inhibit process stability.

3.5.1 Experimental Data Evaluation

Before modelling, the accuracy and reliability of the experimental data were assessed using material mass-balance calculations. Mass balance provides a robust method for verifying laboratory data because it is based on the law of conservation of mass, which states that the mass entering the AD system must equal the mass leaving the system. In this study, balances were performed on COD and nitrogen. Nitrogen balances within the range 90–110% were considered acceptable, indicating sufficient accuracy. The results showed that organically bound nitrogen in the influent was gradually released as TKN during digestion, with effluent TKN values closely matching the influent. COD balances proved more challenging.

Over 95% of biodegradable organics are typically converted to methane, which is insoluble and exits as biogas. However, in this study, hydrogen sulphide (H_2S), a strong inhibitor of methanogens, was stripped from the system using nitrogen gas. While this step minimised competition between SRB and methane-producing bacteria (MPB), it also removed methane from the reactor, thus making direct measurement impossible. Consequently, COD balance calculations could not be completed, and nitrogen balance was relied upon as the main indicator of data reliability. Nitrogen balances were calculated from the average effluent nitrogen values over the 60-day retention period across different batch concentrations. As shown in Table 3.3. Most balances fell within the acceptable range of 95–110%, confirming the accuracy and sufficiency of the data. Only one exception was observed at the 1× concentration, where the nitrogen balance reached 118%. This anomaly is probably attributable to the conversion of organic nitrogen into ammonium during anaerobic processes, which elevated effluent TKN values. Because this was the only significant deviation, it was not considered a major concern for data reliability.

Table 3.3: Nitrogen mass balance

HRT	Batch Concentration	Nitrogen IN	Nitrogen Out	N Balance Percentage
(days)	mg/L	mg/L	mg/L	%
60	0.25x	1827	1864	102%
60	0.50x	2142	1995	93%
60	0.75x	3346	3125	93%
60	1x	3094	3673	118%
60	2x	8456	8122	96%

3.5.2 Feed Biodegradability Characterisation

Characterising feed biodegradability was central to this research, as it enabled partitioning of influent COD and nitrogen into fractions reflecting degradability. In the case of COD, the total influent TWW concentration was divided into BSO, USO, BPO, and UPO. BSO was further subdivided into fermentable organics (FBSO) and VFAs. The results of this categorisation for different feed concentrations (25%, 50%, 75%, 100% and 200% TWW) are presented in Table 3.4 and Figure 3.4 respectively. The particulate COD, which represents the combined contributions of BPO and UPO, showed clear trends across the experimental runs, as illustrated in Figures 3.4 (a) to (e). For all feed concentrations, particulate COD decreased with increasing SRT, indicating substrate degradation.

Beyond a certain point, however, the reduction in particulate COD levelled off, suggesting that the readily biodegradable fraction had been consumed and only UPO remained. These observations are consistent with earlier findings reported by Ikumi (2011). At the highest concentration (200% TWW), the particulate COD trend showed fluctuations between days 0 and 30, which may be attributed to microbial adaptation to the higher substrate load. For the other feed concentrations (25%, 50%, 75%, and 100% TWW), BPO degradation progressed between day 1 and day 30.

Table 3.4: Summary of feed characterisation

Characteristics of tannery raw wastewater							
TWW batches			100%	200%	75%	50%	25%
Total COD	*mg/L as COD*		20388.8	44296.0	14602.0	8722.0	4590.0
Filtered COD	*mg/L as COD*		2666.3	2303.0	2097.2	1666.0	1142.4
TKN	*mg/L as N*		3853.2	8144.3	3139.1	2002.0	1861.6
USO	*mg/L as COD*	8.5%	1623.6	1470.0	1117.2	1038.8	530.4
UPO	*mg/L as COD*	36.0%	8551.3	20000.2	6415.7	1435.7	1484.1
BPO	*mg/L as COD*	48.7%	9171.2	21992.8	6089.1	5620.3	1963.5
BSO	*mg/L as COD*	6.8%	521.3	416.5	490.0	313.6	306.0
	mg/L as COD		156.4	125.0	147.0	94.1	91.8
	mg/L as COD		364.9	291.6	343.0	219.5	214.2
NH3	*mg/L as N*	4.0%	169.1	315.44	117.20	98.00	55.00
Organic N	*mg/L as N*	96.0%	3684.1	7828.8	3021.9	1904.0	1806.6
SO_4^{2-}	*mg/L as SO4*		5141.5	5293.4	4224.4	5989.0	3653.1
Cl^-	*mg/L*		5361.0	5159.1	5195.0	6454.5	4871.3
Na^+	*mg/L*		3574.0	3439.4	3463.3	4303.0	3247.5

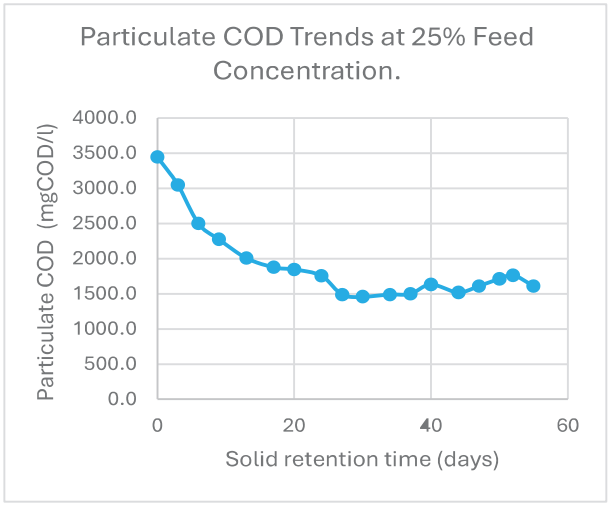

(a)

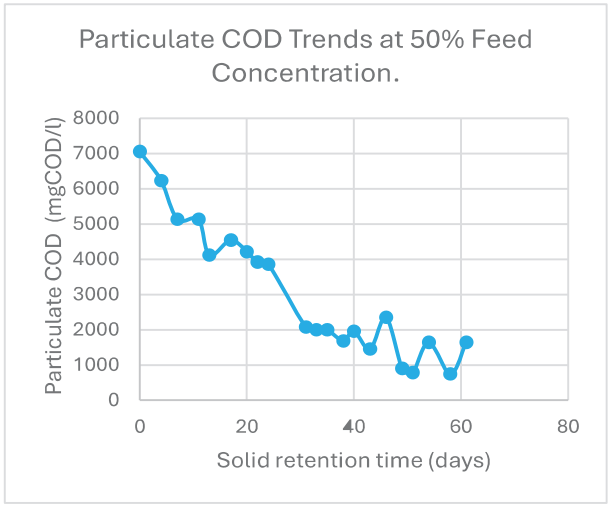

(b)

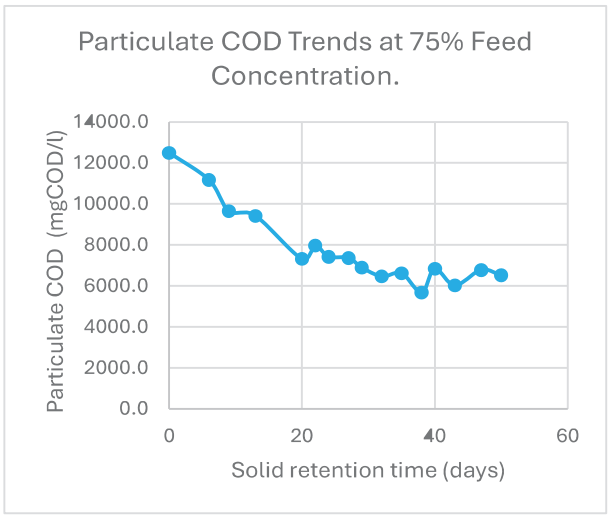

(c)

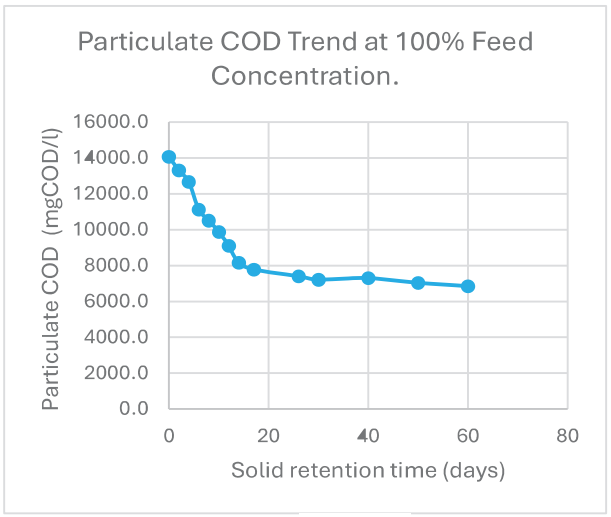

(d)

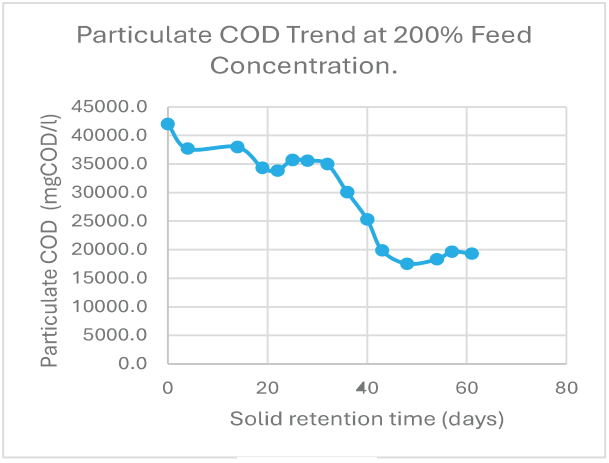

(e)

Figure 3.3: Particulate COD trends at different COD concentrations

Nitrogen characterisation was conducted in a manner similar to COD. In this case, nitrogen was partitioned into FSA, particulate organic nitrogen (X_OrgN), and soluble organic nitrogen (S_OrgN). For the purposes of this study, the soluble organic fraction was assumed to be negligible because it hydrolyses rapidly to FSA.

Figure 3.5 (a) to (e) presents the relationship between influent TKN and FSA release across the various feed concentrations. The trends closely mirrored those observed in particulate COD removal. As BPO degraded, organically bound nitrogen was released into the system as FSA, resulting in a gradual accumulation in the bulk liquid. While TKN values remained largely constant during the 60-day batch runs, the redistribution of nitrogen to FSA confirmed ongoing mineralisation.

At the lowest concentration of 25% TWW, the release of FSA remained nearly constant throughout the experimental run. This outcome was expected, as the low COD concentration limited the availability of BPO for degradation and consequently restricted nitrogen release.

At higher feed concentrations, however, FSA release increased steadily with SRT, reflecting greater mineralisation of nitrogen bound within BPO.

At the beginning of the tests, the total particulate organics (PO) in the TWW batches at 25%, 50%, 75%, 100% and 200% strength were 3447.06, 7056.12, 12504.8, 17722.5 and 41993 mg/L as COD, respectively. The corresponding soluble organic concentrations (SO) were 1142.4, 1666.0, 2097.2, 2666.3, and 2303 mg/L as COD.

These results confirm that higher-strength wastewater supported greater nitrogen release and COD removal but also required longer periods of microbial adaptation for stable degradation. Overall, COD and nitrogen characterisation provided critical insights into substrate availability and transformation during digestion, highlighting how feed strength influences microbial dynamics and reactor performance.

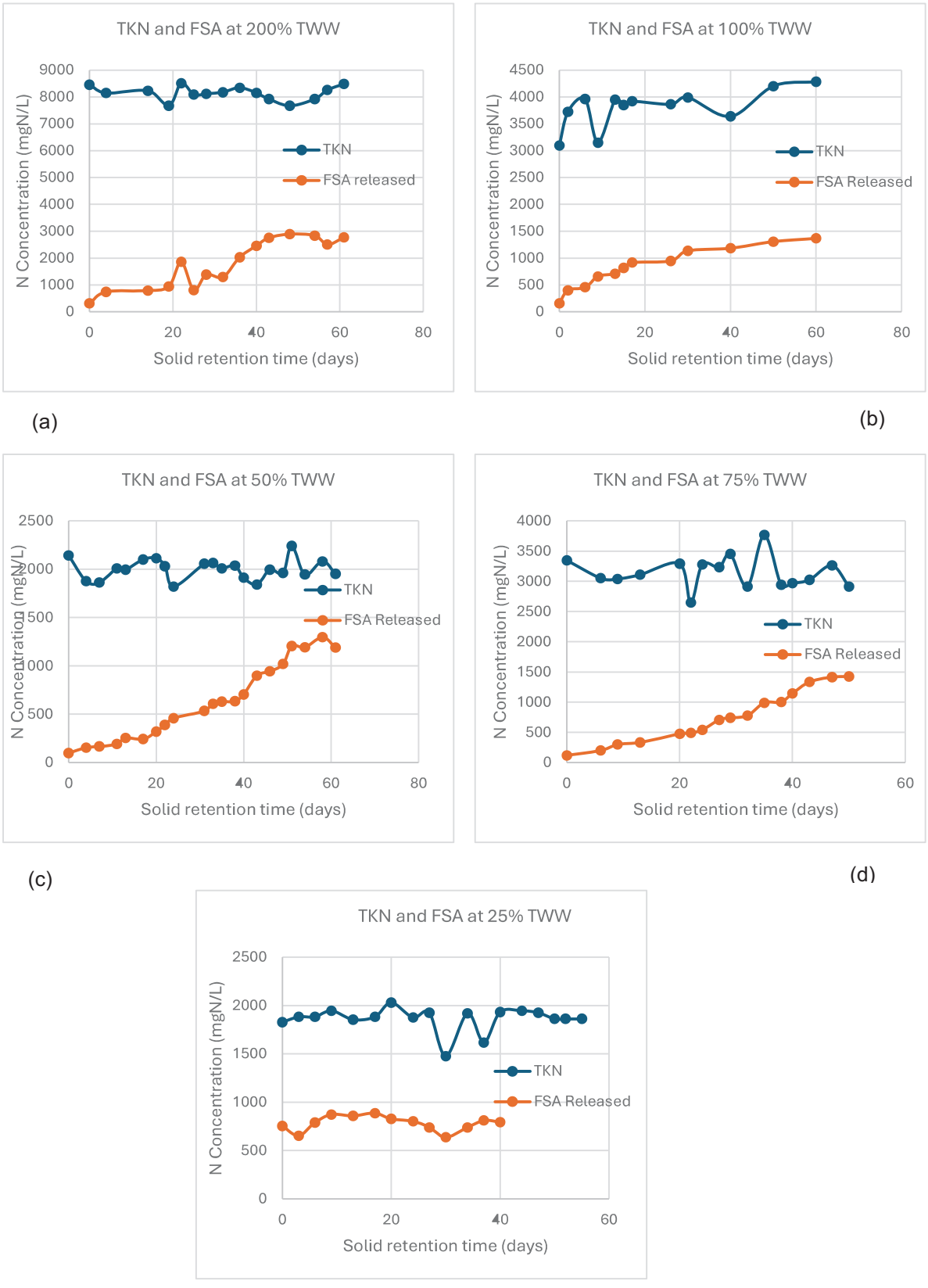

Figure 3.4 (a-e): TKN and FSA at batch Feed concentrations

The active biomass trends for different feed concentrations are shown in Figure 3.6 (a–e) below.

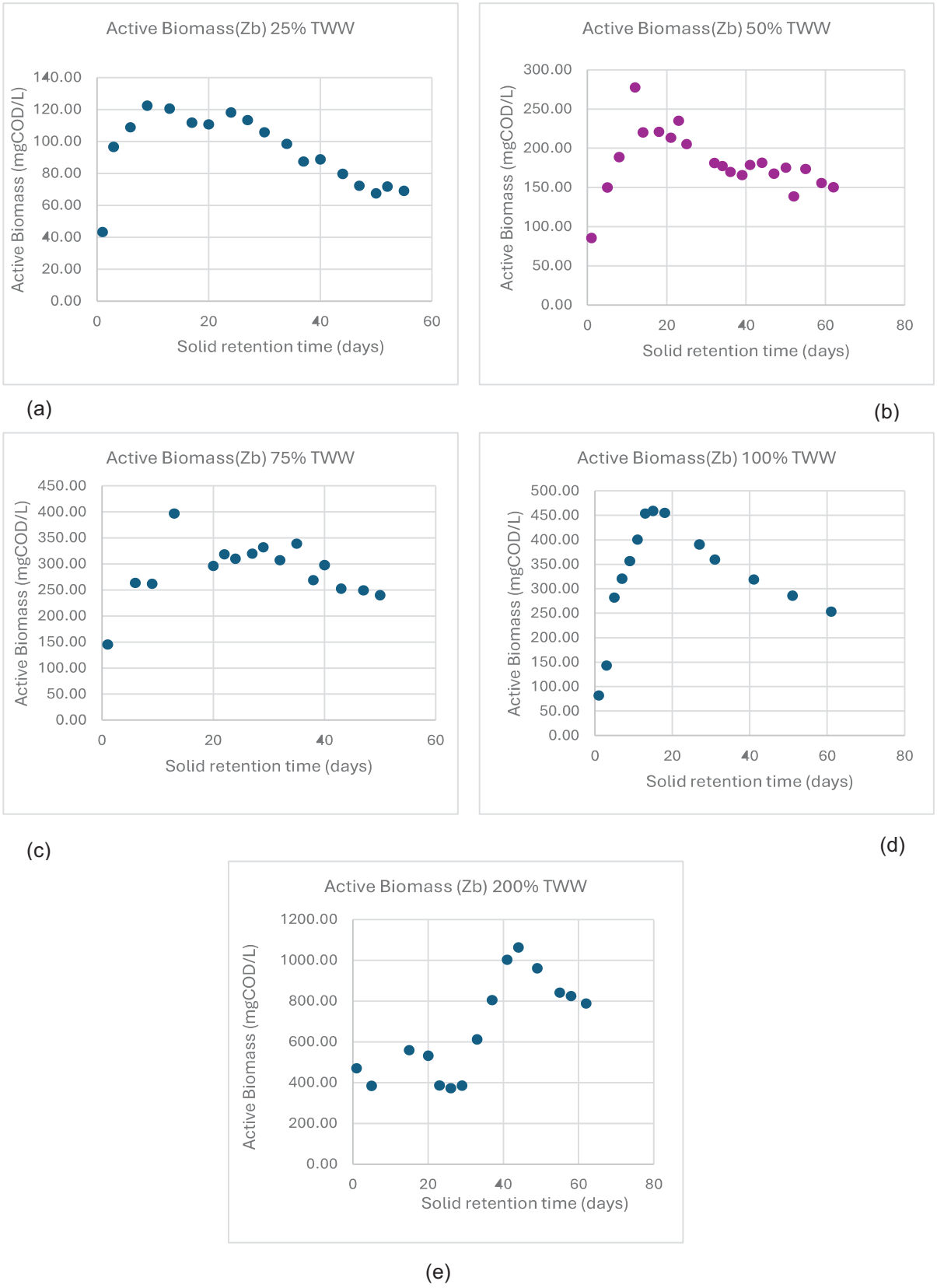

Figure 3.5:(a-e) Active biomass at batch feed concentrations

Across the 25%, 50%, 75%, and 100% TWW concentrations, biomass populations increased significantly from day 1 to day 20. This growth reflects the abundance of substrate during the

early stages of the batch experiments, when the food-to-microorganism (F/M) ratio was favourable. Around day 20, the system reached a peak, with substrate availability balanced against microbial demand. Subsequently, biomass levels declined as substrate availability decreased, consistent with the dynamics expected in batch systems. This trend corresponds closely with the patterns reported by Kemmer *et al.* (1998) (Figure 3.7), who described similar microbial growth phases under comparable conditions.

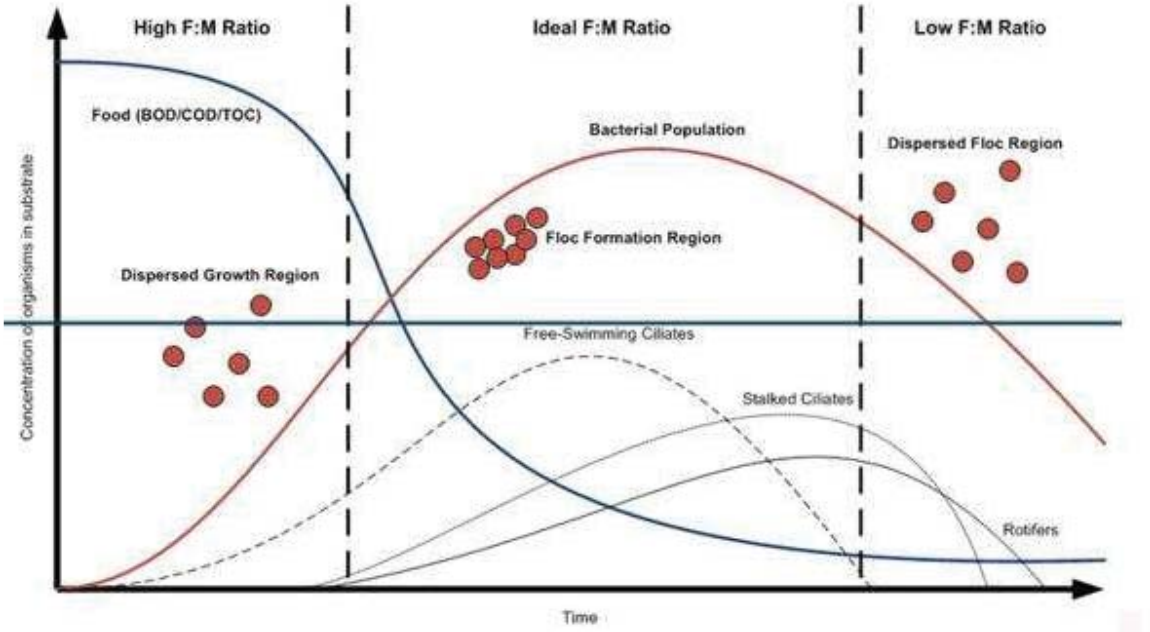

Figure 3.6: Food to microorganism chart (Kemmer, 1998)

In contrast, the biomass behaviour at 200% TWW was notably unstable. Biomass fluctuated between growth and decline over the first 25 days, probably due to substrate inhibition. At such high feed concentrations, excessive organics exert a toxic or inhibitory effect on microbial communities, reducing process stability and performance.

3.5.3 Competition between Methane-Producing Bacteria and Sulphate-Reducing Bacteria

The competition between MPB and SRB is illustrated in Figures 3.8 (a-e). As explained earlier, both groups utilise organic substrates, and their relative performance is shaped by feed concentration and operating conditions. At the lower feed concentrations (25% and 50% TWW), MPB and SRB exhibited similar COD utilisation rates, with neither group showing a clear competitive advantage. A few outliers were observed for MPB, which was probably linked to dissolved hydrogen sulphide (H_2S) removal. Because H_2S was removed from the system using nitrogen or carbon dioxide before it could accumulate, SRB were unable to exploit this potential advantage to outcompete MPB.

At higher feed concentrations (75% and 100% TWW), SRB began to dominate. Their specific COD utilisation rates were consistently higher than those of MPB, indicating that under these conditions, sulphate reduction was favoured over methanogenesis.

The dominance of SRB was even more pronounced at 200% TWW, where MPB activity was significantly suppressed, and COD utilisation rates by SRB were much higher. Interestingly, this effect cannot be attributed to H_2S toxicity, since the stripping procedure was maintained.

Instead, the inhibitory effect appears to be linked to the overall substrate strength, which probably placed MPB at a competitive disadvantage. The COD-to-sulphate (SO_4^{2-}) ratio provides further insight into this trend.

Across the feed concentrations of 25%, 50%, 75%, 100%, and 200% TWW, the COD/SO_4^{2-} ratios were 0.6, 0.4, 0.2, 0.2, and 0.1, respectively (Table 3.5). The decreasing ratio with increasing feed strength indicates that higher concentrations reduced the relative availability of COD per unit sulphate. Under these conditions, SRB outcompeted MPB, as sulphate reduction became the more favourable pathway.

Table 3.5: COD: SO_4^{2-} ratio as per batch feed concentration

Batch feed Concentration	COD: $SO4^{2-}$ Ratio
25% TWW	0.6
50% TWW	0.4
75% TWW	0.2
100% TWW	0.2
200% TWW	0.1

These findings highlight the importance of understanding microbial competition in mixed anaerobic systems. Since methanogenesis and sulphate reduction are the two principal pathways for organic degradation in TWW, their balance directly influences treatment efficiency and biogas recovery.

The next section builds on this understanding by examining the kinetics of hydrolysis under both methanogenic and sulphidogenic conditions, providing quantitative insights into how substrate strength and microbial interactions shape overall system performance.

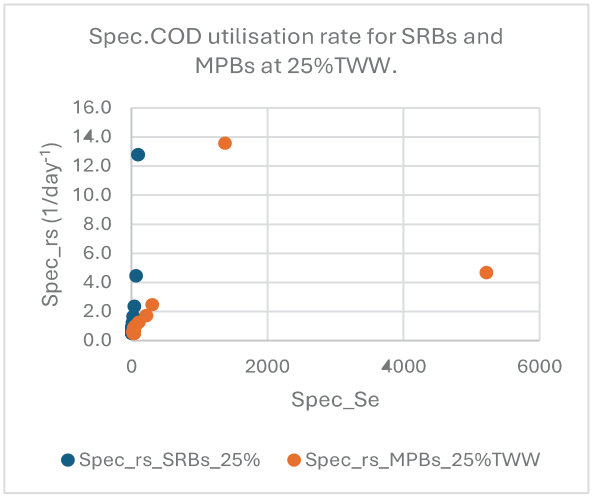

(a)

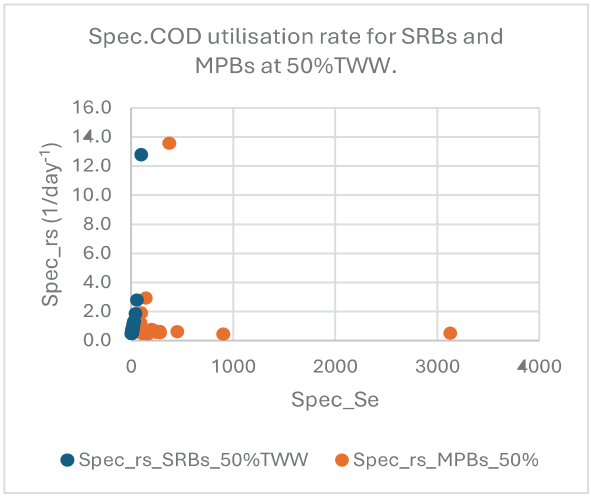

(b)

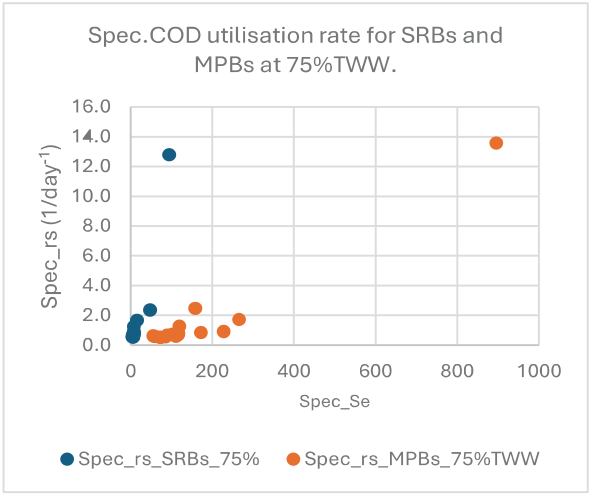

(c)

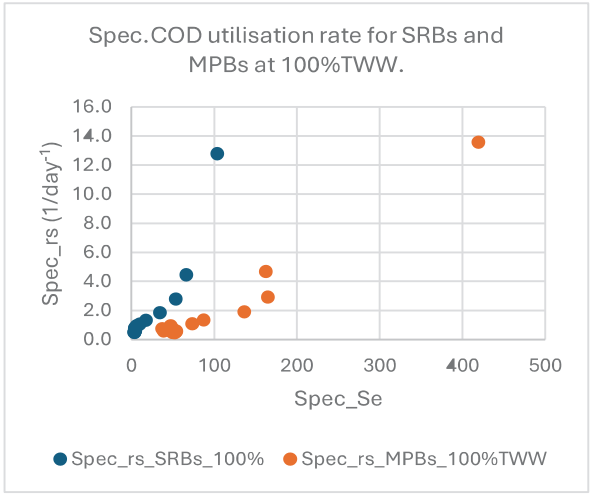

(d)

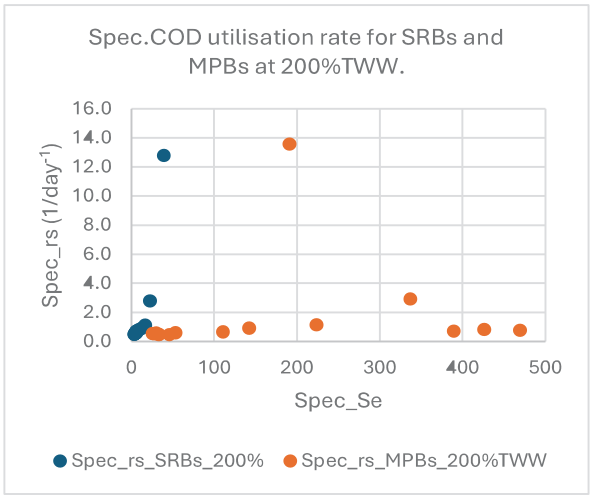

(e)

Figure 3.7 (a-e): Specific COD utilisation rate for SRBs and MPBs at batch feed concentration

3.6 Calibration of the AD Unit process model

3.6.1 Volumetric and specific substrate utilisation rates

The experimental datasets from the SRB process were transformed into specific substrate utilisation rates (rs/Xb) as a function of substrate-to-biomass ratios (Se/Xb). These transformed datasets were analysed using the MATLAB® Curve Fitting Toolbox to determine the Contois kinetic rate constants, including inhibition factors that describe reactions mediated by SRBs.

For this determination, the following parameters were required: influent substrate COD concentration (Si), effluent COD concentration (Se), concentration of substrate COD utilised (CODf), and biomass concentration (Zb).

The influent COD concentration was measured at the beginning of each batch cycle, while effluent COD was measured during sampling (Section 3.3.2.3). The concentration of substrate COD utilised (CODf) for each selected HRT and substrate concentration combination was calculated using Equation 3.4:

$$Su = Si - Se \qquad \text{Equation 3.4}$$

Biomass concentration (Zb) was subsequently determined for each batch at the selected HRTs using Equation (3.2). These values formed the basis for computing volumetric and specific substrate utilisation rates.

$$Z_b = \frac{Y_b * Su}{1 + b_{SRB} * HRT * (1 - Y_b)}$$

Equation 3.5

Where Y_b is the coefficient of biomass yield for each SRB species (= 0.075 gCOD/gCOD).

b_{SRB} is the depth or decay rate for each SRB biomass (= 0.02 d^{-1})

The volumetric substrate utilisation rates (rs) for each CODf used, with respect to HRTs, were determined using Equation 3.3.

$$r_s = \frac{Su}{HRT} \qquad \text{Equation 3.6}$$

All the required parameters were determined above. The specific substrate utilisation rates for each of the Si and HRT were calculated as illustrated in Table 3.6 below.

Table 3.6: Volumetric and specific utilisation rates at different COD concentrations

200% TWW						
HRT	Se	Su	Zb	rs	Se/Zb	rs/Zb
Days	gCOD/L	gCOD/L	gCOD/L	gCOD/L. d	gCOD/gCOD	1/d
1	39.20	5.10	0.34	4.6	116	13.6
5	42.73	1.57	0.05	0.1	885	2.9
15	38.81	5.49	0.25	0.3	156	1.1

20	36.46	7.84	0.34	0.3	106	0.9
23	38.81	5.49	0.19	0.2	202	0.8
26	38.42	5.88	0.19	0.1	200	0.8
29	37.63	6.66	0.21	0.2	176	0.7
33	32.93	11.37	0.42	0.3	79	0.7
37	27.44	16.86	0.64	0.4	43	0.6
41	21.95	22.34	0.85	0.5	26	0.6
44	18.03	26.26	0.98	0.5	18	0.5
49	19.99	24.30	0.85	0.4	24	0.5
55	22.34	21.95	0.71	0.3	32	0.5
58	20.78	23.52	0.74	0.4	28	0.5
62	23.41	20.88	0.62	0.3	38	0.5
100% TWW						
HRT	Se	Su	Zb	rs	Se/Zb	rs/Zb
Days	gCOD/L	gCOD/L	gCOD/L	gCOD/L. d	gCOD/gCOD	1/d
1	15.24	1.22	0.03	0.44	475	13.6
3	13.61	2.84	0.09	0.44	146	4.7
7	13.11	3.35	0.11	0.23	123	2.2
10	12.90	3.56	0.11	0.17	117	1.6
14	11.79	4.67	0.13	0.15	93	1.2
16	10.97	5.49	0.20	0.21	55	1.1
18	10.06	6.40	0.24	0.23	42	1.0
27	9.14	7.32	0.24	0.18	38	0.7
31	8.94	7.52	0.24	0.16	38	0.7
41	8.64	7.82	0.22	0.12	40	0.6
51	8.33	8.13	0.21	0.11	40	0.5
61	8.33	8.13	0.19	0.09	44	0.5
75% TWW						
HRT	Se	Su	Zb	rs	Se/Zb	rs/Zb
Days	gCOD/L	gCOD/L	gCOD/L	gCOD/L. d	gCOD/gCOD	1/d
1	14.01	0.59	0.03	0.40	471	13.6
6	12.25	2.35	0.13	0.33	92	2.5
9	11.96	2.65	0.11	0.19	110	1.7
13	10.09	4.51	0.18	0.23	56	1.3
20	10.58	4.02	0.13	0.12	78	0.9
22	10.19	4.41	0.15	0.13	68	0.9

24	9.70	4.90	0.17	0.14	57	0.8
27	9.31	5.29	0.18	0.13	52	0.7
29	9.11	5.49	0.18	0.12	52	0.7
32	8.82	5.78	0.19	0.12	47	0.7
35	7.84	6.76	0.23	0.14	35	0.6
38	8.82	5.78	0.17	0.10	52	0.6
40	7.15	7.45	0.23	0.14	31	0.6
43	7.94	6.66	0.19	0.10	42	0.6
47	6.37	8.23	0.25	0.13	26	0.5
50	6.37	8.23	0.24	0.12	27	0.5

50% TWW						
HRT	Se	Su	Zb	rs	Se/Zb	rs/Zb
Days	gCOD/L	gCOD/L	gCOD/L	gCOD/L. d	gCOD/gCOD	1/d
1	7.94	1.57	0.02	0.29	372	13.6
5	7.15	2.16	0.05	0.14	145	2.9
8	6.57	3.53	0.07	0.13	98	1.9
12	5.19	2.94	0.12	0.17	42	1.4
14	5.78	3.23	0.06	0.08	92	1.2
18	5.49	3.33	0.07	0.07	78	1.0
21	5.39	3.82	0.06	0.05	87	0.9
23	4.90	3.47	0.08	0.06	65	0.8
25	5.25	3.47	0.03	0.02	200	0.8
32	5.25	3.51	0.02	0.01	236	0.7
34	5.21	3.47	0.02	0.01	277	0.6
36	5.25	3.55	0.01	0.01	451	0.6
39	5.17	3.94	0.02	0.01	248	0.6
41	4.78	4.17	0.04	0.02	128	0.6
44	4.55	4.02	0.04	0.02	128	0.5
47	4.70	4.37	0.02	0.01	285	0.5
50	4.35	3.55	0.03	0.02	148	0.5
55	4.12	4.33	0.04	0.02	107	0.5
59	4.39	4.33	0.03	0.01	163	0.5
25% TWW						
HRT	Se	Su	Zb	rs	Se/Zb	rs/Zb

Days	gCOD/L	gCOD/L	gCOD/L	gCOD/L.d	gCOD/gCOD	1/d
1	4.23	0.36	0.01	0.2	284	13.6
3	4.13	0.46	0.02	0.1	254	4.7
6	4.03	0.56	0.01	0.0	313	2.5
9	3.72	0.87	0.02	0.0	186	1.7
13	3.57	1.02	0.02	0.0	234	1.3
17	3.42	1.17	0.01	0.0	629	1.0
20	2.75	1.84	0.02	0.0	182	0.9
24	2.45	2.14	0.02	0.0	114	0.8
27	2.30	2.30	0.03	0.0	91	0.7
30	2.24	2.35	0.02	0.0	100	0.7
34	2.30	2.30	0.02	0.0	129	0.6
37	2.24	2.35	0.02	0.0	132	0.6
40	2.30	2.30	0.01	0.0	171	0.6
44	2.35	2.24	0.01	0.0	237	0.5
47	2.24	2.35	0.01	0.0	176	0.5
50	2.24	2.35	0.01	0.0	181	0.5
52	2.30	2.30	0.01	0.0	231	0.5
55	2.45	2.14	0.00	0.0	615	0.5

3.6.2 Kinetics of hydrolysis

The hydrolysis kinetics of TWW were assessed across different feed concentrations (25%, 50%, 75%, 100%, and 200%). Figure 3.9 shows that the 25% TWW feed exhibited the fastest hydrolysis rate and therefore served as the zero proxy condition for estimating kinetic parameters. The procedure developed by Harding *et al.* (2020) was applied to derive kinetic constants for hydrolysis under these conditions. The results indicate an inverse relationship between feed concentration and hydrolysis rate. Higher concentrations resulted in slower reaction rates, consistent with the findings of Hansford *et al.* (2004), who reported that inhibitory conditions reduced biological activity and thus reaction rates.

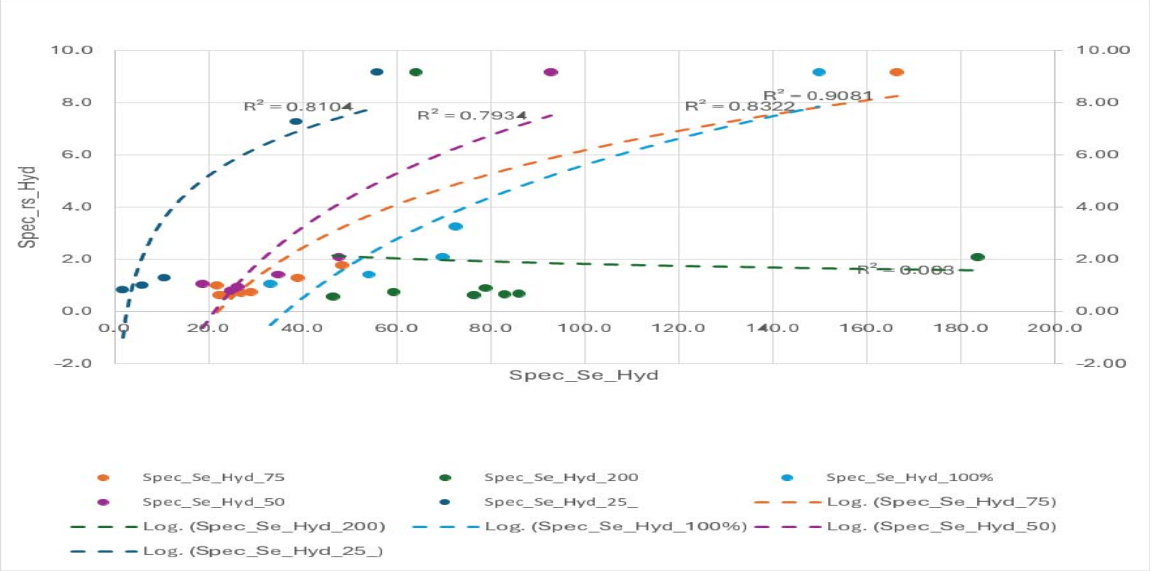

Figure 3.8: Hydrolysis Kinetic Trendlines at Batch Feed Concentration

This relationship is illustrated in Figure 3.10, where curves under inhibitory and non-inhibitory conditions are contrasted.

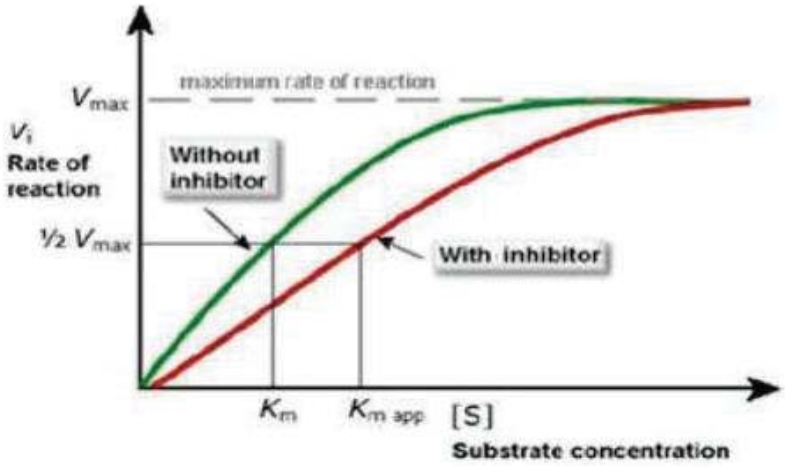

Figure 3.9: Biological reaction with inhibition

In this study, inhibition effects were ascribed primarily to substrate concentration. Although dissolved H_2S is known to inhibit, daily stripping of H_2S from the reactors with nitrogen and carbon dioxide prevented significant accumulation. Without this intervention, microbial activity ceased within the first 10 days of operation. Thus, observed inhibition can be attributed mainly to elevated TWW concentrations. The MATLAB® Curve Fitting Toolbox was employed to estimate the maximum specific hydrolysis rate (K_{max_HYD}) and half-saturation constant (K_{s_HYD}) using nonlinear least-squares regression.

3.6.3 Parameter Estimation for Specific Substrate Utilisation Rate Equations

Experimental data from Section 3.3.4 were fitted to the Contois rate equation using the MATLAB® Curve Fitting Toolbox. The nonlinear least-squares method was applied to determine kinetic constants under various batch TWW conditions. The resulting best-fit constants were

Km = 15.54 and Ks = 40.57. The quality of the curve fit (Goodness of the curve fit) was validated by the following indicators:

- Sum of Squares due to Error (SSE) = 1.02
- R^2 = 0.97
- Adjusted R^2 = 0.96
- Root Mean Square Error (RMSE) = 0.71

These values demonstrate that the Contois equation provided an excellent fit to the experimental data.

3.6.4 Comparison with reported hydrolysis kinetics

Hydrolysis constants were primarily determined at 25% TWW, the concentration yielding the fastest rate. The MATLAB® curve fitting tool confirmed strong fits ($R^2 \geq 0.80$) for datasets that poorly conformed to the Contois mode and were therefore selectively omitted to improve robustness. The estimated constants (Km = 15.549, Ks = 40.568) (Table 3.7) were higher than those reported in earlier studies for primary sludge (Ikumi, 2011; Izzett *et al.*, 1992; O'Rourke, 1968). The discrepancy likely reflects differences in organic composition: TWW is rich in proteins and lipids, whereas primary sludge is predominantly cellulose-based. However, the values obtained in this study are comparable to those reported by Ristow *et al.* (2005) for sulphidogenic treatment of primary sludge, a condition closely aligned with the present experimental setup.

Table 3.7: Estimated kinetic parameters.

Parameters		25% TWW	PS	PS	PS	PS
		This Study	Ikumi	Izzett	O'Rourke	Ristow
Kinetic hydrolysis rates	Km	15.549	1.796	5.270	2.047	11.2
	Ks	40.568	7.962	7.980	0.263	13.0
	R^2	0.9739	0.942	0.900	0.428	-

Figure 3.11 presents the best-fit Contois model for 25% TWW, illustrating the estimated Km and Ks values.

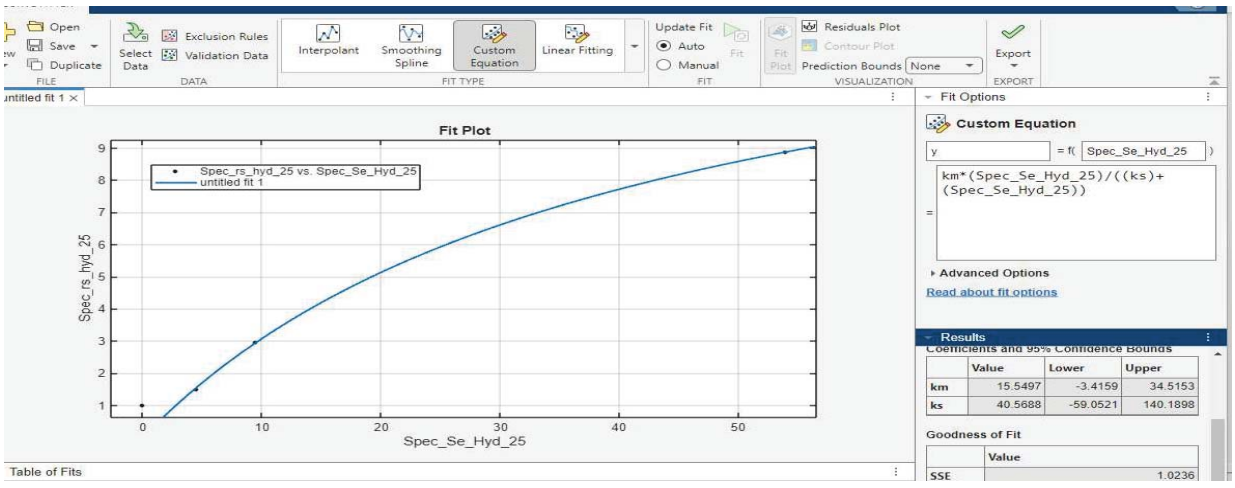

Figure 3.10: MATLAB curve fitting

Theoretically, kinetic constants (Km, Ks) for given wastewater should remain invariant under non-inhibitory conditions, regardless of feed concentration. However, under non-inhibitory conditions, the rate of biologically mediated reactions, fed the same substrate but at different concentrations, should ultimately be described by a single kinetic equation.

3.6.5 Selection of zero proxy and determination of the total inhibition factor

To quantify the effect of inhibition in the AD system, a zero proxy was first established. The zero proxy represents the operational condition under which no inhibition occurs. At this point, the system is assumed to operate under optimum conditions, with minimal competition between MPB and SRB.

For this study, the zero proxy was identified at a feed concentration of 25% TWW. At this concentration, inhibition was negligible, largely because hydrogen sulphide (H_2S), a known inhibitor of methanogenesis, was stripped from the system. The kinetic parameters obtained from MATLAB® curve fitting, specifically

Km = 15.549 and Ks = 40.56 were used as the baseline values for this zero-inhibition state (Harding *et al.*, 2020).

The rate of substrate utilisation was then adjusted for inhibition by applying a rate inhibition factor (FI_T). This factor modifies the kinetic expression to account for the extent of inhibition under different feed concentrations. By definition, a smaller FI_T value corresponds to greater inhibition, while the total inhibition (IT) is calculated as: $I_T = 1 - FI\_T$

At the zero proxy (25% TWW), the inhibition factor was calculated as FI_T = 1.00, corresponding to IT = 0.00. This confirms that no inhibition was present under these conditions. The same procedure was applied to higher feed concentrations (50%, 75%, 100%, and 200% TWW), with the results summarised in Table 3.8 and illustrated in Figure 3.12.

Table 3.8: Experimental runs showing estimation of inhibition factors for reaction rates

%TWW Concentration	CODf	Se (COD)	IT
25	3.448	1.817	1.00
50	7.056	2.643	0.638
75	12.505	7.422	0.473
100	17.723	10.921	0.323
200	41.993	27.969	0.245

To summarise, the total inhibition rate increased progressively with feed concentration. At 25% TWW, inhibition was absent. However, as the concentration increased, inhibition became more pronounced, reaching 0.755 at 200% TWW.

This trend indicates that, although H_2S inhibition was effectively minimised by stripping across all concentrations, additional inhibitory effects emerged at higher substrate loads. These were attributed primarily to substrate inhibition, which exerted a stronger influence as feed strength increased.

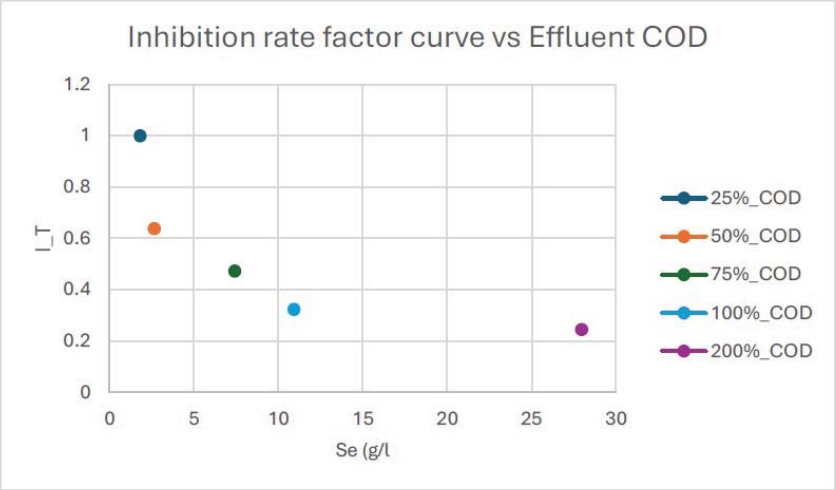

Figure 3.11: Inhibition rate factor curve versus effluent COD.

The inhibition analysis demonstrates that while low-strength TWW can be digested with minimal inhibitory effects, higher-strength feeds impose significant constraints on microbial activity. This finding highlights the importance of optimising feed concentration to maintain balanced microbial competition and stable system performance.

3.6.6 Curve Fitting for Inhibition Kinetics

The inhibition dataset was modelled using the substrate inhibition function proposed by Wayman and Tseng, as described by Han and Levenspiel (1987). MATLAB® Curve Fitting Toolbox produced the best-fit curve shown in Figure 3.13.

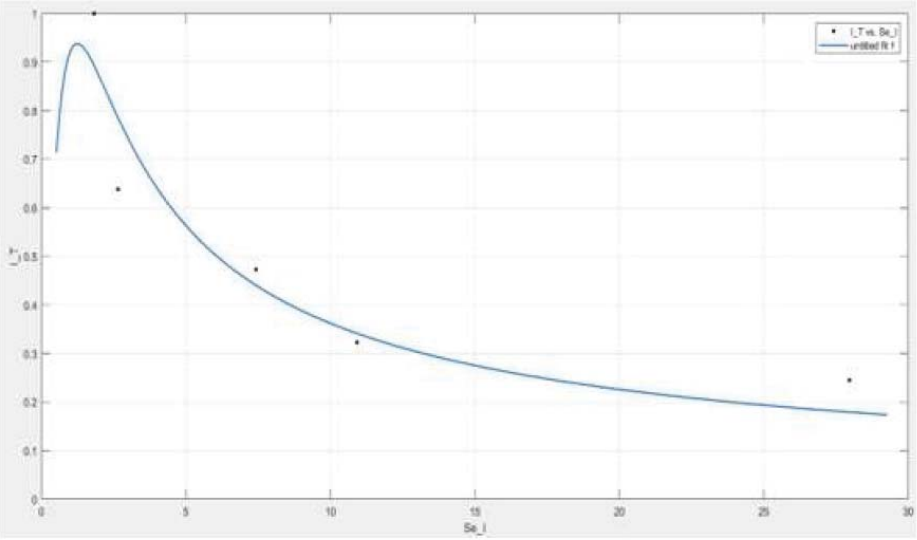

Figure 3.12**: MATLAB curve fitting for inhibition rate against effluent COD**

Overall, the experimental results demonstrate that the Contois equation effectively describes the kinetics of TWW under varying conditions. The estimated kinetic constants (Km = 15.54, Ks = 40.56; R^2 = 0.97) are consistent with those observed in sulphidogenic systems and indicate that substrate concentration is the dominant inhibitory factor. These insights provide a reliable framework for modelling and optimising TWW treatment processes.

CHAPTER 4: MICROALGAL-BACTERIAL POLISHING SYSTEM FOR TANNERY WASTEWATER TREATMENT

4.1 Introduction

TWW is among the most challenging industrial effluents to treat because it contains high loads of organic matter, nitrogen, salts, and heavy metals, particularly chromium (Saranya & Shanthakumar, 2020a, 2020b). Conventional secondary treatments can reduce pollutant levels but often leave behind residual nitrogen and other compounds that pose risks to the environment.

In recent years, researchers have explored microalgal-bacterial (MAB) systems as an innovative tertiary treatment option, building on the principle of phyco-remediation (PR), where microalgae use photosynthesis to capture CO_2, release O_2, and assimilate nutrients (Chen *et al.*, 2016; Sharmila *et al.*, 2022). They integrate pollutant removal with resource recovery, thereby contributing to both environmental protection and circular economy goals.

The MAB systems (Schematic shown in Figure 4.1) are particularly promising because they not only polish wastewater but also generate valuable biomass for bioenergy, animal feed, or biofertilizers, aligning with circular economy goals (Mpofu *et al.*, 2023; Ranjan & Welz, 2022). Strains such as *Chlorella* and *Scenedesmus/Tetradesmus* have demonstrated strong adaptability and nutrient uptake in treated TWW, particularly when supported by upstream interventions such as secondary bioremediation, chemical treatment, or ozonation (Nambukrishnan & Singaram, 2022; Saranya & Shanthakumar, 2020a, 2020b; Urbina-Suarez *et al.*, 2025).

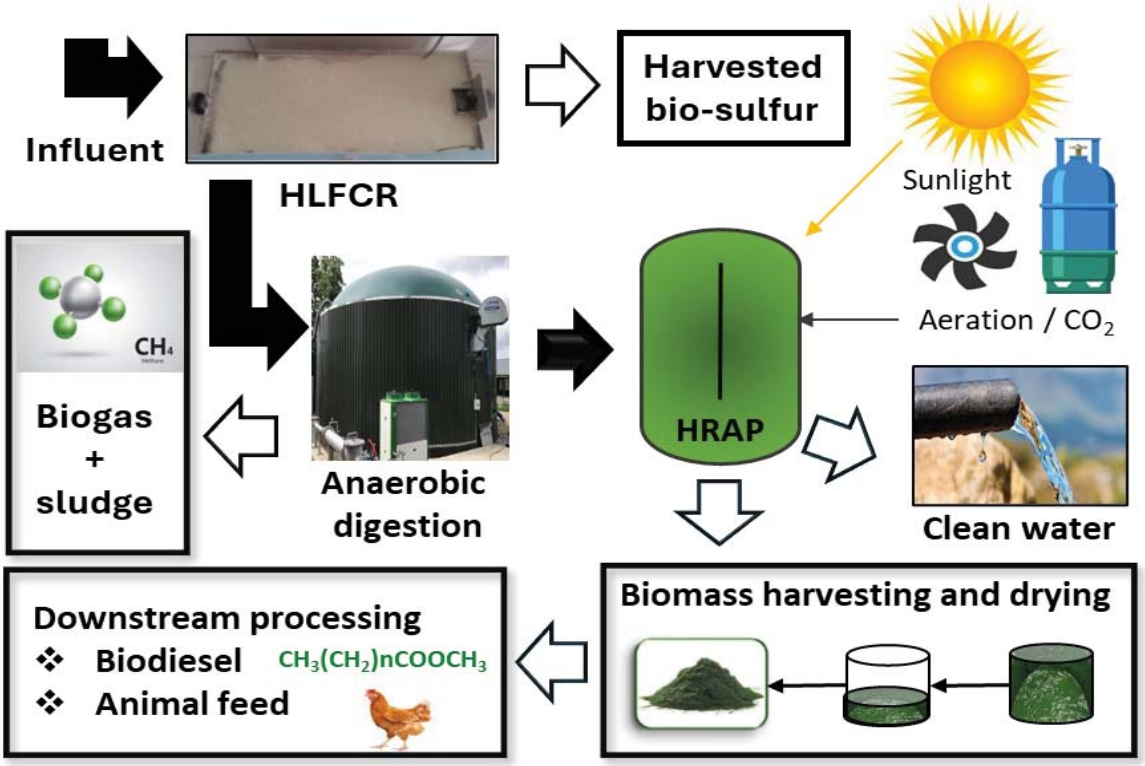

Figure 4.1: Schematic depicting a proposed microalgal-bacterial TWW biorefinery

The success of these systems depends on careful strain selection, operational control of HRT, and balancing microbial interactions. Figure 4.2 shows the major metabolic interactions between bacteria and microalgae in microalgal-bacterial wastewater treatment systems. Microalgae assimilate ammonium directly into biomass, whereas bacteria convert ammonia into nitrite and nitrate; both processes occur in tandem under appropriate conditions (Arun *et al.*, 2021; Welz *et al.*, 2023). Advances such as algal-bacterial granulation and biorefineries demonstrate the potential of these systems not only to clean wastewater but also to generate valuable biomass and reduce treatment costs (Ahmad *et al.*, 2023; Ranjan & Welz, 2022). While challenges remain, including the management of toxic metals and high sodium levels, MAB systems represent a promising step toward sustainable wastewater treatment solutions for resource recovery in the leather industry.

4.1.1 Key considerations in nutrient and pollutant removal

A. Nitrogen Species

Microalgae assimilate ammonium (NH_4^+) directly into cellular material (González-Camejo *et al.*, 2022; Salbitani & Carfagna, 2021), while bacteria oxidise ammonia to nitrite (NO_2^-) and nitrate (NO_3^-) in conventional activated sludge systems (Welz *et al.*, 2023). In MAB systems, both pathways operate simultaneously (Arun *et al.*, 2021). Their balance is influenced by wastewater composition, HRT, light, and dissolved gases (Arun *et al.*, 2021). Adding CO_2 enhances algal uptake, whereas oxygen produced by algal photosynthesis supports bacterial nitrification, thereby reducing aeration requirements (Caparroz *et al.*, 2024; Aditya *et al.*, 2023). For complete N removal, alternating aerobic and anoxic phases - or exploiting anoxic zones within granules- is required.

B. Phosphorus and Sulphur Species

Phosphate (PO_4^{3-}) is often limiting in TWW, so its removal is usually not prioritised in MAB systems (Monzon Martinez *et al.*, 2025; Ngobeni *et al.*, 2024; Gao *et al.*, 2023). Conversely, sulphur species such as hydrogen sulphide (HS^-) and sulphate (SO_4^{2-}) are abundant and can be toxic, requiring careful monitoring. Studies have shown high removal efficiencies of these compounds under controlled conditions (Arutselvan *et al.*, 2022; Das *et al.*, 2017).

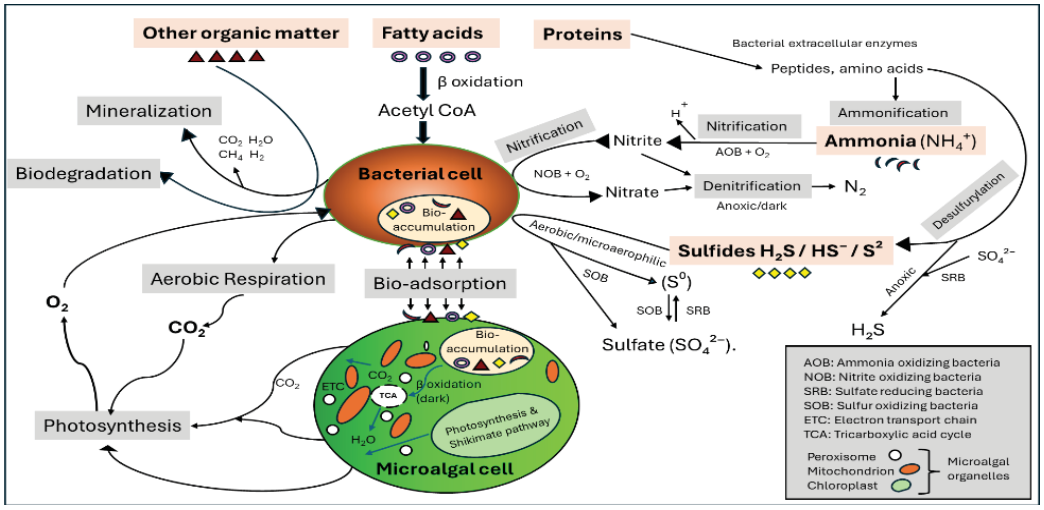

Figure 4.2: Bacteria–Microalgae Metabolic Interactions in Wastewater Systems

4.1.2 Captions and Heavy Metals

Microalgae can take up heavy metals, such as chromium, a major pollutant in TWW (Saranya & Shanthakumar, 2020a, 2020b). However, accumulation in biomass raises disposal concerns unless recovery technologies are developed (Ngobeni *et al.*, 2024). Sodium uptake by microalgae has also been reported (Arutselvan *et al.*, 2022), but removal rates are negligible compared to typical TWW concentrations (Mpofu *et al.*, 2022; Ranjan & Welz, 2025). In such cases, complementary technologies such as membranes are more suitable.

4.2 Microalgae Bacterial (MAB) Experiments

4.2.1 Introduction to Experimental Setup

A series of experiments was conducted during this project (Figure 4.3). The initial studies were performed with microalgal strains only. Firstly, the four most promising microalgae strains were selected from a range of indigenous and commercial strains for their superior ability to grow in TWW, and their remediation potential was assessed. Thereafter, the strains were applied as a consortium, and their TAN removal potential was assessed under different simulated seasonal conditions of temperature and light duration (photoperiod). The biomass generated by the single strains and the consortium was fully characterised, and its potential for downstream applications was assessed. The microalgal consortium was then used in MAB studies, both in flasks and in photobioreactors. Previous studies have shown that metabolically active bacteria are present in TWW (Horn *et al.*, 2022); therefore, the flasks and reactors were inoculated only with microalgae, not bacteria. The data obtained from the MAB studies were used as input in the MAB model (Section 5.3).

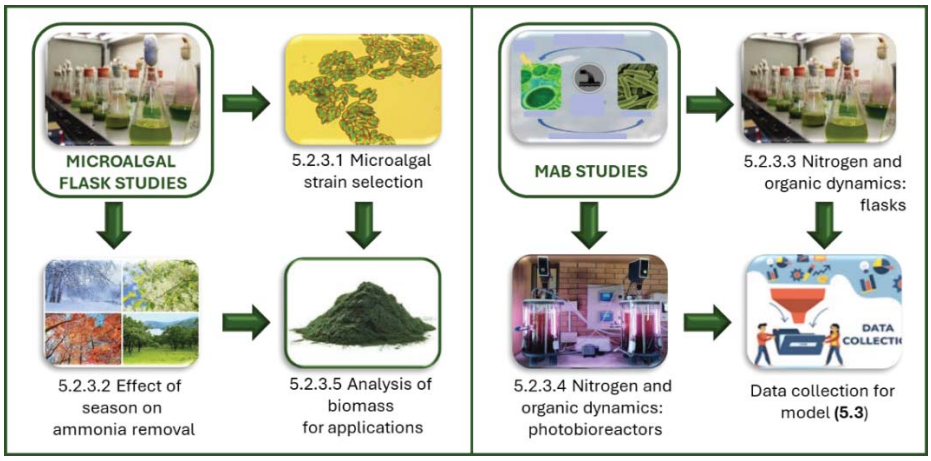

Figure 4.3: Experimental Design for Microalgal and MAB Studies

4.2.2 Experimental testing protocols

4.2.2.1 Tannery wastewater

Composite partially treated TWW was collected from a local tannery and frozen until required after mixing and aliquoting into 20 L polypropylene containers. Two large batches were obtained more than a year apart, with notably different characteristics (Table 4.1). Where it was necessary for experimental purposes to increase the amount of NH3 or P, ammonium oxalate ($(NH_4)_2C_2O_4$) and/or potassium dihydrogen phosphate (KH_2PO_4), respectively, were added to obtain the desired nutrient balances (Section 5.3.4).

Table 4.1: Chemical characteristics of the raw TWW (n=3)

(Parameters in mg/L except for pH (units) and T.Alk (mg $CaCO_3$/L))

Parameter	Batch 1	Batch 2
pH	7.8	6.6 ± 0.02
CODt	876 ± 4	5190 ± 20
CODs	489 ± 4	5000 ± 39
VOA	101 ± 11	1246 ± 43
NH_3-N	7.4 ± 0.4	40.7 ± 1.1
NO_3^--N	< 0.5	4.8 ± 0.40
NO_2^--N	0.05	0.97 ± 0.06
T.Alk	162 ±3	782 ± 68
TP	0.3 ± 0.04	8.4 ± 0.06
SO_4^{2-}	1040 ± 85	1657 ± 80
Cl	1975 ± 64	1373 ± 23
S^{2-}	-	5.4 ± 0.41

CODt = total chemical oxygen demand; CODs = soluble chemical oxygen demand; VOA = volatile organic acids; NH_4-N = ammonia as nitrogen; NO_3^--N = nitrate as nitrogen; NO_2^--N = nitrite as nitrogen; T.ALK = total alkalinity; TP = total phosphorus; SO_4^{2-} = sulphate; Cl^- = chloride; S_2^- = sulphide.

4.2.3 Analytical Procedures

The pH was measured using an Eutech pH 700 instrument (Eutech Instruments, Singapore) with a pH probe. The wastewater chemical analyses were conducted using a Merck Spectroquant Pharo (Darmstadt, Germany) instrument, with standards and controls according to the manufacturer's instructions. The biomass was dried in an oven at 60°C overnight, then crushed to a fine powder using a pestle and mortar and characterised. Major and minor elements were quantified using a Thermo ICap 6200 ICP-AES instrument for trace analyses, and an Agilent (Santa Clara, USA) 7900 ICP-MS instrument for ultra-trace analyses at the Central Analytical Facility (CAF) at Stellenbosch University (Stellenbosch, South Africa).

The carbon, hydrogen, nitrogen, and sulphur (CHNS) content (% wt/wt) was determined using an Elementar Vario EL cube elemental analyser (Hamburg, Germany) according to the manufacturer's instructions, also at CAF. The protein content was determined by multiplying the N content by 5.8 (Gnaiger & Bitterlich, 1984). The fatty acids were qualitatively and quantitatively evaluated using an Agilent 7890A Gas Chromatography–Flame Ionisation Detector (GC-FID) System with a HP88 (100 m x 250 µm, 0.250 µm) column.

The carbohydrate content was determined using the Anthrone spectroscopic method as described by Chen and Vaidyanathan (2013). The dry cell weight (DCW) evaporation method was used to quantify the amount in the flask and in the photobioreactor experiments.

4.2.4 Flask Studies

The microalgal strains were grown in Erlenmeyer flasks (250-1000 mL) and in shaking incubators at 160 revolutions per minute (rpm), or under static conditions, with photoperiods as specified in the results and discussion. Light was provided by 17 W, 31 μmol/sec Sylvania (Budapest, Hungary) Gro-Lux LED grow bulbs, which emit light primarily in the blue and red regions of the visible spectrum.

4.2.5 Photobioreactor Studies

Two 20 L (16.7 L working volume) photobioreactors were used (Figure 5-4). Each was supplied with light by three equally spaced Sylvania (Budapest, Hungary) Grolux F8W/T5 fluorescent bulbs, which emit light primarily in the blue and red regions of the visible spectrum. The initial photosynthetic photon flux density ranged from approximately 11-21 µmol/m². s^{-1} from interior to exterior of the reactors, dropping to as low as 1 µmol/m². s^{-1} in the interior due to the formation of MAB biofilm on the surface of the reactors during the experiments. The reactors were each aerated at 12 L/min (0.72 L/L.min-1). The temperature was controlled using heat exchangers, with water from a heated water batch controlled by a programmable logic controller (PLC) and a transmitter. Temperature, pH, and redox were also monitored in real time using the PLC and corresponding probes (Figure 4.4). Further details of the experimental procedures and analyses specific to each experiment are provided in the corresponding subsections.

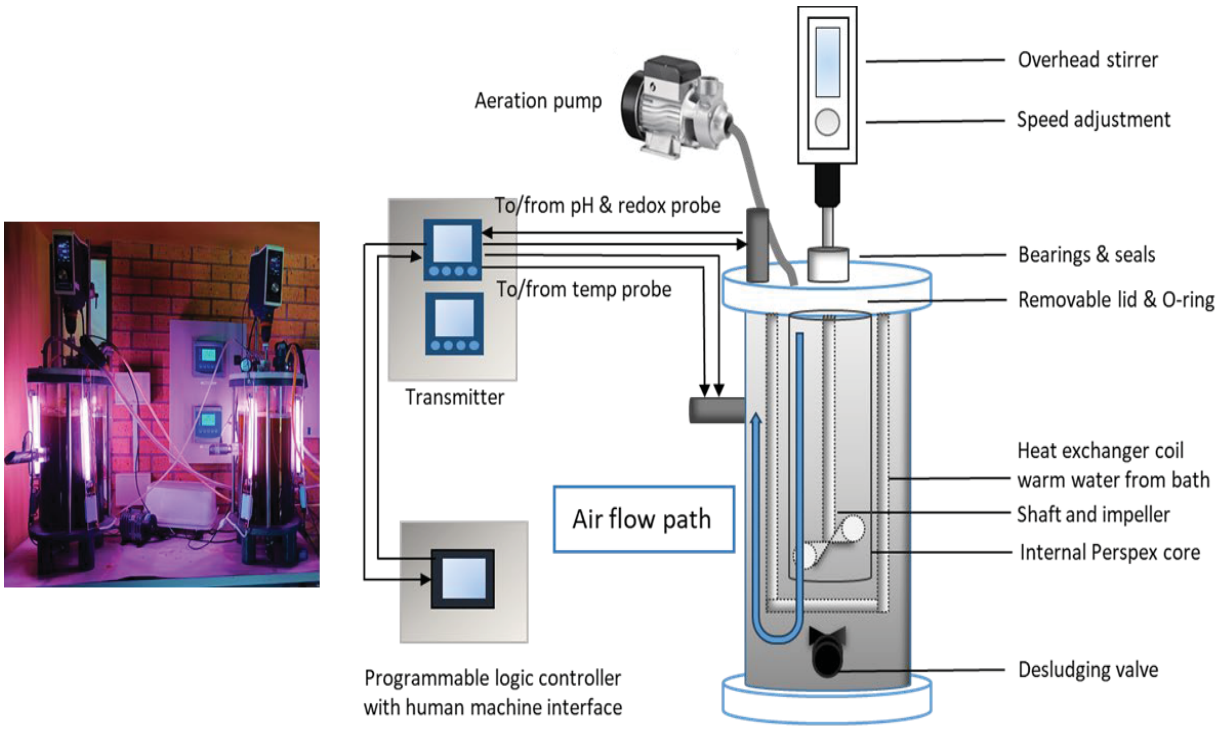

Figure 4.4: Picture and annotated diagram of the photobioreactors

4.2.6 Results and Discussion

4.2.6.1 Microalgal strain selection, acclimation and remediation potential: flask studies

The four microalgae strains selected comprised three indigenous strains isolated from TWW and winery wastewater, and one commercial strain acclimated to grow in 50% raw TWW (Figure 4.5). The indigenous strains were identified using molecular and microscopic methods, designated as *Tetradesmus obliquus CPUT-L1, Tetradesmus dimorphus CPUT-L2 and Neochloris sp. CPUT-W1, and* registered in the National Centre for Biotechnology Information (NCBI) database (Ranjan *et al.*, 2025).

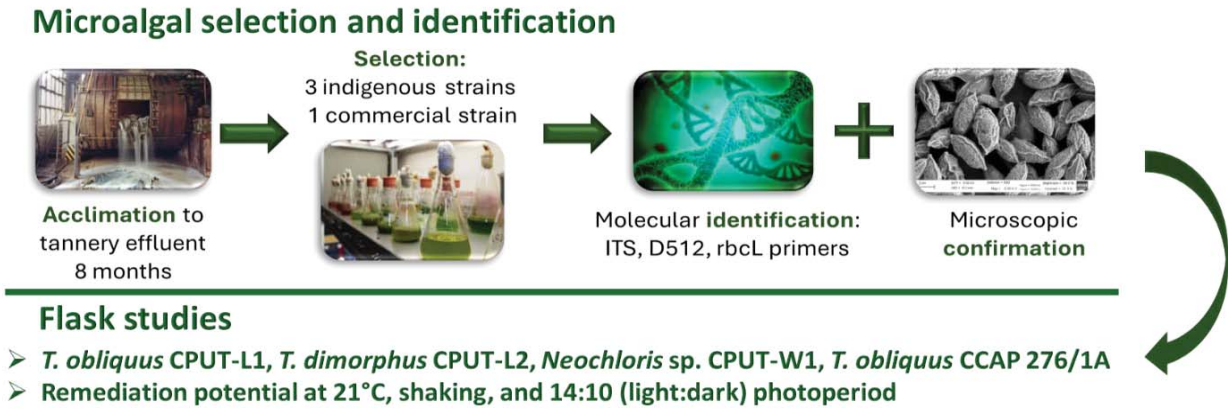

Figure 4.5**:** Experimental Procedures for Microalgae Selection, Identification and Remediation

The strains were grown in duplicate flasks containing sterilised TWW (batch 1, Table 4.1) for 60 days. The growth rates were typically highest for the first 10 days of the experiment, and the stationary phases were reached at around 48 days (Figure 4.6). There were no significant differences in the growth profiles obtained for *T. obliquus* CPUT-L1 *and T. dimorphus* CPUT-L2 (paired t-TEST $p>0.05$), but highly significant differences in the growth profiles between the other strains ($p<0.0001$). In terms of biomass, the highest amounts measured (in descending order) were 1.50±0.017 g/L (*T. obliquus* CCAP 276/1A), 1.40±0.07 g/L (*T. obliquus* CPUT-L1), 1.31±0.11 g/L (*T. dimorphus* CPUT-L2) and 1.11±0.04 g/L (*Neochloris* sp. CPUT-W1).

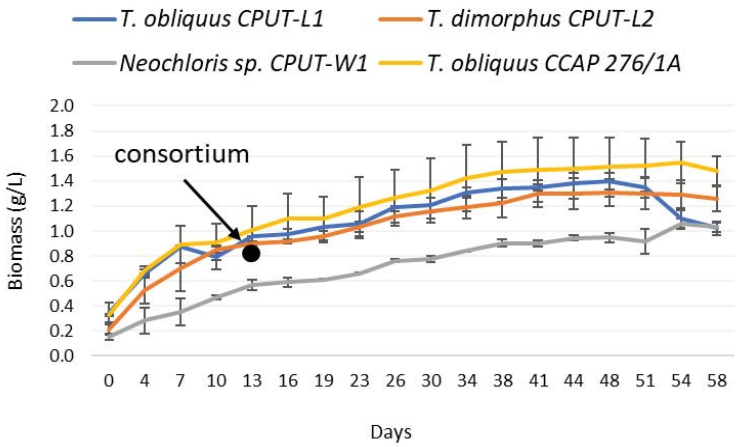

Figure 4.6: Growth Profiles of Microalgal Strains in Tannery Wastewater (Ranjan et al., 2025)

The soluble COD (CODs) concentrations were largely unchanged during the experiment, but there were 63-84% increases in the CODt and 23-36% increases in the TOC (Figure 4.7). Notable increases in influent VOA concentration to 101 mg/L were observed, with 53% for *Neochloris* sp. CPUT-W1 to 163% for *T. obliquus* CPUT-L1, indicating fermentative microalgal metabolic activity.

The increases in TOC and CODt can be explained by microalgae's ability to fix atmospheric CO_2 and replicate via autotrophic photosynthetic growth in the presence of light. These results highlighted the importance of bacteria in MAB systems in facilitating the utilisation of soluble COD (CODs) and the subsequent removal from TWW (Watanabe & Isdepsky, 2021). In contrast to this study, others have reported effective removal of COD in TWW by microalgae; however, in these cases, the wastewater was not sterilised and therefore likely contained bacterial populations, as shown by Horn *et al.* (2022).

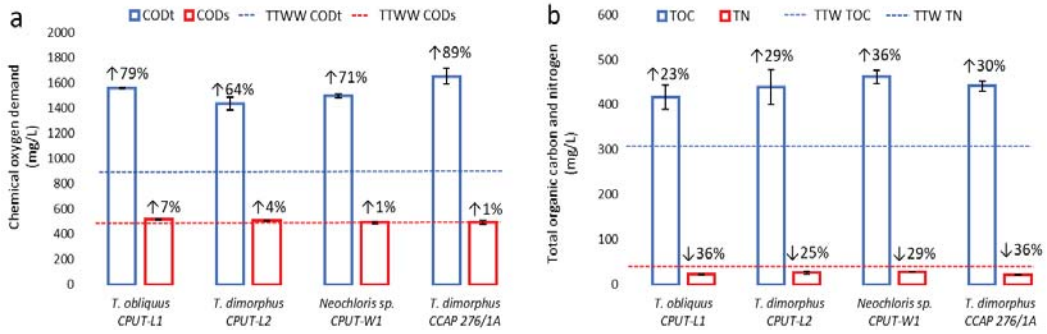

Figure 4.7: Total and Soluble COD, TOC and TN at Experimental End (Ranjan et al., 2025)

NH3-N concentrations decreased from the relatively low value (12 mg/L) in the TWW to below the detection limit of the test (1 mg/L) for all strains after 13 days. During rapid NH_3-N utilisation, there were accompanying increases in pH and decreases in T.Alk, reversing after 10 and 4 days, respectively (Figure 4.8). The increase in alkalinity after 4 days was attributed to CO2 fixation and possible proton uptake (Zerveas *et al.*, 2021). This increase in T.Alk from microalgal growth is a clear example of how microalgae and bacteria can operate synergistically in MAB systems, in which microalgae provide the alkalinity required by the AOB. In summary, the selected microalgal strains showed promise for polishing TWW following treatment in HLFCR and AD, as evidenced by their ability to grow in TWW and utilise NH_3. The results of this study show that microalgae require bacteria to synergistically increase COD and NH_3 removal.

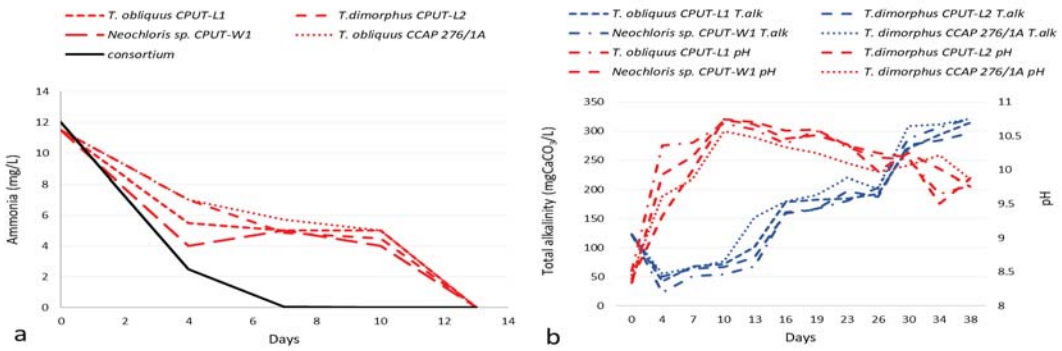

Figure 4.8: Ammonia (a), Total Alkalinity and pH (b) in Microalgal Monocultures (Ranjan et al., 2025)

This central composite design (CCD) experiment was based on the hypothesis that climatic factors could be important functional determinants for PR of TWW in full-scale systems such as HRAPs (Figure 4.9). The NH_3-N utilisation rate and biomass abundance from a consortium of the four microalgal strains in equal densities grown in TWW (batch 1) were determined under simulated winter, autumn/spring and summer conditions (temperature: 8.0°C, 17.5°C, 27.0°C, respectively; photoperiod: 10:14 hrs, 12:12 hrs, 14:10 hrs light: dark, respectively) with varied initial NH_3-N concentration and inoculum sizes (Figure 4.9).

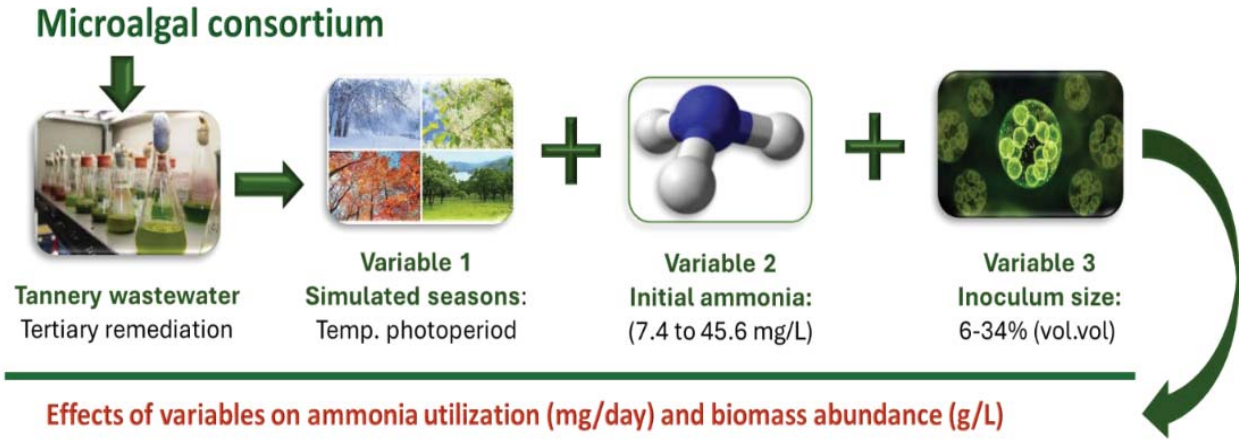

Figure 4.9: Experimental outline for seasonal microalgal consortium study

Neither the initial amount of biomass nor the initial NH_3 concentration had a significant effect on the growth of the microalgae at the end of the 14-day experiment Figure 4.10 a, b; Ranjan & Welz, 2025). However, growth was highly dependent on climatic factors. In this case, the amount attained was highest in the flasks from the summer-simulated (0.72 ± 0.07 g/L), followed by autumn/spring simulated (0.50 ± 0.11 g/L) and winter-simulated (0.39 ± 0.06 g/L) temperature and photoperiod conditions (Figure 4.10c; Ranjan & Welz, 2025).

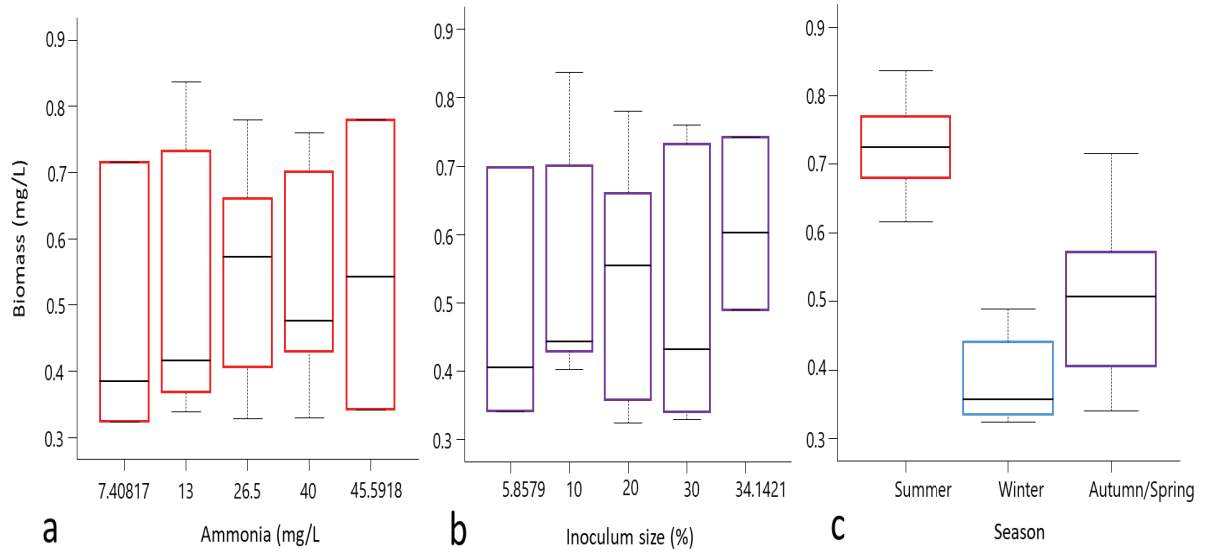

0

Figure 4.10: Effects of Ammonia, Inoculum Size and Season on Biomass Growth (Ranjan & Welz, 2025)

There were increases in the CODt in all flasks (Figure 4.11), for the same reasons alluded to when the microalgae were grown singly (Section 5.2.3.1). In comparison to the CODt (Figure 4.11 a-c), the CODs (Figures 5-11 d) were relatively stable.

The measured CODt was highest in summer- and lowest in winter-simulated conditions, with a relatively high overall correlation between biomass and CODt (Pearson's R=0.795), and moderate correlations in the winter-simulated (Pearson's R=0.540) and summer-simulated (Pearson's R=0.479) conditions, and a low correlation in the autumn/spring-simulated conditions (Pearson's R=0.369). The results can be explained by the fact that similar microalgal strains (*T. obliquus* and various Neochloris spp.) have been shown to grow both autotrophically and heterotrophically (Krzemińska *et al.*, 2014; Sutherland & Ralph, 2021). Autotrophic (photosynthetic) microalgal growth is expected to be highest in summer when the photoperiod is longest and lowest in winter when the photoperiod is shortest. Conversely, heterotrophic metabolism should be more marked in winter.

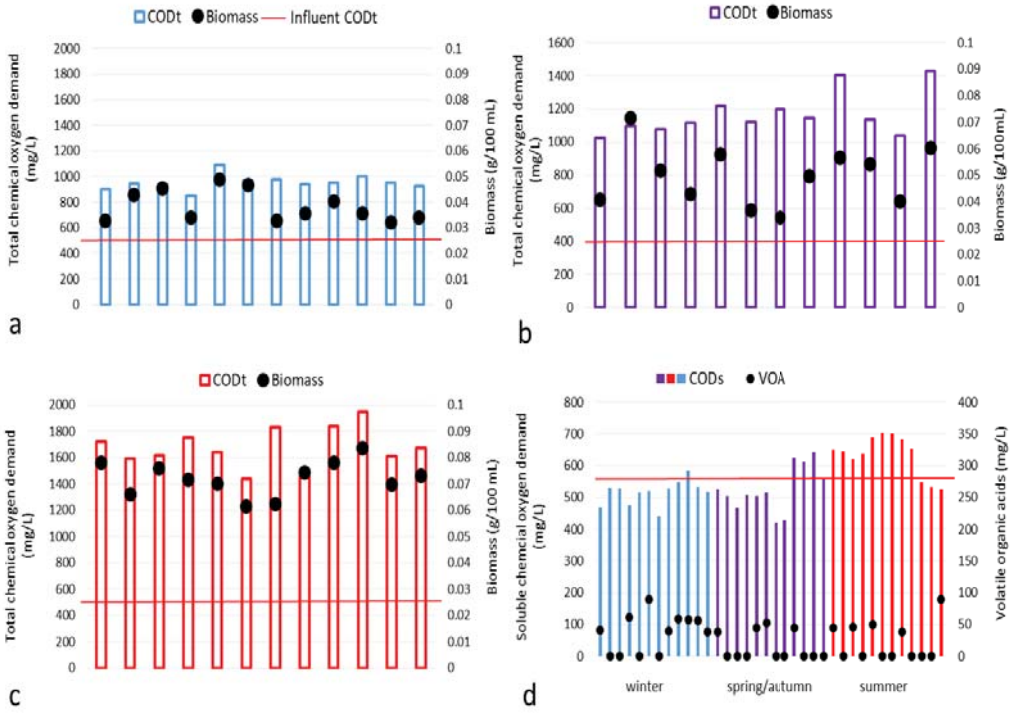

Figure 4.11: Seasonal comparison of total and soluble COD, biomass and volatile organic acids (Ranjan & Welz, 2025)

There were temporal pH increases of approximately 2 units (9 to 11) in all the runs (data not shown), corresponding to decreases in NH_3-N concentrations (Figure 4.12 a-c). In the summer-simulated runs, NH_3-N was completely utilised within 10 days, while complete NH_3-N utilisation only occurred in 17% and 42% of the winter and spring/autumn-simulated runs, respectively, at the end of the experimental period, clearly demonstrating the positive effect of increased temperature and/or photoperiod on NH_3-N utilisation. This aligns with increased microalgal growth from winter through to summer. There were highly significant correlations ($p<0.001$) between the initial NH_3-N and the NH_3-N utilisation rate for each simulated season (Figure 4.12 d-f), with high Pearson's correlation coefficients in the summer (R=0.932) and winter (R=0.843) simulated experiments, and a moderately high coefficient in the autumn/spring-simulated experiments (R=0.619).

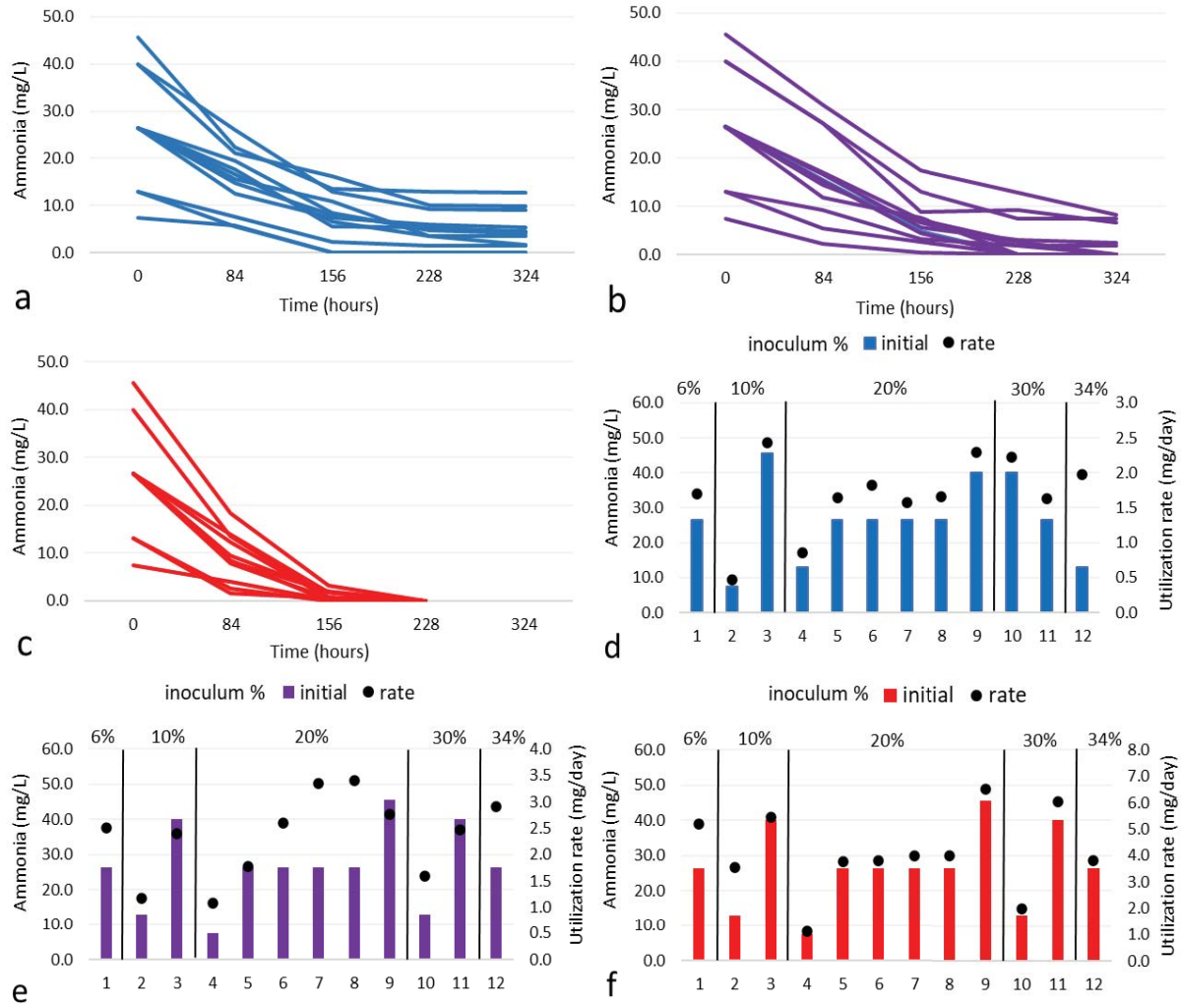

Figure 4.12: Seasonal ammonia concentration trends and relationships with utilisation rate and inoculum size (Ranjan & Welz, 2025)

In summary, the microalgal consortium successfully removed NH3-N, and removal rates depended on initial NH_3-N concentrations and simulated climatic conditions. Many studies focus on optimising microalgal growth conditions that are unrealistic for full-scale implementation. While fundamental knowledge provides valuable information, this experiment highlighted the importance of studying microalgal growth and remediation under climatic conditions likely to occur in the geographic area where the systems will be installed. Building on the results of the MAB, remediation was conducted.

4.2.6.2 Removal of organics and nitrogen removal dynamics in microalgal-bacterial systems: flask studies

4.2.6.3 Effect of light intensity: preliminary study

High light intensities can damage microalgal chlorophylls, impeding growth. This can adversely affect the removal of NH_3-N via the microalgal growth route (Lewis *et al.*, 2018). To assess the possibility of light sensitivity under simulated SA summer conditions, flask experiments (500 mL flasks, 350 mL working volume) were conducted using two light intensities (~140–187 $\mu mol/m^2 \cdot s^{-1}$ and ~33-50 $\mu mol/m^2 \cdot s^{-1}$) designated as standard light and low light, respectively.

Batch 2 of TWW was filtered and balanced in terms of macronutrients (5:1 N:P ratio). The high initial CODs (2693 mg/L) in the flasks ensured sufficient organic electron donors for denitrification. The experiment was conducted under the same summer-simulated temperature and photoperiod conditions as the microalgal-only experiments, using a 20% (vol/vol) inoculum.

The light intensity had no significant ($p>0.05$) effect on the removal of CODs (Figure 4.13 a) In comparison to the pure microalgal systems, where the CODs concentration showed no notable changes, 62% to 74% removal took place in the MAB flasks after 28 days. Almost complete NH_3-N removal was achieved in all flasks within 7 days, but NH_3-N removal was slightly higher under standard light conditions for the first 3 days (Figure 4.13 b).

It was assumed that this difference was due to increased photosynthesis and greater microalgal growth under higher light intensity, as the biomass concentration was higher in flasks exposed to standard light conditions (0.615 g/L) than in those exposed to low light conditions (0.435 g/L).

In contrast to the pure microalgal systems: (i) the pH in the MAB flasks remained relatively stable - between 6-8 in comparison with 9-11 in the pure microalgal flasks, and (ii) there was a decrease in T.alk from around 600 $mgCaCO_3$/L to <200 $mgCaCO_3$/L in comparison with an increase from around 50 $mgCaCO_3$/L to 300 $mgCaCO_3$/L after 7 days in the pure microalgal systems (Figure 4.13 c). These results reflect nitrification by AOB and concomitant consumption of T.Alk in the MAB systems.

Although good nitrification occurred, there was a build-up of NO_2^{2-}-N and NO_3^{2-}-N at both light intensities (Figure 4.13 d), with some overall increases in the sum of these inorganic N sources assumed to be due to protein degradation. The protein concentration in the TWW used in this study was 287±13 mg/L.

The increased NO_2^{2-}-N formation under low-light conditions supports the theory that higher NH3-N utilisation for microalgal uptake and lower bacterial nitrification occur under standard light than under low-light conditions. Overall, the results indicated that standard light conditions did not inhibit microalgal photosynthesis. In fact, the rate of microalgal growth was higher with more intense light.

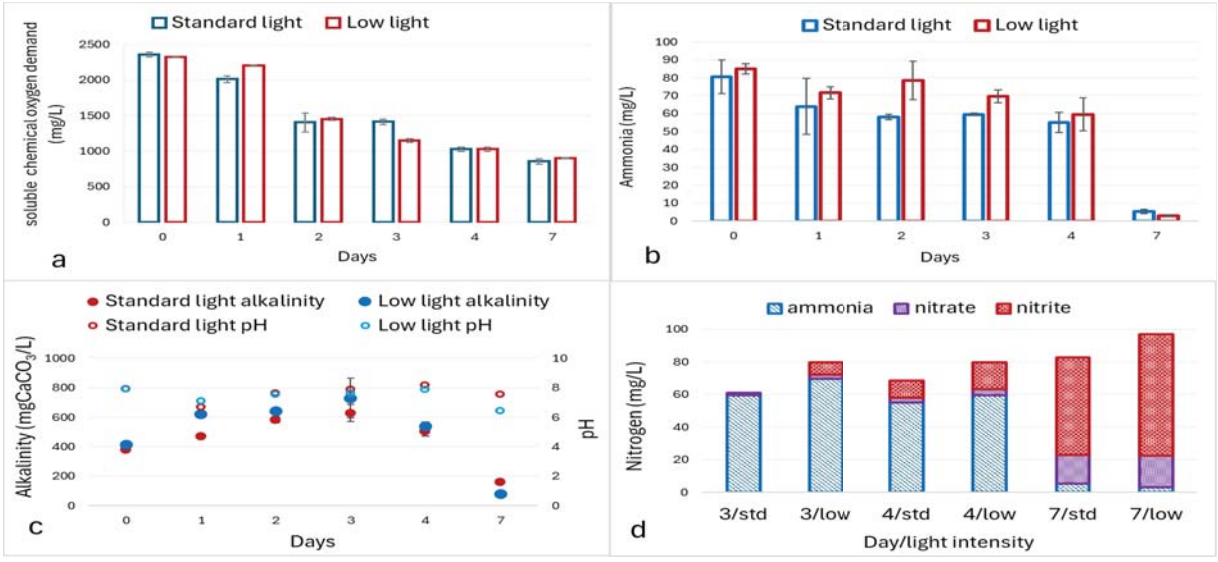

Figure 4.13: Effect of light intensity on soluble COD, ammonia, alkalinity, pH and nitrogen metabolism

A second, more comprehensive experiment was conducted to assess biomass growth, COD removal, and nitrogen dynamics using an inoculum containing bacteria acclimated to NH_3-N and TWW in a photobioreactor, as well as in a pre-acclimated microalgal consortium. The experiment was again conducted under summer-simulated temperature and photoperiod conditions and two light intensities. The flasks contained 25% (vol.vol) inoculum consisting of 50% settled biomass from the photobioreactor and 50% of the microalgal consortium.

The inoculum was added to attain two different densities (0.5 g/L and 0.05 g/L), designated as 0.5 g/L inoc. and 0.05 g/L inoc. Four of the five experiments were conducted with continuous shaking, whereas one was conducted under intermittent shaking and static conditions that coincided with light–dark cycles.

The rationale of using aeration during the light cycle and static conditions during the dark cycle was to create alternating aerobic and anoxic environments to encourage nitrification-denitrification. Photosynthesis does not take place during the dark cycle that simulates night, so microalgae do not produce O_2, which could interfere with denitrification. It was assumed that microalgal growth was the primary contributor to the measured biomass because microalgal cells are much larger than bacterial cells.

Macroscale visible growth of green microalgae was also observed in the flasks. Higher initial inoculum, continuous shaking and standard light intensity all promoted better overall microalgal growth (Figure 4.14). However, light intensity did not affect growth rates for the first 3 days. Thereafter, stationary and even decline phases were reached under low light, but the biomass continued to increase in the flasks subjected to standard light intensity.

The decrease in biomass under low light intensity was attributed to microalgal growth inhibition resulting from acidification of the flask contents, as discussed later in this report. Overall, the results indicated that biomass retention (SRT) will need to be flexible to optimise microalgal growth in full-scale MAB HRAPs treating TWW over different seasons.

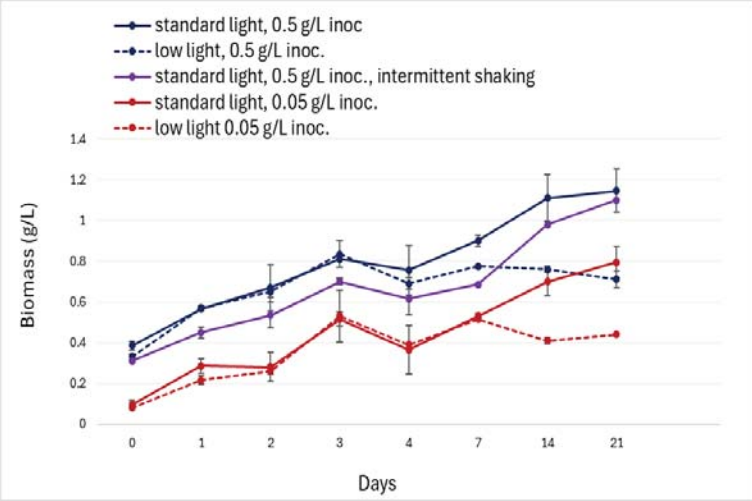

Figure 4.14: Temporal changes in biomass under different cultivation conditions

Given that the TWW had already been treated, good COD removal was achieved (Figure 4.15). Removal was attributed to bacterial mineralisation, as essentially no removal was observed in the microalgal-only experiments. Removal trends in all the flasks with continuous shaking/aeration were similar on a temporal scale despite the different inoculum densities, with 70-72% removal achieved at the end of the experiment. It was hypothesised that high doubling

times of well-acclimated heterotrophs may have reduced the numerical differences in the flasks with lower inoculum densities. Lower COD removal (63%) was observed under intermittent-shaking static conditions, attributed to reduced heterotrophic organic degradation under anoxic conditions during the dark cycle.

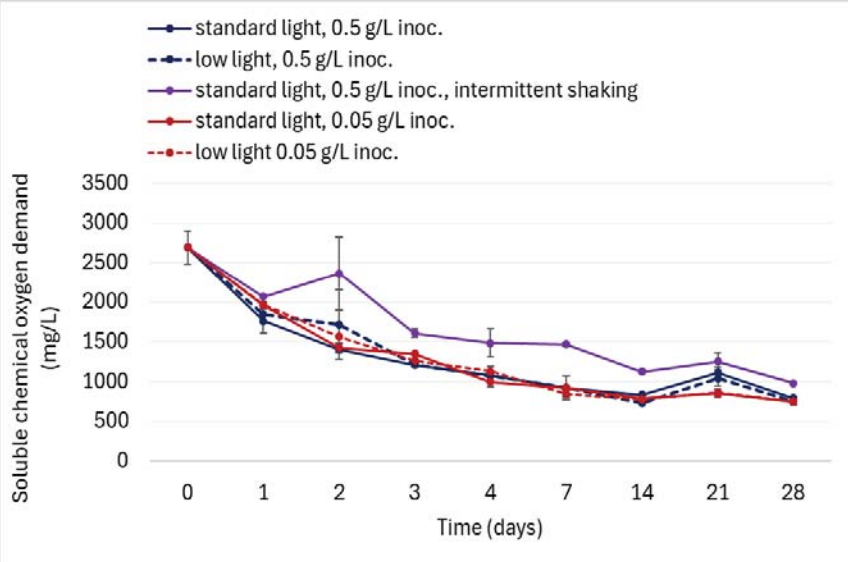

Figure 4.15: Temporal changes in soluble chemical oxygen demand under different cultivation conditions

Ammonia-nitrogen showed similar initial declines, followed by increases over the first three days under all operational conditions (Figure 4.16a). Thereafter, the NH_3-N concentrations declined more rapidly in the flasks with higher inoculum densities and continuous shaking. This was attributed to higher densities of slow-growing autotrophic AOB.

However, after 2 weeks, similar reductions were noted in all flasks that were continuously aerated. As expected from nitrification by AOB, NH_3-N removal was accompanied by consumption of T.Alk (Figure 4.16b). Of particular interest were the contrasting changes in pH under standard and low light intensities after 4 days.

The optimal pH range for microalgae such as Scenedesmus and Tetradesmus is 7.0-8.5, and the test strains used in the project grow well at pH values up to 11 (Ranjan *et al.*, 2025). This alkaliphilic nature is attributable to the strains being selected for their ability to grow in TWW, which is typically alkaline (Ranjan *et al.*, 2025). On the other hand, AOB are known to prefer pH values of 7.5-8.0 (Nagabalaji *et al.*, 2023; Arutselvan *et al.*, 2022).

In this study, the pH was theoretically optimal for the growth of both groups during the first 3-4 days, but became too alkaline for AOB thereafter when light intensity was high. This was assumed to be due to higher photosynthetic rates and concomitant CO_2 fixation when more light was available.

In contrast, as light intensity decreased, the pH was predicted to become too acidic for both groups. This is supported by the observation that biomass reached a plateau or decreased after 4 days in flasks with low light intensity and pH (Figures 5.14 and 5.16c).

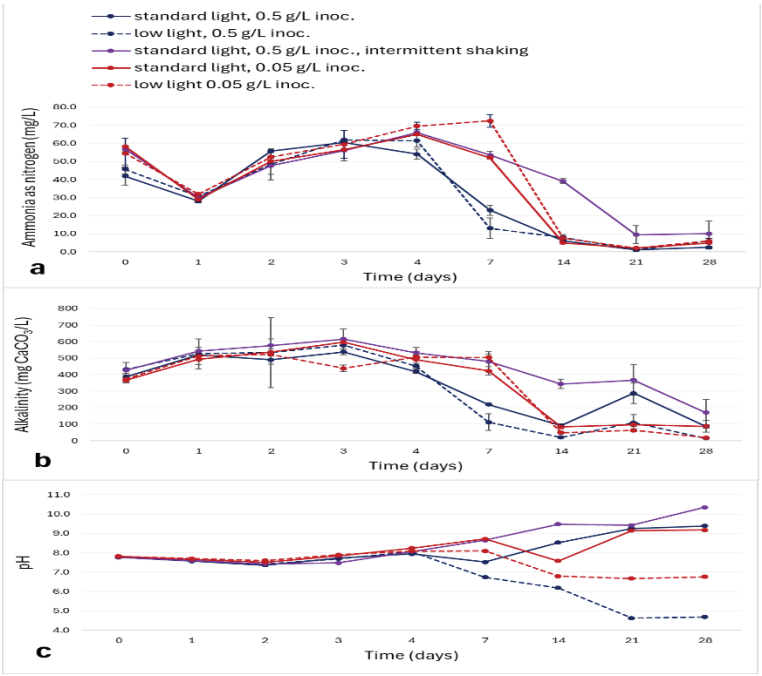

Figure 4.16: Temporal changes in ammonia-nitrogen, total alkalinity and pH under different cultivation conditions

In terms of nitrification-denitrification, there was a notable build-up of NO_2^{2-}-N and/or NO_3^{2-}-N from nitrification by AOB and NOB, respectively, after 4-7 days in the continuously aerated flasks. As expected, the formation of NO_2^{2-}-N and NO_3^{2-}-N coincided with NH_3-N reduction. It is difficult to make assumptions about more specific metabolic processes, given contributions from microalgal uptake and from the actions of nitrifiers, denitrifiers, and protein-hydrolysing taxa. However, intermittent shaking/aeration achieved the desired goal of promoting denitrification, as evidenced by reduced NO22--N, NO32-N, and combined NO22--N + NO32-N + NH_3-N concentrations in those flasks (Figure 4.17).

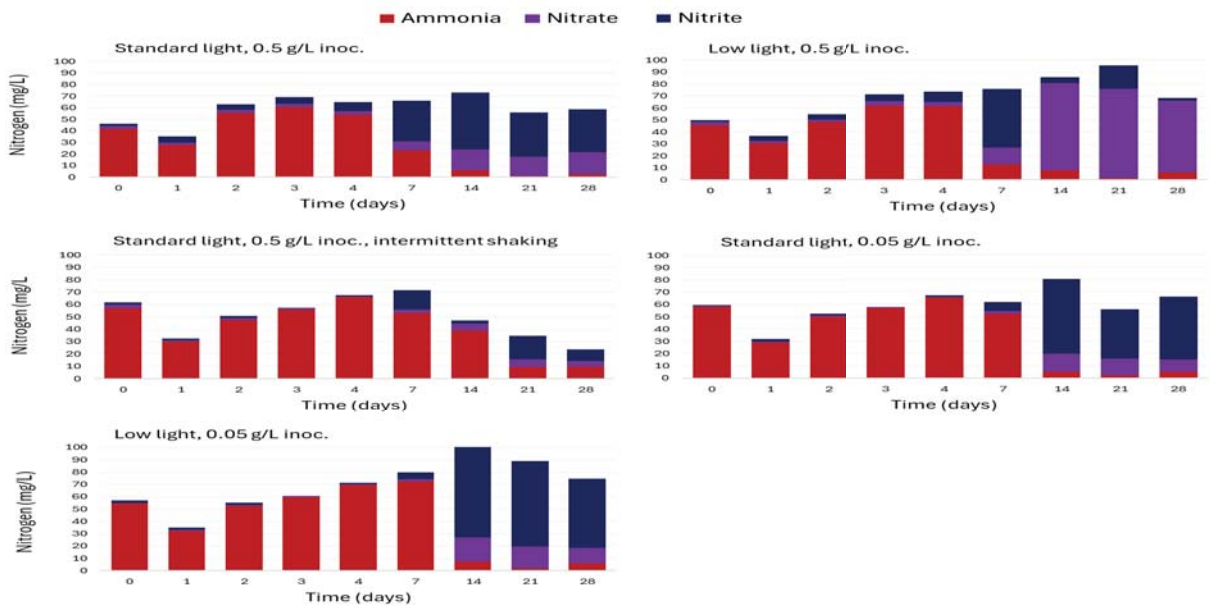

Figure 4.17: Inorganic nitrogen speciation under different cultivation conditions

Overall, the results of this experiment highlight the need to balance microalgal growth (to provide alkalinity) with bacterial growth (for consumption of T.alk and production of acid breakdown products) to: (i) maintain the pH in an ideal range to attain sufficient microalgal biomass for downstream applications, and (ii) promote functionality of both microalgae and bacteria in terms of CODs and N removal. It is also important to create conditions conducive to denitrification to prevent the build-up of other N species that may be toxic within MAB systems and to the environment. In this study, denitrification was effectively accomplished by intermittent aeration. Similar results may be achieved in continuous systems with dedicated aerobic and anoxic reactor zones, or in granular MAB systems. When comparing the results of the four flask studies, N and COD removal were markedly enhanced when bacteria and microalgae were used in conjunction.

4.2.7 Effects of aeration and addition of readily available organics on total nitrogen removal in a microalgal-bacterial photobioreactor

Building on the results obtained from flask studies, two photobioreactors were operated in batch mode for 69 days, with TWW (batch 1) containing relatively low concentrations of CODt (876±4 mg/L), CODs (489±4 mg/L), and NH_3-N (7.4 mg/L). The temperature (27°C) and photoperiod (14:10 light: dark) were set to mimic summer conditions, as in the MAB flask studies.

All the NH_3-N was removed within a few days after start-up, together with a slight decrease in T.alk, suggesting some AOB metabolic activity (Figures 4.18 a, b). On day 8, ammonium sulphate was added to increase the NH_3-N to a concentration (234 mg/L) expected from TWW after HLFCR-AD remediation (Mpofu *et al.*, 2023). The majority of NH_3-N was removed within 20 days, accompanied by consumption of most of the T.alk and a decrease in pH, as expected for bacterial nitrification. In contrast to the flask studies under low light, the pH remained within the range conducive to both microalgal and nitrifier growth.There was a sharp increase in CODt and, to a lesser extent, in CODs within 2 days after start-up, attributable to microalgal growth. This was consistent with the microalgae-only reactor studies. The aeration mode was changed on day 44, resulting in another spike in microalgal growth and increases in CODt and CODs. Overall, of the CODs in this batch of TWW was poor, probably because the TWW had already undergone secondary remediation so that the residual organics were recalcitrant in nature, and/or due to contributions from endogenous decay with the photobioreactors.

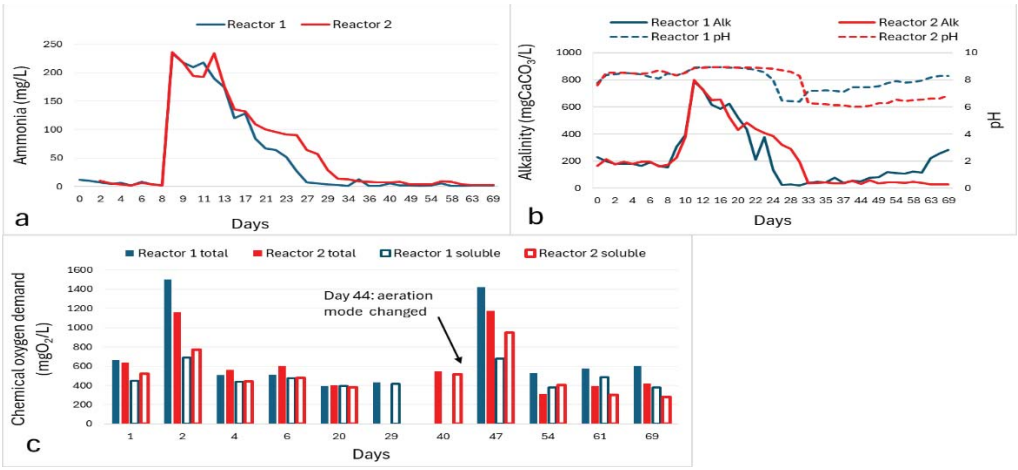

Figure 4.18: Ammonia, total alkalinity, pH and COD concentrations in the bulk liquid of two photobioreactors

The concentrations of NO_3^{2-}-N and NO_2^{2-}-N in the TWW were low at the start of the experiment (<0.5 mg/L and 0.05 mg/L, respectively). After start-up, NH3-N and NO2-N accumulated in the reactors, again indicating bacterial nitrification (Figure 4.19). To stimulate denitrification, the aeration mode was changed from 1 hr (on-off) intermittent aeration for 24 hours to 1 hour (on-off) intermittent aeration during the light cycle, and no aeration during the dark cycle. The rationale was to provide CO_2 via aeration for microalgal growth and photosynthesis during the light cycle (day) and anoxic conditions for denitrifying heterotrophs during the dark cycle (night).

There was minimal response to the change in aeration, and it was hypothesised that insufficient readily biodegradable COD was available to the denitrifiers. At this point (day 61), there were negligible differences in the NO_3^{2}--N and NO_2^{2}-N in the bulk liquid of reactors 1 and 2, which had been run under the same conditions. To test the hypothesis, excess readily biodegradable COD was added to reactor 1, but not reactor 2, on day 62, and the hypothesis was confirmed as there was almost complete removal of NH_3-N and NO_2^{2}-N in reactor 1 by day 69 (Figure 4.19). The added CODs were expended almost immediately, supporting the theory that the CODs in the TWW itself were recalcitrant.

In summary, MAB systems are promising for remediating TWW after HLFCR and AD, achieving complete N removal when operated under alternating aerobic and anoxic conditions. Further studies are required to optimise operational parameters across different climatic conditions, and results should be validated using multiple batches of TWW. Thereafter, it may be appropriate to pilot the HLFCR–AD–MAB system at a local tannery.

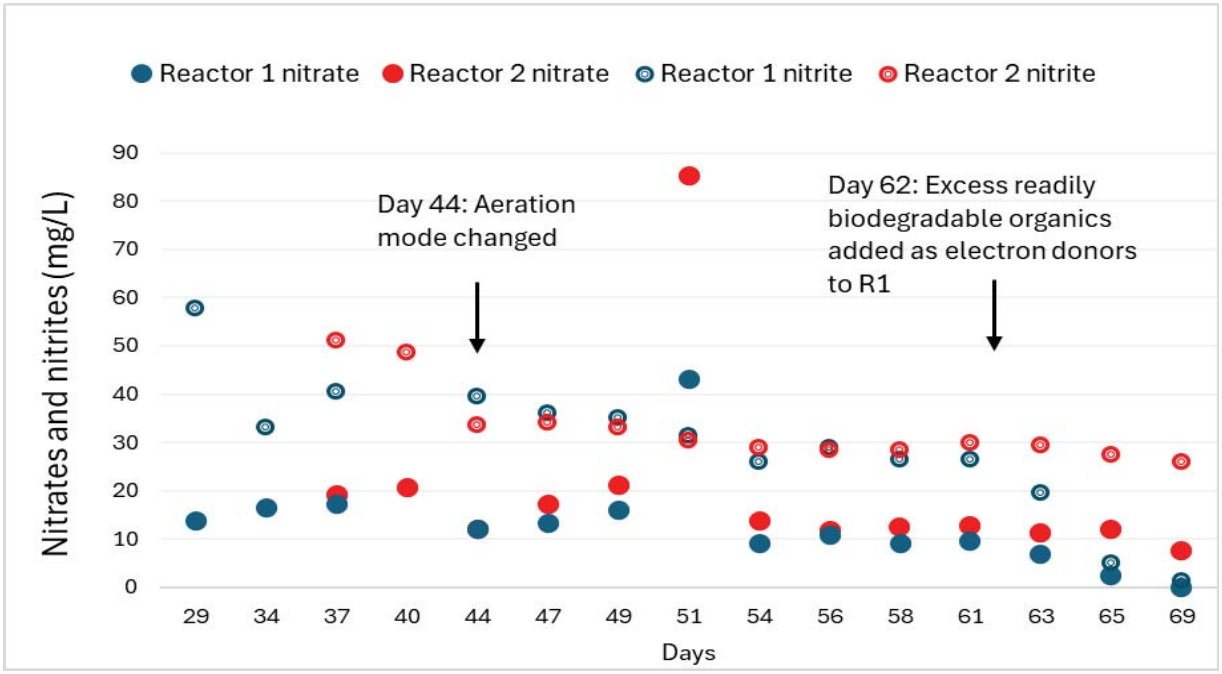

Figure 4.19: Nitrate and nitrite concentrations in the bulk liquid of two photobioreactors

Table 4.2 summarises the compositions of the dried microalgal biomasses when cultivated as individual strains. A consistent finding across all strains was the relatively low lipid content, particularly when compared with previously reported values for *T. obliquus*, *T. dimorphus*, and *Neochloris oleoabundans* grown under N limitation or mixotrophy (Santos *et al.*, 2013; Sehgal et al., 2019; Ranjan *et al.*, 2025). Conversely, the protein concentrations observed in this study were comparatively high and more stable, indicating a shift in metabolic allocation under the

nutrient conditions provided by the TWW. The literature supports this trend: protein levels ranging from 19–56% (wt./wt.) in *T. obliquus*, 18–35% (wt/wt) in *Neochloris* species, and similar ranges in *Scenedesmus* and *T. dimorphus* grown in diverse wastewater matrices had been reported previously, confirming the potential of these taxa as high protein feedstocks (Oliveira *et al.*, 2021; Baldisserotto *et al.*, 2024; Ekinci *et al.*, 2019). Given that it also contained a wide range of vital trace elements, the biomass produced here shows promise for use in aquaculture and poultry feed applications. These applications have two main advantages: (i) they help to meet the increasing demand for sustainable protein substitutes, and (ii) they comply with the circular bioeconomy principles by turning an industrial waste stream into a product with added value (Bhatti *et al.*, 2023; Cicci *et al.*, 2024).

Table 4.2: Physicochemical characteristics of the dried microalgal biomass of the study strains

	T. obliquus CPUT-L1	*T. dimorphus* CPUT-L2	*Neochloris* sp. CPUT-W1	*T. obliquus* CCAP 276/1A
Macromolecules (%wt.wt)				
Proteins	24.5	33.5	36.8	37.2
Carbohydrates (GE)	17.9	19.1	19.8	12.7
Fatty acids	10.2	13.3	7.40	9.44
Elemental CHNS (%wt.wt)				
Carbon	52.8	45.9	42.6	46.0
Hydrogen	9.61	9.11	8.44	9.22
Nitrogen	4.26	5.79	6.35	6.42
Sulphur	0.30	0.48	0.42	0.43
Major cations (g/kg)				
Sodium (Na)	8.30	7.14	7.77	4.88
Magnesium (Mg)	8.06	8.68	8.74	9.96
Phosphorus (P)	12.3	13.1	19.6	27.3
Potassium (K)	5.20	5.67	8.23	9.42
Calcium	6.46	3.78	4.89	6.63
Minor cations (g/kg)				
Aluminium (Al)	0.805	0.714	0.720	0.614
Silica (Si)	1.97	0.865	1.35	1.58
Manganese (Mn)	4.86	2.78	3.44	3.32
Iron (Fe)	1.25	0.744	1.02	0.895
Zinc (Zn)	0.176	0.0851	0.119	0.128
Minor cations (mg/kg)				
Boron (B)	30.4	38.9	41.7	24.6
Vanadium (V)	0.900	0.842	1.08	1.09

Chromium (Cr)	20.7	41.2	42.5	15.5
Cobalt (Co)	1.48	0.824	0.979	2.78
Nickel (Ni)	2.81	2.52	2.58	1.79
Copper (Cu)	11.6	8.20	6.38	9.53
Arsenic (As) (0.1)*	0.310	0.277	0.265	0.206
Strontium (Sr)	16.3	14.0	8.43	10.2
Molybdenum (Mo)	0.531	0.275	0.471	0.459
Cadmium (Cd) (0.05)*	0.047	0.055	0.044	0.083
Tin (Sn) (50)*	0.906	1.00	1.53	0.974
Antimony (Sb)	0.089	0.250	0.059	0.063
Barium (Ba)	31.4	17.2	19.4	23.2
Mercury (Hg) (1.2)*	0.029	0.018	0.014	0.014
Lead (Pb) (0.05)*	2.30	2.51	3.32	3.56

*For edible oil (FAO/WHO, 2021) GE = glucose equivalent; selenium was below the detection limit

Upstream processes must still be carefully considered. While Cr-free tanning would significantly lower this risk, wet blue (Cr) tanning can jeopardise the feed safety of the biomass unless this waste stream is segregated from the process. The elemental characterisation further revealed that concentrations of tin (Sn), mercury (Hg), and lead (Pb) were all well below FAO/WHO food safety limits (FAO/WHO, 2021). Conversely, arsenic (As) and cadmium (Cd) were occasionally detected at levels slightly above thresholds for specific food commodities but remained within acceptable ranges for others. These results underscore the need for long-term monitoring of batch variability to ensure consistent quality if the biomass is to be used in feed formulations (Rose *et al.*, 1996; Khan *et al.*, 2024; Ranjan *et al.*, 2025).

Beyond direct feed applications, protein-rich biomass offers opportunities in the bioenergy sector. When co-digested with secondary TWW sludge, microalgal biomass can enhance methane yields and reduce the inhibition commonly observed when digesting tannery wastes alone. Such co-valorisation strategies not only produce renewable energy in the form of biogas but also yield nutrient-rich digestates that can be applied as biofertilizers, closing nutrient cycles at both industrial and agricultural levels (Ekinci *et al.*, 2019; Hidaka *et al.*, 2017). When microalgal consortia, rather than monocultures, were grown in TTWW, similar patterns emerged (Table 4.3) (Ranjan & Welz, 2025). Seasonal changes affected protein, carbohydrate, and fatty acid concentrations, but overall trends were consistent. Fatty acid levels remained too low for biodiesel to be considered a viable downstream option under the studied conditions. Instead, the biomass became increasingly valuable due to rising protein and carbohydrate concentrations, particularly under summer-simulated conditions with elevated temperatures and longer photoperiods.

These results parallel observations from *T. dimorphus* and *N. oleoabundans*, where N-rich environments promote protein accumulation at the expense of lipids. The high N load of TTWW, therefore, appears particularly advantageous for producing protein-rich biomass, reinforcing its potential as an alternative protein source for feed and aquaculture nutrition (Safi *et al.*, 2021; Cicci *et al.*, 2024; Gallego *et al.*, 2025). Given the biomass's high protein content, vital

carbohydrates, and mineral nutrients, particularly Ca, Mg, P, K, and N, it also has the potential to be used as an organic fertiliser. Such valorisation pathways are pertinent and timely, given the global challenges of meeting demand for soil amendments and proteins. Toxic metal accumulation remains a major drawback, as it was in feed applications.

Lead levels were often above FAO/WHO limits, and Cd and As levels were also high (FAO/WHO, 2021). Before biomass can be safely implemented at scale, these safety concerns require more research into metal-removal strategies, such as upstream pretreatment of TWW or selective harvesting techniques. Thus, although biodiesel production is not feasible due to low lipid levels, TWW-grown microalgal biomass demonstrates strong potential for downstream use in feed, fertiliser, and bioenergy applications. Ensuring metal safety and maintaining compositional consistency will be critical to unlocking its value in a sustainable biorefinery framework (Ranjan *et al.*, 2025; Ranjan & Welz, 2025). Table 4.3 below shows the physicochemical characteristics of the dried microalgal biomass of the study consortium grown under various simulated seasonal conditions.

Table 4.3: Physicochemical characteristics of dried microalgal biomass grown under different simulated seasonal conditions

	Winter Low	Winter High	Spring/A. Low	Spring/A. High	Summer Low	Summer High
***Macromolecules* (%wt.wt)**						
Proteins	32.8	34.9	37.4	33.0	30.6	18.5
Carbohydrates (GE)	5.5	4.6	8.0	18.5	16.4	22.3
Fatty acids	3.33	3.80	5.15	6.40	3.70	4.39
***Elemental CHNS* (%wt.wt)**						
Carbon	39.2	40.7	42.4	45.3	44.5	46.7
Hydrogen	6.77	7.10	7.48	8.19	8.36	8.77
Nitrogen	5.67	6.02	6.44	5.69	5.28	31.4
***Major cations* (g/kg; mg/L)**						
Sodium (Na)	9.47	10.3	8.50	5.51	6.46	5.31
Magnesium (Mg)	25.6	24.6	15.4	10.6	18.5	7.81
Phosphorus (P)	7.07	7.89	4.80	3.44	4.11	2.59
Potassium (K)	4.72	3.38	4.39	5.13	4.62	3.53
Calcium (ca)	10.2	8.65	9.04	6.48	5.61	2.72
***Minor cations* (g/kg; mg/L)**						
Silica (Si)	1.65	0.18	0.48	0.60	0.37	0.65
***Minor cations* (g/kg; µg/L)**						
Aluminium (Al)	4.93	4.15	3.56	2.49	3.61	2.34
Manganese (Mn)	16.8	15.4	11.6	8.76	10.4	6.64
Iron (Fe)	3.66	1.97	2.74	2.05	2.34	1.79
Zinc (Zn)	0.75	0.69	0.44	0.33	0.41	0.19
***Minor cations* (mg/kg; µg/L)**						
Boron (B)	20.8	15.2	14.7	9.14	34.7	20.9
Vanadium (V)	0.96	0.74	0.82	0.71	0.61	0.58
Chromium (Cr)	67.6	47.1	50.8	38.9	45.4	34.2
Cobalt (Co)	1.20	1.16	0.99	0.66	0.87	0.54
Nickel (Ni)	9.71	7.49	3.78	1.83	2.31	1.65
Copper (Cu)	35.8	37.3	25.8	35.4	20.8	17.5
Arsenic (As) (0.1 mg/kg)*	0.99	0.94	0.80	0.63	0.59	0.54

Selenium (Se)	0.33	0.14	0.26	0.22	0.24	0.16
Strontium (Sr)	31.8	31.8	28.1	20.7	18.9	11.2
Molybdenum (Mo)	0.48	0.33	0.44	0.47	0.39	0.37
Cadmium (Cd) (0.05 mg/kg)*	0.15	0.11	0.10	0.06	0.07	0.05
Tin (Sn) (50)*	6.19	1.88	5.52	3.96	5.18	3.72
Antimony (Sb)	0.28	0.12	0.14	0.16	0.14	0.12
Barium (Ba)	65.0	58.1	56.1	42.2	44.9	38.1
Mercury (Hg) (1.2 mg/kg)*	0.21	0.31	0.23	0.23	0.17	0.46
Lead (Pb) (0.05 mg/kg)*	6.55	6.06	4.86	4.35	3.48	2.82

*For edible oil (FAO/WHO, 2021) GE = glucose equivalent; BDL = below detection limit; TTWW = treated TWW.

4.3 Microalgae Bacterial Systems Modelling

Microalgal modelling has a long research history (Droop, 1968; Bernard *et al.*, 2009), but only recently have these models been integrated into biological wastewater treatment systems. Early work by Buhr and Miller (1983) explored the simultaneous growth of algae and bacteria in High-Rate Algal Ponds (HRAPs), a common feature of advanced pond systems.

More recent approaches have adapted frameworks such as the River Water Quality Model No. 1 (RWQM1), which describe nutrient cycling and microbial processes (Gehring *et al.*, 2010; Reichert *et al.*, 2001). Table 4.4 below provides an overview of recent developments in the modelling of MAB systems.

Table 4.4: Features, processes and components of integrated mechanistic microalgae–bacteria models

Basic model	Simulation platform	Processes	Components	Limitations	Experimental validation	References
RWQM1 (Reichert *et al.*, 2001)	COMSOL Multiphysics	10 processes Microalgal processes: growth on NH_3, NO_3^-, endogenous respiration, inactivation, chemical equilibrium and gas transfer	10 components Microalgae biomass (XALG), ammonium nitrogen (SNH_4-N), ammonia-nitrogen (SNH_3), nitrate (SNO3-N), dissolved oxygen (SO_2), bicarbonate ($SHCO_3$-), carbon dioxide (SCO_2), carbonate (SCO_3), hydrogen ion (SH), hydroxide ion (SOH)	Light attenuation and bacterial processes are excluded.; hydrodynamic equations must be integrated	The model was calibrated using a 1.30m^2 surface area batch mesocosm algal culture with a depth of 0.55 m	(Solimeno *et al.*, 2015)
Algal dynamics - (Solimeno *et al.*, 2015)	MATLAB/Simulink	6 processes Algal growth on NH_4, NO_3, algal decay; bacterial growth and	8 components Algae biomass (Xalg), bacteria biomass (Xbac), dissolved	pH dynamics and algal inhibition by excess light	Calibrated with two 1 L lab-scale PBRs treating sewage in batch mode	(Zambrano *et al.*, 2016)

Bacterial dynamics - ASM1		decay; oxygen transfer	substrates (nitrate SNO_3, ammonium SNH_4) and dissolved gases (carbon dioxide SCO_2, oxygen SO_2)	and CO_2 are not considered		
Algal dynamics – their own input **Bacterial dynamics – Modified ASM3 (Iacopozzi *et al.*, 2007)**	Aquasim 2.0	23 processes Algal processes include growth and endogenous respiration. Bacterial processes include aerobic growth, endogenous respiration, and anoxic growth and endogenous respiration	17 components components Soluble inert organics SI, ammonium (SNH_4), nitrate (SNO_3), nitrite (SNO_2), nitrogen gas (N2), dissolved oxygen (SO_2), readily degradable substrate (SS), AOB biomass (XAOB), NOB biomass (XNOB), inert particulate organics (XI), heterotrophic biomass (XH), phototrophic biomass (XP), organics stored by heterotrophs (XSTO)	Limited algal processes considered	The model was calibrated and validated using data from a 2 L PSBR operating with a 4-day HRT for centrate wastewater treatment	(Arashiro *et al.*, 2017)
Algal dynamics – BIO_ALGAE **(Solimeno *et al.*, 2017)** **Bacterial dynamics – Modified ASM3 (Iacopozzi *et al.*, 2007)**	COMSOL Multiphysics	25 processes Algal processes: growth on SNH_4, SNO_3, endogenous respiration and decay. Bacterial processes: aerobic growth on SNH_4, SNO_3, anoxic growth (SNO_3, SNO_2), endogenous respiration, decay Nitrifying activity: growth, endogenous respiration and decay of XAOB and XNOB,	19 components Algal biomass (XALG), heterotrophic bacteria (XH), nitrite-oxidising bacteria (XNOB), ammonia-oxidising bacteria (XAOB), slow degradable organic matter (XS), inert particulate organic matter (XI), ammonium nitrogen (SNH_4-N), ammonia-nitrogen (SNH_3), nitrate (SNO_3-N), nitrite (SNO_2-N), phosphate (SPO_4-), dissolved oxygen(SO_2), carbon dioxide (SCO_2), bicarbonate	Integration of CFD can enhance the prediction of more precise pH dynamics, dissolved oxygen profiles, and other component profiles	The model was calibrated and validated using data from two HRAPs (3.5m², 0.3 m depth) with a 4.5-day HRT for municipal wastewater treatment	(Solimeno *et al.*, 2017)

		hydrolysis and chemical equilibrium	($SHCO_3$-), carbonate (SCO_3), hydrogen ion (SH), hydroxide ion (SOH), Inert soluble organic matter (SI), readily biodegradable soluble organic matter (SS)			
Algal dynamics – Modified ASM-2d with their own inputs	MATLAB	6 processes Algal uptake and storage of nitrogen and phosphorus; photoautotrophic growth; heterotrophic growth; decay	11 components Soluble ammonium nitrogen (SNH_4), Soluble nitrate + nitrite nitrogen (SNO), Inorganic soluble P (SPO_4), Internal cell quota N (XAlgN), Internal cell quota P (XAlgPP), Alkalinity (SAlk), Dissolved oxygen (SO_2), Carbon source (SA), Slowly biodegradable organic matter (XS), Algal biomass concentration (XAlg), non-biodegradable organic matter (XI)	Bacterial processes are not considered; aspects such as light attenuation, toxicity, photo-oxidative damage, and temperature effects are neglected	Model was calibrated and validated using data from a 24 L airlift PER in SBR mode with synthetic medium	(Wágner *et al.*, 2016)
MRQWM1 **(Broekhuizen *et al.*, 2012)** **BIO_ALGAE2** **(Solimeno *et al.*, 2019)**	Aquasim 2.0	19 processes Algae processes: growth on SNH, SNO_3 Heterotrophic bacterial processes: aerobic – aerobic respiration, decay, growth on SNH, SNO_3, respiration. Anoxic – growth on SNO_2, SNO_3, respiration, hydrolysis	17 components phototrophic algae (XALG), Ammonium oxidising bacteria (XAOB), Nitrite oxidising bacteria (XNOB), Heterotrophic bacteria (XH), Slowly biodegradable organic matter (XS), Readily biodegradable particulate matter (SS), Inert particulate matter (SI), Total inorganic carbon (SIC), organic nitrogen (SND), Total ammoniacal	n.d	The model was configured and calibrated using data from a 56 m^2 raceway pond treating synthetic wastewater	(Casagli *et al.*, 2021)

		Nitrifying bacteria: Aerobic XAOB – ammonification, decay, growth, respiration, XNOB – growth, respiration, decay.	nitrogen (SNH), Nitric nitrogen (SNO_3), Nitrous nitrogen (SNO_2), Total inorganic phosphorus (SPO_4), nitrogen gas (SN_2), Water (SH_2O), Dissolved oxygen (SO_2)			

The RWQM1 model accounts for algal growth on nitrogen (N) and phosphorus (P), but it does not include carbon limitation - a major factor in algal growth in wastewater environments (Gehring *et al.*, 2010). Other models have focused on narrower processes, such as algal growth (Sah *et al.*, 2011) or ammonia removal (Halfhide *et al.*, 2015).

Van der Steen *et al.* (2015) modified the Activated Sludge Model No. 3 (ASM3) to represent biomass growth for nitrifying bacteria and algae. However, most existing models have limitations. They often use a few parameters, neglect interactions between algae and bacteria, or ignore the effects of high dissolved oxygen (DO) on algal activity.

The BIO_ALGAE model (Solimeno *et al.*, 2015; 2017) addresses these gaps by simulating both algal and bacterial growth, incorporating carbon limitation, light attenuation, photorespiration, and temperature effects. Although promising, it has been tested primarily on synthetic media and urban wastewater, rather than on TWW, which exhibits highly variable characteristics.

This study aims to refine and validate an algal-bacterial (MAB) model within a plant-wide modelling framework, specifically for TWW treatment, improving prediction and optimisation of biomass production and nutrient removal.

4.3.1 Model Implementation

The modified MAB model was developed using the UCT Plant-Wide Model (PWM_SA) (Ikumi, 2020) as the foundation. PWM_SA was chosen because:

- It has been extensively applied to South African wastewater treatment scenarios.
- It includes a generic speciation and ion pairing routine that links stoichiometrically to the proposed MAB processes.
- It is implemented in WEST®, a simulation platform that allows integration of multiple unit processes in a single network.

PWM_SA already supports a ‘supermodel’ approach, enabling the connection of various unit operations. UCT’s collaboration agreement with DHI (the developer of WEST®) provides direct access to model code, enabling the creation and international sharing of new models.

The extended PWM_SA model incorporates:

- Growth and decay of MAB strains (e.g., *Tetradesmus obliquus*, *T. dimorphus*, *Neochloris* sp.) known for their resilience in TWW.
- Heterotrophic growth of MAB during dark phases.

- The effects of light intensity on growth and decay kinetics.

Because this MAB model is built within PWM_SA, it is fully compatible with other treatment processes (e.g., activated sludge, hybrid linear flow channel reactors) for integrated, system-wide simulations. It also runs faster simulation runs. This allows for the omission of processes 4-7 from the current BIO_ALGAE model shown in Table 4.5 below, since they are comprehensively catered for in the algebraic speciation routine of the proposed modified MAB model (i.e., they are already part of the speciation and ion pairing routine of Brouckaert *et al.* (2022), which is part of the current PWM_SA model).

Table 4.5: Mathematical description of the processes of the model (process rates)

Processes	Process rate [M L^{-3} T^{-1}]
1. **Microalgae growth on N (ammonia and nitrates) and P (phosphates)**	$\rho_1 = \mu_{ALG} \times \frac{N}{KN+N} \times \frac{P}{KP+P} \times \frac{I}{KI+I} \times e^{-\beta I} \times \frac{1}{\left(1+\frac{S}{Ki_S}\right)} \times \frac{1}{\left(1+\frac{S\_NH_4}{Ki_N}\right)} \times X_{ALG}$
2. **Microalgae endogenous respiration (aerobic)**	$\rho_2 = \mathrm{k_{resp,ALG}} * \frac{S\_O_2}{\mathrm{K_{O2,ALG}} + S\_O_2} * \mathrm{X_{ALG}}$
3. **Death of microalgae (anaerobic)**	$\rho_3 = \mathrm{k_{death,ALG}} * \mathrm{X_{ALG}}$
4. **Oxygen transfer to the atmosphere**	$\rho_{O2} = \mathrm{Ka,O2} * \left(\mathrm{S_{O2}^{SAT}} - S\_O_2\right)$
5. **Carbon dioxide transfer to the atmosphere**	$\rho_{O2} = \mathrm{Ka,CO2} * \left(\mathrm{S_{CO2}^{SAT}} - S\_CO_2\right)$
6. **Ammonia transfer to the atmosphere**	$\rho_{NH3} = \mathrm{Ka,NH3} * \left(\mathrm{S_{NH3}^{SAT}} - S\_NH_3\right)$
7. **7 – 10. Speciation and ion pairing reactions for ammonia, carbonate, phosphate and sulphate weak acid systems (already available as part of the current PWM_SA model, as described by Brouckaert *et al.* 2016 and Brouckaet *et al.*, 2022; see Section 2.8.1)**	
Where: • **N = concentrations of nitrogen (mgN/L)** • **P = concentrations of phosphorus (mgP/L)** • **S concentrations of sulphide (mgS/L)** • **S_NH_4 = Concentrations of NH_4^+** • **S_NH_3 = Concentrations of NH_3** • **S_O = Concentrations of dissolved oxygen (DO)** • **KN = half-saturation constants for N** • **KP = half-saturation constants for P** • **I = light intensity (µmol photons m−2s−1)**	• Ka,O2 = Mass transfer coefficient for oxygen • Ka,CO2 = Mass transfer coefficient for carbon dioxide • Ka,NH3 = mass transfer coefficient for ammonia • S_{O2}^{SAT} = Saturation concentration of oxygen • S_{CO2}^{SAT} = Saturation concentration of carbon dioxide • S_{NH3}^{SAT} = Saturation concentration of ammonia • μ_{ALG} = Maximum growth rate of microalgae

• **KI = half-saturation constant for light (µmol photons m−2s−1)** • **β = photoinhibition coefficient** • **Ki_S = inhibition constant for sulphide (mgS/L)** • **Ki_N = inhibition constant for ammonia (mgN/L)**	• $k_{resp,ALG}$ = Endogenous respiration constant • $k_{death,ALG}$ = Death constant
NB: The parameters for processes 4 – 6 have been calibrated (the values from Solemino *et al.*, 2019 shall be applied) and are deemed not to change with the incorporation of the new MAB biomass to be investigated in this study. Also, the speciation and ion pairing processes are already included in the current PWM_SA model (Brouckaert *et al.*, 2022). Hence, the scope of model calibration for this study includes the calibration of the stoichiometric and kinetic constants governing the growth and death of the new Mab biomass (i.e., the parameters associated with Equations 1, 2, and 3).	

4.3.2 Model Calibration Process

Model calibration was supported by controlled batch experiments in 500 mL flasks (working volume 350 mL). Four types of duplicate reactors were run under different conditions:

1. Batch 1: 70 mL inoculum (2 g/L) + 280 mL TWW, standard light intensity (140–187 µmol/m²·s).
2. Batch 2: Same as Batch 1 but at low light intensity (33–50 µmol/m²·s).
3. Batch 3: 70 mL inoculum (0.2 g/L) + 280 mL TWW, standard light intensity.
4. Batch 4: Same as Batch 3 but at low light intensity.

Reactors were incubated at 160 rpm with LED grow lights emitting blue and red spectra. The inoculum was pre-cultivated in controlled photobioreactors. Model parameters for MAB growth and decay were tuned by comparing simulated results with experimental data, minimising errors across key variables, including COD removal, biomass growth, and nitrogen transformation. The main results are presented below.

- **COD Removal**

According to the model, COD removal is primarily mediated by ordinary heterotrophic organisms (OHOs), which are typically found in activated sludge systems used to treat organic wastewater. The current PWM_SA model already contained the stoichiometric and kinetic equations used to replicate the metabolism of OHOs; hence, it did not require further adjustments to account for COD removal processes. Figure 4.20 below compares model-simulated and experimentally measured COD concentrations in laboratory-operated and tested batch reactors. To obviate this stage of model calibration, the COD from the influent wastewater (tannery effluents) was completely soluble. Hence, the variabilities that would be brought about by the particulate organic components were eliminated – i.e., the unbiodegradable particulates (which accumulate in the reactor without breakdown) and biodegradable particulates (which depend on hydrolysis prior to utilisation by biomass).

The graphs below (Figure 4.20) show that the simulated model shows that the experimentally measured data for COD concentrations in all the batch tests are well matched. This indicates that the PWM_SA model replicated COD removal without further adjustments to model

stoichiometry or OHO-biometabolism parameters. An important factor to consider is the nitrogen content of fermentable soluble biodegradable organics. This is because, prior to utilisation, the FBSO is broken down, thereby releasing organically bound N as ammonia. The released ammonia increases the amount already present in the influent, thereby increasing the substrate available to the biomass. Some is used by the OHOs as a nutrient for growth, and the rest is made available for the chemical autotrophs (MAB) and autotrophic nitrifying organisms (ANOs).

Henze *et al.* (2008) stated that when the OHO dies, its remains can be broken down into biodegradable particulate organic components (which are later hydrolysed for release of further nutrients that could be used by the biomass) and endogenous residue (an unbiodegradable component of the dead biomass). A major factor limiting OHO biomass growth was oxygen availability. The oxygen available in the batch reactor was primarily generated as a byproduct of photosynthetic metabolism in the MAB. Because of this limitation, the kinetics of OHO biomass growth were much slower than would occur in conventional AS systems. Hence, although OHOs have a yield of 0.67 (mgCOD of biomass/mgCOD of organics used), the OHO biomass produced was relatively low for these reactors.

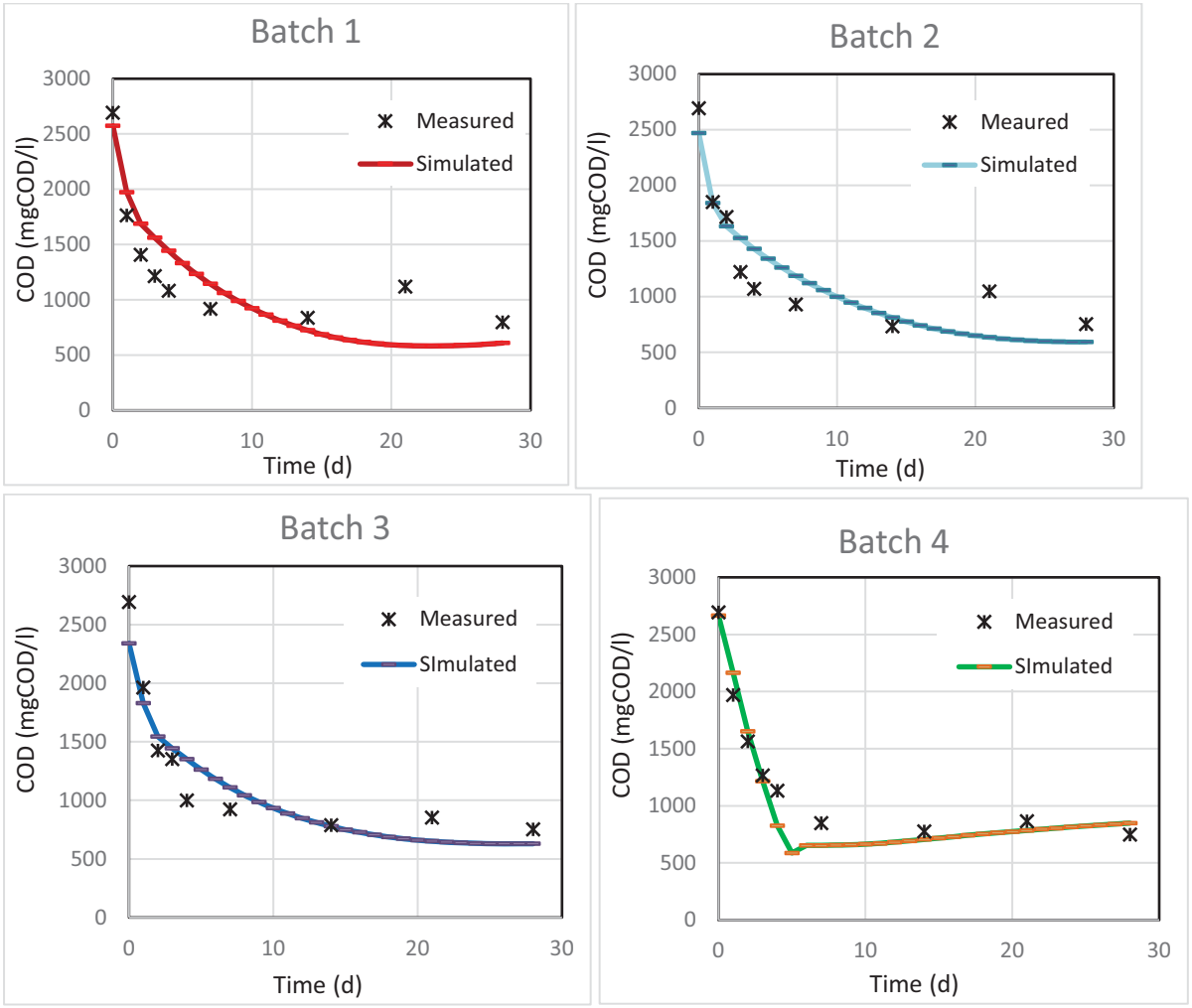

Figure 4.20: Model predicted versus experimentally measured data for COD utilisation

- **Biomass Growth**

In the absence of OHO biomass, the other expected microorganisms in the batch reactor included ANOs and MAB. The ANOs have a very low yield compared to the MAB biomass. However, the ANOs were observed to collaborate with the MAB for ammonia removal (i.e., both utilised large quantities of ammonia for growth). In addition to ammonia, the MAB is modelled to utilise other nitrogen sources, such as nitrates (NO_3), for growth. The MAB and ANO biomass also require small amounts of phosphate as a nutrient and use dissolved carbon dioxide as a carbon source for anabolism.

As noted in the graphs below (Figure 4.21), the model replicated biomass (MAB) growth very well. This means that the split of N use was accurately captured between ANOs and MAB biomass. The kinetics of MAB death and growth were therefore calibrated to suit the various conditions of the batch tests used in this study. Given this, the allocation of ammonia, used as a substrate by both microorganisms, could be evaluated.

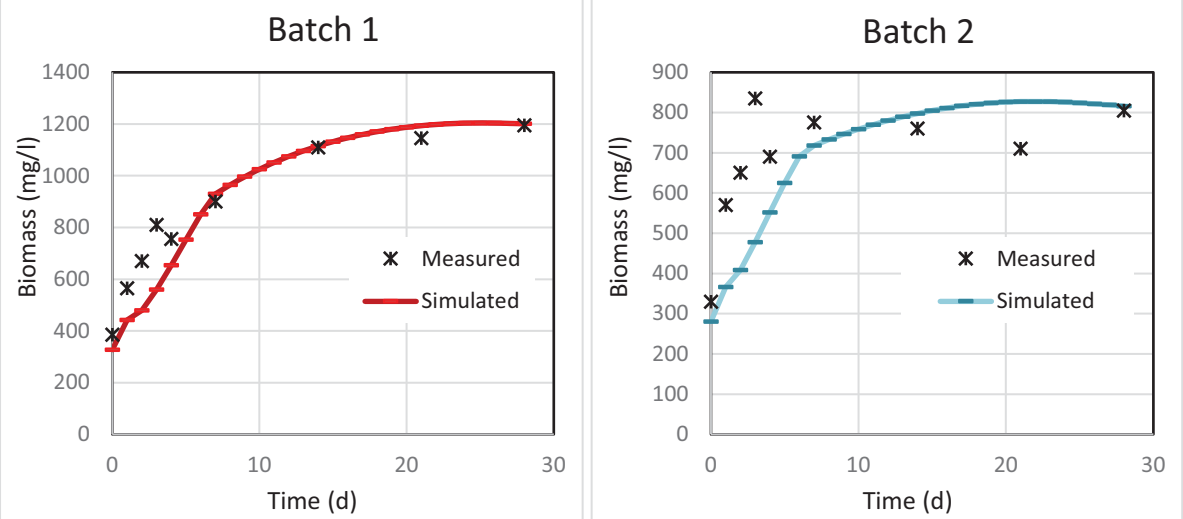

Figure 4.21: Model predicted versus experimentally measured data for MAB biomass growth

- **Ammonia Utilisation**

The sources of ammonia in the MAB system are primarily the influent wastewater and the N released during the hydrolysis of biodegradable organics (including dead biomass). Ammonia is primarily used by either the ANOs (largely as an electron donor for their catabolic processes) or the MAB. The calibration of ammonia utilisation using batch reactor tests was quite complex because it relied a lot on knowing (i) the initial concentrations of the ANO and MAB biomass in the reactor and (ii) the accuracy of the MAB death rate and the rate of fermentation of the FBSO.

The graphs below (Figure 4.22) compare model-simulated and experimentally measured data. The model replicates the trend in ammonia utilisation reasonably well. However, the experimentally measured value shows an initial increase in ammonia, followed by a subsequent reduction. This may be due to the ANOs' acclimatisation prior to subsequent growth and ammonia uptake, or to insufficient oxygen to promote ANO growth during the early phase of the batch test. Given that the ANOs do not constitute a significant portion of the biomass population, it is understandable that the biomass prediction was well replicated, whereas NH4 utilisation

was not. The sudden increase in ammonia during this early stage of the batch reactor can be attributed to the N released by the organics broken down (and not utilised) at the start of the batch test. From the 4th day onward, ammonia utilisation accelerates, resulting in nitrate formation.

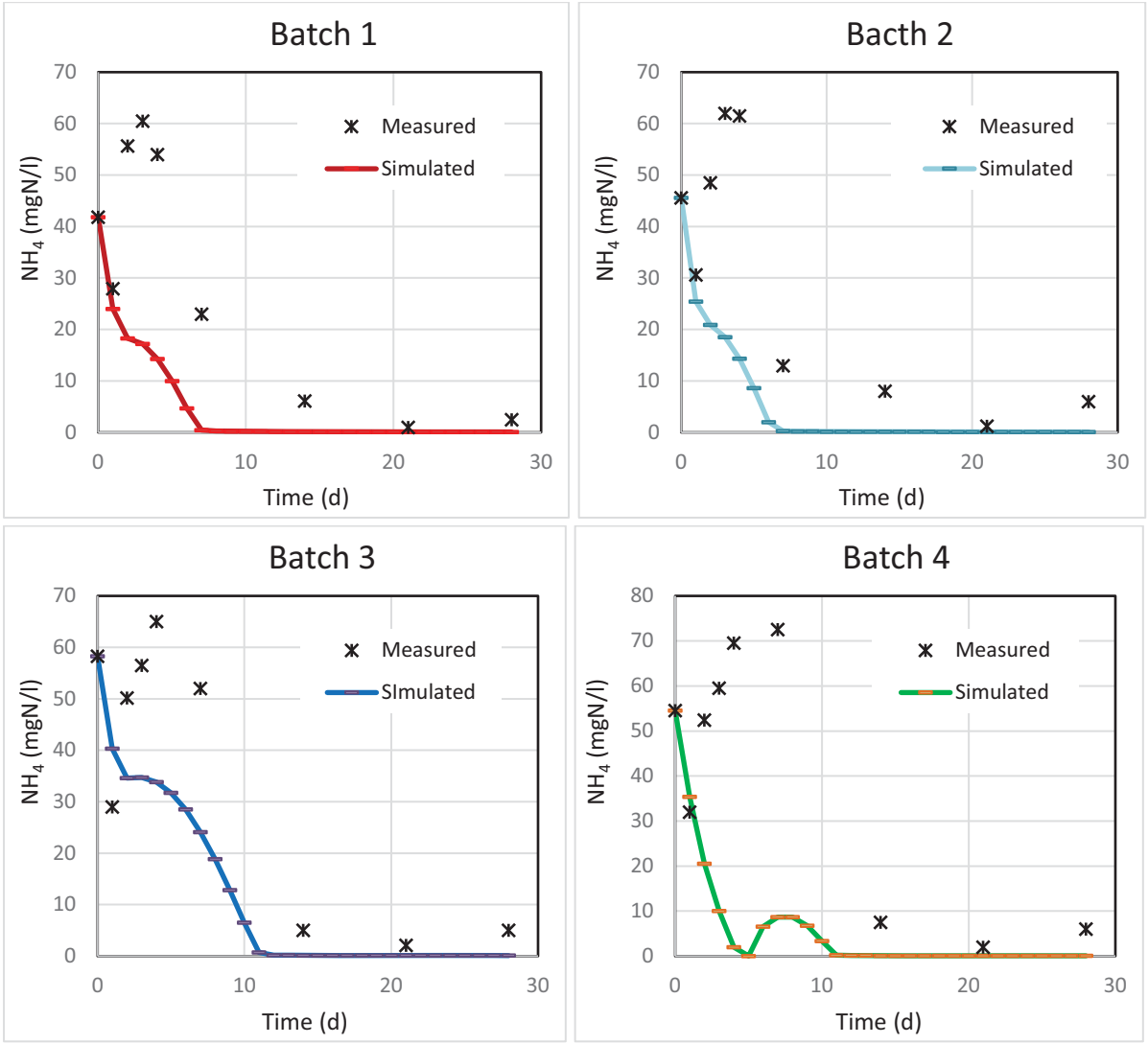

Figure 4.22: Model predicted versus experimentally measured data for ammonia utilised

- **Nitrates Generation**

The nitrates are generated from the process of nitrification (mediated by ANOs). However, the nitrates could be used by either MABs (as N source) or by facultative OHOs (as an electron donor during the absence of oxygen- i.e. anoxic conditions; Henze *et al.*, 2008). The graphs below (Figure 4.23) show that the model can capture the trend in nitrate generation across all batch tests used in this study. Further work may later be used towards selectively evaluating the ANOs' utilisation of nitrates – this could be done through aeration of the reactors (to eliminate the effect of facultative OHOs) and carrying out the test in the dark (to eliminate the influence of MAB). In this way, once ANO growth is calibrated, the MAB's distinct function can be more easily calibrated against the experimental data.

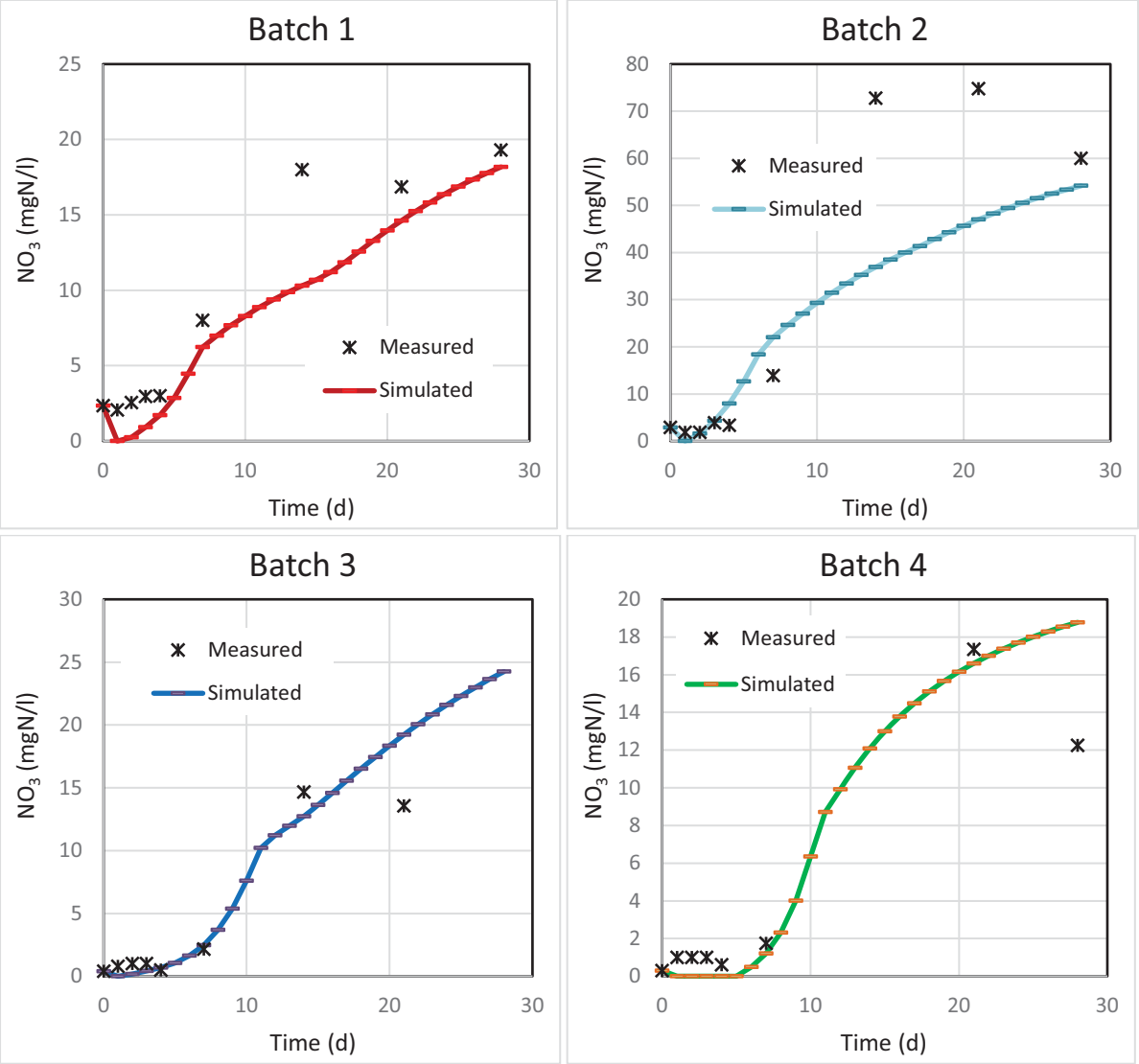

Figure 4.23: Model predicted versus experimentally measured data for nitrates generated

4.4 Closure

This study demonstrates the value of integrating algal-bacterial (MAB) processes into a plant-wide modelling framework for TWW treatment. By extending the UCT PWM_SA model to include microalgal and nitrifying biomass growth, we have created a tool capable of simulating the dynamic interactions between algae, bacteria, and wastewater constituents under realistic conditions.

The batch reactor experiments provided critical data for calibrating key growth, decay, and nutrient utilisation parameters. The close agreement between simulated and observed COD removal, biomass production, and nitrogen transformation confirms that the model accurately represents the dominant biological processes. Importantly, this approach highlights the role of oxygen generated by microalgae in supporting heterotrophic activity, as well as the complementary function of MAB and ANO populations in ammonia removal.

While the model performs well in predicting system behaviour, further refinement is needed to represent early-phase ammonia dynamics better and to disentangle nitrate consumption

pathways under different operating conditions. Future work should focus on validating the model at larger scales, exploring its sensitivity to light intensity and diurnal cycles, and adapting it for real-time control and optimisation of TWW treatment systems.

Overall, this work lays the foundation for the use of advanced, integrated models to design and optimise sustainable, low-energy treatment solutions for high-strength industrial wastewaters, thereby supporting both environmental compliance and resource recovery goals.

CHAPTER 5: PLANT-WIDE DYNAMIC MODELLING, SYSTEM INTEGRATION, AND PERFORMANCE EVALUATION

5.1 Introduction

This study demonstrates that single technologies cannot reliably treat TWW in isolation. Instead, a purpose-designed, integrated treatment train is required. This process comprises a two-stage HLFCR, downstream AD, and tertiary polishing via a microalgal-bacterial (MAB) reactor – a configuration capable of meeting regulatory standards while enabling resource recovery.

Building on previous chapters that established the independent kinetics of the HLFCR, AD, and MAB subsystems, this chapter consolidates them into a dynamic plant-wide model. Implemented in DHI WEST using the UCT PWM_SA framework, the model evaluates reactor sizing and retention time (HRT/SRT) optimisation and assesses system stability under complex TWW loading.

As illustrated in Figure 5.1 The subsystems are linked in series: the HLFCR facilitates sulphate reduction and sulphur recovery, thereby protecting the AD from sulphide inhibition. At the same time, the AD recovers methane, and the MAB system performs nitrogen polishing. The compatibility of these models enabled the seamless, dynamic transfer of all state variables (including organic, sulphur, and nitrogen species) during simulation.

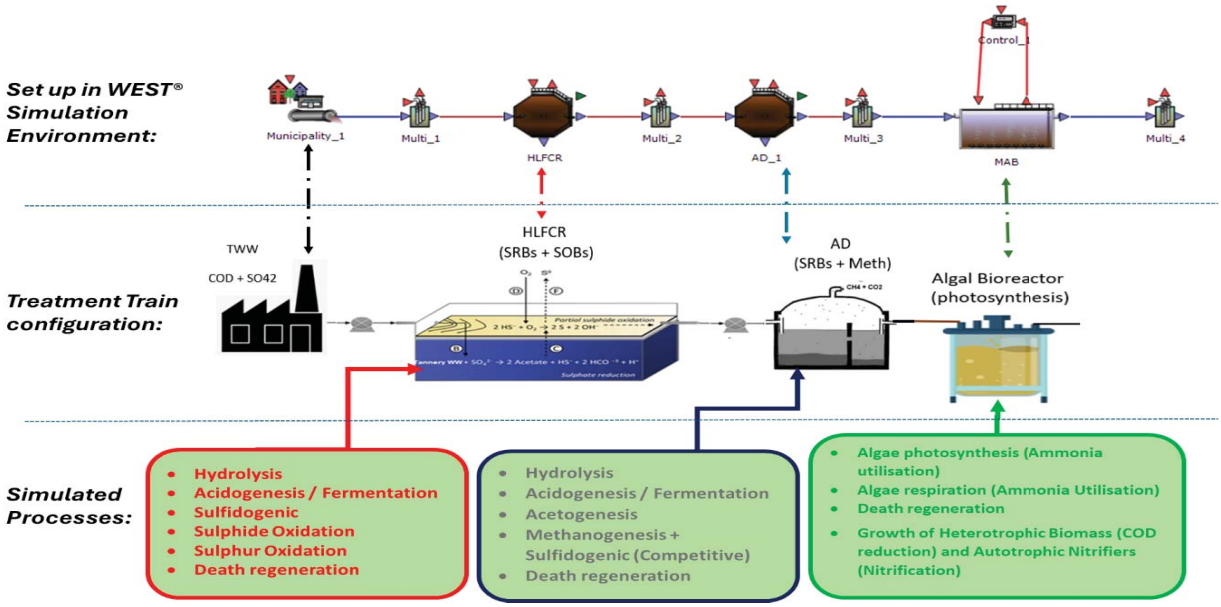

Figure 5.1: Plant-wide configuration of the integrated HLFCR–AD–MAB treatment train in the PWM_SA dynamic model

5.2 Influential Characteristics

Based on experimental work by Opus (2025), the unbiodegradable soluble and particulate fractions of treated wastewater were determined, along with measured total and soluble TKN and COD concentrations used to define influent components. The COD and TKN block diagrams for TWW concentration are shown in Figures 5.2 and 5.3 respectively.

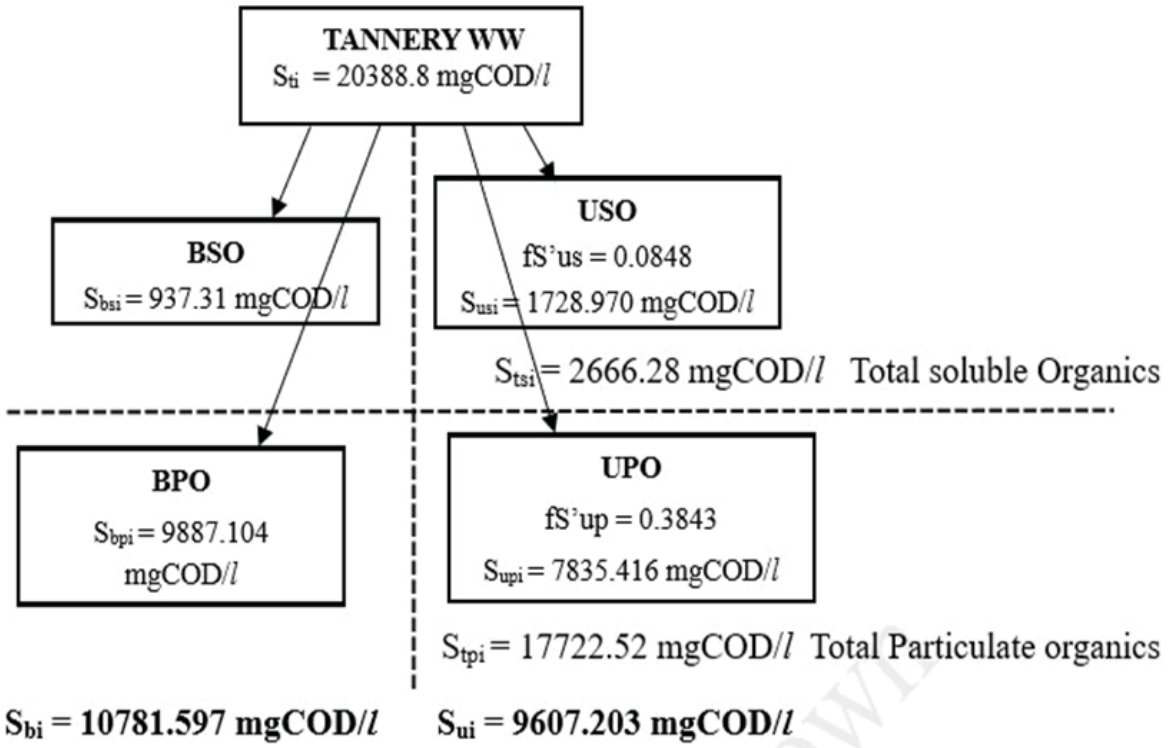

Figure 5.2: TWW COD characteristics block diagram

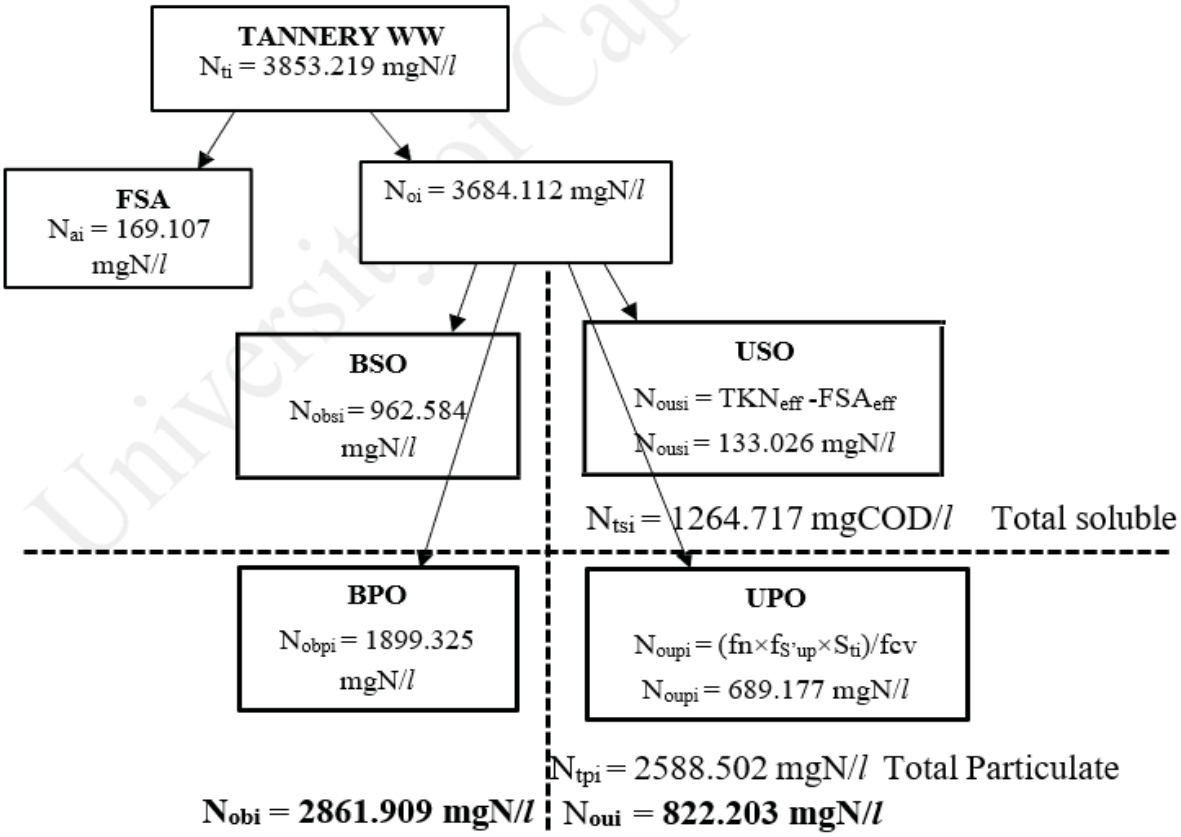

Figure 5.3: TWW TKN Characteristics block diagram

The COD and TKN characteristics were then translated by Opus (2025) into a typical PWM_SA model in our components, as shown in Table 5.1 towards carrying out the simulation exercise.

Table 5.1: Characteristics of the RAW TWW

Tannery Wastewater Batches					
Name	**Denotation**	**Units**	**Percentages**		**Values**
Total COD (Unfiltered)	T-COD	mgCOD/l			20388.8
Soluble COD (filtered)	T-COD (Filt)	mgCOD/l			2666.3
Total Kjeldahl Nitrogen	TKN	mgN/l			3853.2
Model Input Components					
Name	**Denotation**	**Units**	**Percentages**		
Unbiodegradable Soluble organics	S_U (USO)	mgCOD/l	8.48%		1623.6
Unbiodegradable Particulate Organics	X_U (UPO)	mgCOD/l	38.43%		8551.3
Biodegradable Particulate Organics	X_B_Org (BPO)	mgCOD/l	46.24%		9171.2
Glucose	S_GLU (BSO)	mgCOD/l	6.85 %	50%	521.3
Propionate	S_Pr (BSO)	mgCOD/l		15%	156.4
Acetate	S_VFA (BSO)	mgCOD/l		35%	364.9
Ammonia	S_NHx	mg/l as N	4.0%		169.1
Organic nitrogen	X_N_Org	mgN/l	96.0%		3684.1
Sulphates	S_SO4	$mgSO_4^{2-}$ /l			5141.5
Chlorides	S_CL	mg/l			5361.0
Sodium	S_Na	mg/l			3574.0

The elemental composition of PO was established using the Volcke *et al.* (2006) procedure, with carbon and phosphorus proportions derived from Mpofu *et al.* (2022), and COD and nitrogen proportions derived from the study's experimental data. The results determined in this way by Opus (2025) are shown in Table 5.2 below.

Table 5.2: Elemental composition of the TWW

Particulate Organics (PO)
$C_{4.506}H_7O_{2.004}N_{0.745}P_{0.013}$
Unbiodegradable Particulate Organics (UPO; Denoted In Model As X_U_Inf)
$C_{4.734}H_7O_{1.988}N_{0.766}P_{0.028}$
Biodegradable Particulate Organics (BPO; Denoted In Model As X_B_Inf)
$C_{4.339}H_7O_{2.017}N_{0.730}P_{0.003}$

The elemental characterisation of the BPO to the form $C_{4.339}H_7O_{2.017}N_{0.730}P_{0.003}$ allows for the determination of the hydrolysis products up to the simplest products of biological metabolism, like CO_2, NH_4^+, CH_4, $H_2PO_4^-$, etc.

For the given influent characteristics, an influent flow rate of 1,000 m³/d (1 ML/d) was selected for all simulations. The simulations performed included the following:

- HLFCR sizing optimisation for sulphate control
- AD SRT selection and sizing for biogas generation
- MAB volume optimisation for N removal
- Evaluation of resource recovery for adjusted influent (via significant changes in SO_4/COD and N/COD ratios).

5.3 HLFCR Optimisation for Sulphate Control

The first step in applying the model to simulate TWW treatment was to size the reactor. HLFCR reactor size optimisation was performed to determine the optimal reactor size for sulphate removal in TWW. This involved simulating SO_4 removal as a function of HLFCR volume. The Figure 5.4 presents the results of this simulation.

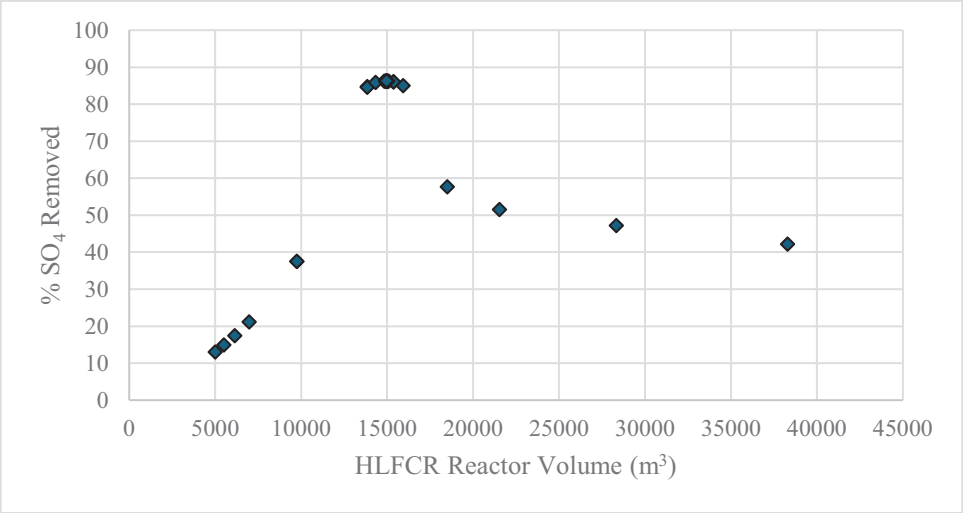

Figure 5.4: The % sulphates removed with adjusted reactor volume (i.e., sizing for SO_4 removal)

As shown in Figure 5.4 The simulation-based sizing process indicated an optimal HLFCR volume of approximately 14950 m³, achieving approximately 86.3% sulphate removal while maintaining controlled dissolved sulphide. This is in line with the function of the HLFCR within the TWW treatment train – i.e. sulphur buffering reactor, preventing sulphide toxicity to AD.

5.4 Performance of AD with Sulphate Pre-Removal

Following size optimisation of the HLFCR for sulphate removal, the reactor was virtually connected to the AD for subsequent simulations; these sequential simulations required optimising the AD SRT to maximise biogas production. Noting that, for a completely mixed AD reactor (HRT = SRT), the connection of the AD to the HLFCR (i.e., the fixed HLFCR effluent is the AD influent feed), requires the adjustment to SRT AD inflow connected to HLFCR; AD volume adjustment is required for its SRT optimisation.

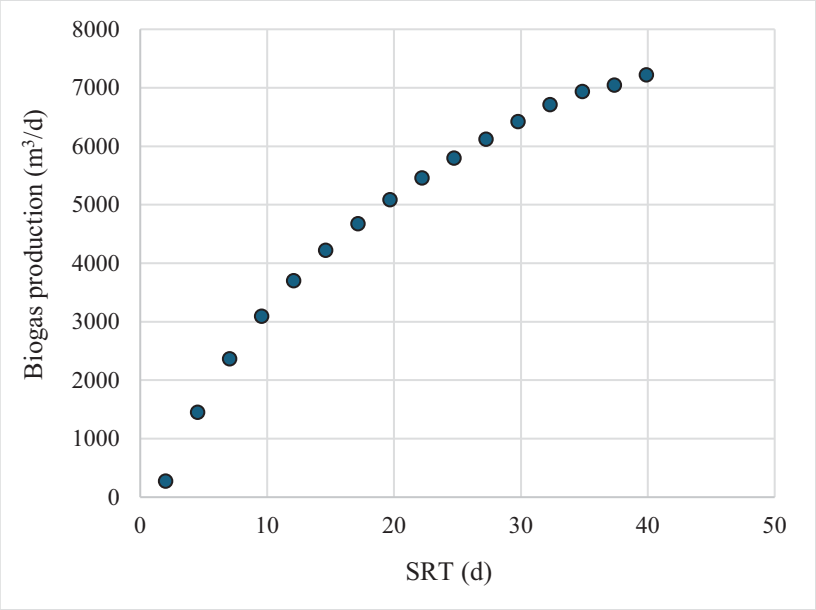

Figure 5.5: The biogas production with adjusted SRT (i.e., sizing for methane generation)

Figure 5.5 shows that, in the simulated AD SRT optimisation, biogas production begins to level off after 30d SRT, with little difference between 30d and 40d. The simulations also demonstrate that sulphate control via the HLFCR upstream of the AD restores methanogenic dominance in the AD, thereby stabilising biogas generation and associated energy recovery.

5.5 MAB Nitrogen Polishing Behaviour

Completing the treatment train for the TWW treatment system required the final connection of the HLFCR-AD to the MAB unit process. Having optimised the size for the HLFCR and AD systems, the MAB was virtually connected to the HLFCR -AD (hence the effluent from the AD was the influent feed to the MAB system). For this complete treatment train, the first set of simulations involved adjusting the MAB reactor size towards optimising nitrogen (N) removal.

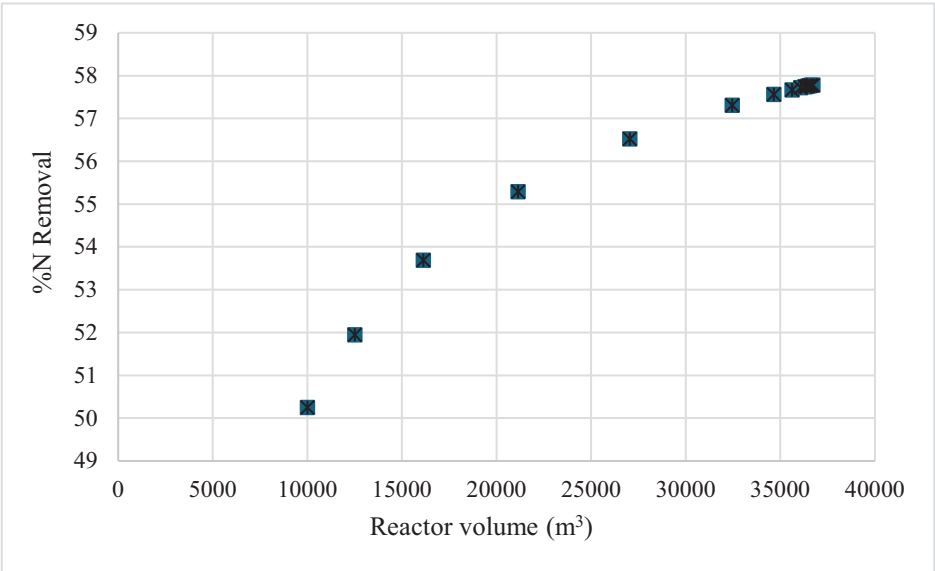

Figure 5.6: MAB reactor volume adjustment with N removal

Figure 5.6 shows that increasing the MAB reactor volume from 10 ML to 35 ML yielded only about 8% improvement in N removal, indicating that: (i) the N removal is limited by carbon/redox balance, not volume, and (ii) it is important to have integrated upstream management of COD (i.e., via the AD process the preceded the MAB). Therefore, N polishing performance depends on whole-system interactions rather than standalone sizing.

5.6 System-Wide Scenario Analysis

On finally sizing and connecting the HLFCR-AD- MAB unit operations for the treatment train fed TWW, a set of dynamic simulations was performed, based on the following scenarios of influent variability:

- Scenario 0 (S0) - Base scenario with default current influent
- Scenario 1 (S1) - Influent has increased SO_4/COD ratio by 50% of current Influent
- Scenario 2 (S2) - Influent has decreased SO_4/COD ratio by 50% of current Influent
- Scenario 3 (S3) - Influent has increased N/COD ratio by 50% of current Influent
- Scenario 4 (S4) - Influent has decreased N/COD ratio by 50% of current Influent

When performing these simulations, there was a check for:

i. The quantity of influent COD that was converted to biogas and the amount that remained as residual COD.
ii. The quantity of sulphates that was converted to elemental sulphur and the amount that went out as residual sulphates and sulphides.
iii. The nitrogen that was converted to nitrates, denitrified to nitrogen gas and used to grow MAB biomass.

Table 5.3 together with Figures 5.7 and 5.8 shows the conversion of sulphate to sulphur and sulphides in the HLFCR unit process, and the biogas generation from the subsequently connected AD unit process.

Table 5.3: Biogas and sulphur recovery from HLFCR-AD of the integrated system

Variable	Scenario 0: Base	Scenario 1: +50% SO_4/COD	Scenario 2: -50% SO_4/COD
Biogas generated (gCOD/l Influent)	16,2	23,8	16,6
Elemental sulphur (mgS/l Influent)	10,0	12,5	6,4
Residual Sulphides (mgS/l Influent)	10,6	11,1	6,5
H_2S production (gS/l Influent)	15,4	18,8	9,0

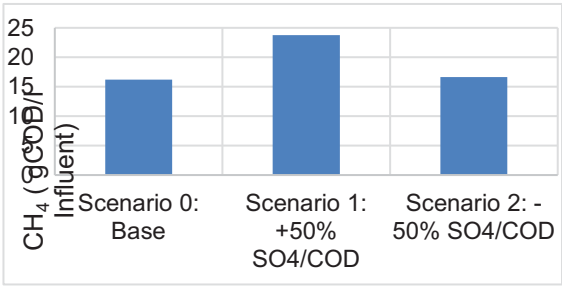

Figure 5.7: Methane generation in the integrated system under adjusted influent SO_4/COD ratios

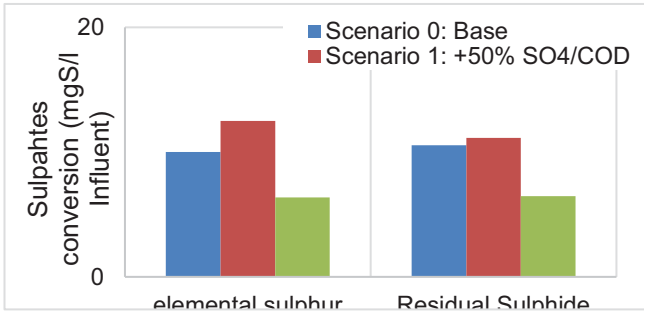

Figure 5.8: Sulphate Transformation in the Integrated System (Adjusted SO_4/COD)

Evaluating the sulphur fate under different influent SO_4/COD ratios, it is notable that the HLFCR consistently converts sulphate to elemental sulphur and some sulphides. However, the graph shows that the residual sulphide carryover is sufficiently limited to ensure maintenance of AD stability (i.e., due to upstream sulphur control). Hence, according to simulations of the integrated virtual system, the HLFCR maintains sulphur conversion even under load shifts; without it, AD inhibition could occur. Table 5.4 and Figure 5.9 present the findings from Scenarios 3 and 4, in which the MAB polishing step of the integrated system was evaluated in response to adjustments in nitrogen load.

Table 5.4: Nitrogen removal in MAB polishing of an integrated system

Variable	Scenario 0: Base	Scenario 3: +50% N/COD	Scenario 4: -50% N/COD
Nitrogen to nitrates	84,2	113,1	49,9
Nitrates denitrified	110,8	143,0	64,1
N for biomass growth	125,6	164,1	77,8

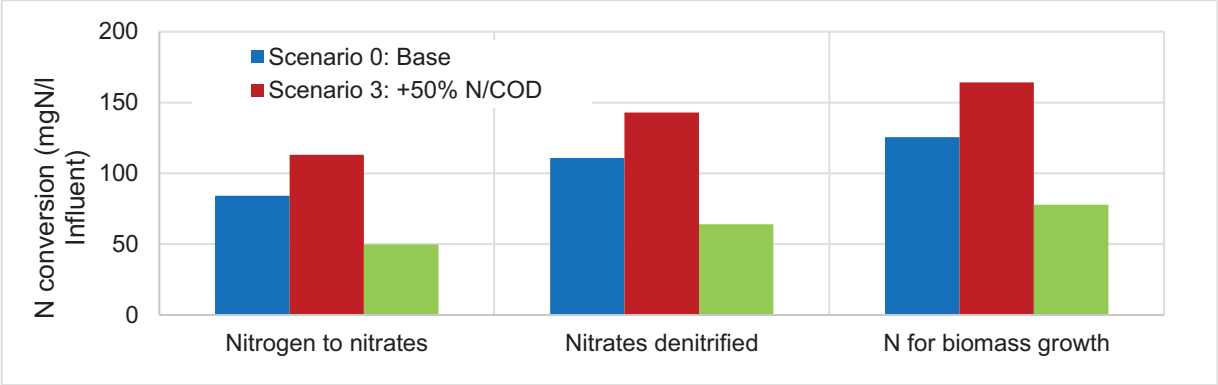

Figure 5.1: Nitrogen conversion pathways within the integrated system

The differences in the results for S0, S3, and S indicate that nitrogen removal in the system is governed by the N/COD balance, thereby necessitating integrated control. The biomass contributing to N removal in the MAB reactor comprises microalgae and ANOs. However, for denitrification to occur, the facultative heterotrophic biomass is required to mediate the process (Henze *et al.*, 2008). The removal of organics in the AD prior to the MAB does not necessarily limit denitrification, because the death and decay of MAB biomass provide a source of organic

carbon (an electron donor for denitrification) to react with the nitrates generated by the ANO biomass population.

5.7 Closure

The integrated simulations confirm that the HLFCR - AD - MAB system behaves as a coupled sulphur–carbon–nitrogen biogeochemical platform. Stability, compliance, and resource recovery are achieved only when these cycles are managed in concert. The results from the system-wide simulation demonstrate the importance of cycle coupling for ensuring stability that would otherwise be difficult to achieve using single technologies. The integrated train showcases, system synergy such that: (i) the operation of AD alone would result in sulphide inhibition (and poor biogas generation), (ii) the MAB alone would result in carbon limitation, (iii) the HLFCR alone would result in presence of residual COD & N. Hence there is significant benefit in the integrated setup which simultaneously produces methane from AD, elemental sulphur from HLFCR, and algal biomass (from MAB reactor) confirming the circular economy feasibility of the process.

CHAPTER 6: CONCLUSIONS AND RECOMMENDATIONS

This study demonstrates that TWW cannot be reliably treated using a single technology. Instead, consistent performance requires a purpose-designed, integrated treatment train comprising a two-stage HLFCR, downstream AD, and tertiary polishing using a microalgal-bacterial (MAB) reactor. Together, these units form a system capable of meeting regulatory discharge requirements while enabling resource recovery and water reuse.

Experimental results, supported by dynamic plant-wide modelling, identify upstream sulphate control in the HLFCR as the key factor governing overall system stability. By removing sulphate and converting sulphide into recoverable elemental sulphur, the HLFCR mitigates sulphide toxicity and restores favourable conditions for methanogenesis in the AD unit. Within the digester, TWW behaviour is well described by Contois-type kinetics, with clear evidence of substrate-driven inhibition at high organic loading rates. These relationships define practical operating envelopes that maintain process stability and optimise methane production.

At the tertiary stage, MAB polishing effectively closes the nitrogen cycle under realistic operational controls. Intermittent aeration coordinated with light–dark cycles, together with the addition of modest amounts of readily biodegradable carbon, supports ammonia and nitrate removal while promoting algal growth. The resulting algal biomass constitutes a valuable co-product, provided that appropriate metal risk management strategies are in place.

Overall, the integrated HLFCR–AD–MAB system represents a transition from end-of-pipe pollution control to resource-optimised water management. The treatment train produces effluent that is suitable for discharge or reuse while recovering renewable methane, elemental sulphur, and protein-rich biomass. The dynamic plant-wide model developed in this study further strengthens this approach by serving as a decision-support tool for reactor design, operational optimisation, and risk management under variable influent conditions.

Two immediate priorities emerge from this work. First, pilot-scale validation of the complete HLFCR-AD-MAB train under diurnal and seasonal variability is needed to confirm its robustness, refine control strategies, and quantify lifecycle costs and benefits. Second, further model development should focus on short-term nitrogen dynamics - including acclimation, hydrolysis, and storage processes, as well as carbon-management strategies such as internal fermentation or minimal external dosing. These refinements will enhance the model's predictive capability and its usefulness for guiding real-world operation.

REFERENCES

Achouri, O., Panico, A., Bencheikh-Lehocine, M., Derbal, K. and Pirozzi, F. (2017) 'Effect of chemical coagulation pretreatment on anaerobic digestion of tannery wastewater', Journal of Environmental Engineering, 143(9), p. 04017039.

Aditya, L., Vu, H.P., Johir, M.A.H., Mahlia, T.M.I., Silitonga, A.S., Zhang, X., Liu, Q., Tra, V.-T., Ngo, J.J. and Nghiem, L.D. (2023) 'Role of culture solution pH in balancing CO_2 input and light intensity for maximising microalgae growth rate', Chemosphere, 343, 140256. https://doi.org/10.1016/j.chemosphere.2023.140255

Ahmad, S.F.K., Lee, K.T. and Vadivelu, V.M. (2023) 'Emerging trends of microalgae bio-granulation in wastewater treatment: A bibliometric analysis from 2011 to 2023', Biocatalysis and Agricultural Biotechnology, 50(4), 102684. https://doi.org/10.1016/j.bcab.2023.102684

Ahmed, M.D.D., Maraz, K.M. and Amin Khan, R. (2021) 'Prospects and challenges of chrome tanning: Approach a greener technology in the leather industry', Scientific Review, (73), pp. 42–49. https://doi.org/10.32861/sr.73.42.49

Alex Kibangou, V., Lilly, M., Mpofu, A.B., de Jonge, N., Oyekola, O.O. and Welz, P.J. (2022) 'Sulfate-reducing and methanogenic microbial community responses during anaerobic digestion of tannery effluent', Bioresource Technology, 347, 126308. https://doi.org/10.1016/j.biortech.2021.126308

Amen, T.W.M., Eljamal, O., Khalil, A.M.E. and Matsunaga, N. (2018) 'Evaluation of sulfate-containing sludge stabilization and the alleviation of methanogenesis inhibition at mesophilic temperature', Journal of Water Process Engineering, 25, pp. 212–221. https://doi.org/10.1016/j.jwpe.2018.08.004

Andreotti, V. (2017) 'Microalgae in aquaculture wastewater: a new forecasting method of production in a marine system', Universitat Politècnica de Catalunya, 4(1), pp. 9–15. (Note: this appears incomplete—if it's a thesis/report, send the full details and I'll correct it.)

Annachhatre, A.P. and Suktrakoolvait, S. (2001) 'Biological sulfate reduction using molasses as a carbon source', Water Environment Research, 73(1), pp. 118–126. https://doi.org/10.2175/106143001X138778

Arashiro, L.T., Rada-Ariza, A.M., Wang, M., Van der Steen, P. and Ergas, S.J. (2017) 'Modelling shortcut nitrogen removal from wastewater using an algal-bacterial consortium', Water Science and Technology, 75(4), pp. 782–792.

Armitano, J., Méjean, V. and Jourlin-Castelli, C. (2013) 'Aerotaxis governs floating biofilm formation in Shewanella oneidensis', Environmental Microbiology, 15(11), pp. 3108–3118. https://doi.org/10.1111/1462-2920.12158

Arun, S., Ramasamy, S. and Pakshirajan, K. (2021) 'Mechanistic insights into nitrification by microalgae-bacterial consortia in a photo-sequencing batch reactor under different light intensities', Journal of Cleaner Production, 321, 128752. https://doi.org/10.1016/j.jclepro.2021.128752

Arutselvan, C., Narchonai, G., Pugazhendhi, A., Seenivasan, H.K., Lewis, O.F. and Thajuddin, N. (2022) ‘Phycoremediation of textile and tannery industrial effluents using microalgae and their consortium for biodiesel production’, Journal of Cleaner Production, 367, 133100. https://doi.org/10.1016/j.jclepro.2022.133100

Bagheri Novair, S., Biglari Quchan Atigh, Z., Asgari Lajayer, B., Shu, W. and Price, G.W. (2024) ‘The role of sulphate-reducing bacteria (SRB) in bioremediation of sulphate-rich wastewater: Focus on the source of electron donors’, Process Safety and Environmental Protection. https://doi.org/10.1016/j.psep.2024.01.103

Baldisserotto, C., Gessi, S., Ferraretto, E., Merighi, S., Ardondi, L., Giacò, P., Travagli, A. and Pancaldi, S. (2024) ‘Cultivation modes affect the morphology, biochemical composition, and antioxidant and anti-inflammatory properties of the green microalga’, Protoplasma. https://doi.org/10.1007/s00709-024-01958-7

Batstone, D.J., Keller, J., Angelidaki, I., Kalyuzhnyi, S.V., Pavlostathis, S.G., Rozzi, A., Sanders, W.T.M., Siegrist, H. and Vavilin, V.A. (2002) ‘The IWA Anaerobic Digestion Model No. 1 (ADM1)’. (Note: please confirm source type—often this is a scientific paper/report. Provide journal/report details and I’ll finalise.)

Berben, T. (2019) Comparative analysis of sulfur oxidation pathways in haloalkaliphilic thiocyanate-utilizing species of the genus Thioalkalivibrio. (PhD thesis). ISBN 9789491407697. (Institution/location needed for full Harvard.)

Bernard, O., Masci, P. and Sciandra, A. (2009) ‘A photobioreactor model in nitrogen limited conditions’. (Note: incomplete—journal/conference details needed.)

Bhatti, S., Richards, R., Wall, C.L., MacPherson, M.J., Stemmler, K., Lalonde, C.G., Patelakis, S.J.J., Tibbetts, S.M. and McGinn, P.J. (2023) ‘Phycoremediation and simultaneous production of protein-rich algal biomass from aquaculture and agriculture wastewaters’, Journal of Chemical Technology and Biotechnology, 98, pp. 1918–1935. https://doi.org/10.1002/jctb.7409

Broekhuizen, N., Park, J.B.K., McBride, G.B. and Craggs, R.J. (2012) ‘Modification, calibration and verification of the IWA River Water Quality Model to simulate a pilot-scale high rate algal pond’, Water Research, 46(9), pp. 2911–2926. https://doi.org/10.1016/j.watres.2012.03.011

Bryantseva, K., Gorlenko, V.M., Kompantseva, E., Imhoff, J.F., Suling, J. and Mityushina, L. (1997) ‘Thiorhodospira sibirica gen. nov., sp. nov., a new alkaliphilic purple sulfur bacterium from a Siberian soda lake’, International Journal of Systematic Bacteriology, 45. (Note: year/volume/pages appear inconsistent in your entry—please confirm and I’ll correct.)

Buhr, H.O. and Miller, S.B. (1983) ‘A dynamic model of the high-rate algal-bacterial wastewater treatment pond’, Water Research, 17(1), pp. 29–37.

Camiloti, P.R., Oliveira, G.H.D. and Zaiat, M. (2016) ‘Sulfur recovery from wastewater using a micro-aerobic external silicone membrane reactor (ESMR)’, Water, Air, & Soil Pollution, 227(1). https://doi.org/10.1007/s11270-015-2721-y

Caparroz, M., Guzman, J.L., Berenguel, M. and Acién, F.G. (2024) ‘A novel data-driven model for prediction and adaptive control of pH in a raceway reactor for microalgae cultivation’, New Biotechnology, 82, pp. 1–13. https://doi.org/10.1016/j.nbt.2024.04.001

Cardoso, R.B., Sierra-Alvarez, R., Rowlette, P., Flores, E.R., Gómez, J. and Field, J.A. (2006) 'Sulfide oxidation under chemolithoautotrophic denitrifying conditions', Biotechnology and Bioengineering, 95(6), pp. 1148–1155. https://doi.org/10.1002/bit.21084

Casagli, F., Zuccaro, G., Bernard, O., Steyer, J.-P. and Ficara, E. (2021) 'ALBA: A comprehensive growth model to optimize algae-bacteria wastewater treatment in raceway ponds', Water Research, 190, 116734. https://doi.org/10.1016/j.watres.2020.116734

Chabane, Y.N., Marti, S., Rihouey, C., Alexandre, S., Hardouin, J., Lesouhaitier, O., Vila, J., Kaplan, J.B., Jouenne, T. and Dé, E. (2014) 'Characterisation of pellicles formed by Acinetobacter baumannii at the air-liquid interface', PLOS ONE, 9(10), e111660. https://doi.org/10.1371/journal.pone.0111660

Chatterjee, S. and Hausinger, R.P. (2022) 'Sulfur incorporation into biomolecules: recent advances', Critical Reviews in Biochemistry and Molecular Biology. https://doi.org/10.1080/10409238.2022.2141678

Chen, S., Li, X., Ma, X., Qing, R., Chen, Y., Houzhen, Z., Yu, Y., Li, J. and Tan, Z. (2023) 'Lighting the way to sustainable development: Physiological light control strategy in microalgae-based wastewater treatment under illumination', Science of the Total Environment, 903, 155298. (Note: https://doi missing in your entry—add if you want it included.)

Chowdury, K.H., Nahar, N. & Deb, U.K. 2020. The Growth Factors Involved in Microalgae Cultivation for Biofuel Production: A Review. Computational Water, Energy, and Environmental Engineering, 09(04): 185–215.

Cicci A., Scarponi P., Cavinato C., Bravi M. 2024 Microalgae production in olive mill wastewater fractions and digestate slurry: Bioremediation effects and suitability for energy feed uses. Science of the Total Environment 932: 172773 https://doi.org/10.1016/j.scitotenv.2024.172773

Colman, D. R., Lindsay, M. R., Amenabar, M. J., & Boyd, E. S. (2019). The Intersection of Geology, Geochemistry, and Microbiology in Continental Hydrothermal Systems. Astrobiology, 19(12), 1505–1522. https://doi:10.1089/ast.2018.2016. ISSN:15311074.

Cope, K. (2021). A Report on Vegetable Tanning. ISSN:1920-4159.

Corominas, L., Rieger, L., Takács, I., Ekama, G., Hauduc, H., Vanrolleghem, P. A., Oehmen, A., Gernaey, K. V., Van Loosdrecht, M. C. M., & Comeau, Y. (2010). New framework for standardized notation in wastewater treatment modelling. Water Science and Technology, 61(4), 841–857. https://doi:10.2166/wst.2010.912. ISSN:02731223.

Costa, R. B., O'Flaherty, V., & Lens, P. N. L. (2020). Biological treatment of organic sulfate-rich wastewaters. In Environmental Technologies to Treat Sulfur Pollution: Principles and Engineering -2nd Edition (pp. 167–213). IWA Publishing. https://doi:10.2166/9781789060966_0167. ISBN: 9781789060966.

da Fontoura JT, Rolim GS, Farenzena M, Gutterres M (2017) Influence of light intensity and tannery wastewater concentration on biomass production and nutrient removal by microalgae Scenedesmus sp. Process Safety and Environmental Protection 111: 355–362. https://doi.org/10.1016/j.psep.2017.07.024

Dahl, C. (2020). A biochemical view on the biological sulfur cycle. In Environmental Technologies to Treat Sulphur Pollution: Principles and Engineering (pp. 55–96). IWA Publishing. https://doi:10.2166/9781789060966_0055. ISBN: 9781789060966

Das C, Naseera K, Ram A, Meena RM, Ramaiah N (2017). Bioremediation of tannery wastewater by a salt-tolerant strain of Chlorella vulgaris. Journal of Applied Phycology 29: 235-243 https://doi.org/10.1007/s10811-016-0910-8

Devi, A., Verma, M., Saratale, G.D., Saratale, R.G., Ferreira, L.F.R., Mulla, S.I. & Bharagava, R.N. 2023a. Microalgae: A green eco-friendly agents for bioremediation of tannery wastewater with simultaneous production of value-added products. Chemosphere, 336(June): 139192. https://doi.org/10.1016/j.chemosphere.2023.139192

Droop, M.R. 1968. Vitamin B12 and Marine Ecology. IV. The Kinetics of Uptake, Growth and Inhibition in Monochrysis Lutheri. Journal of the Marine Biological Association of the United Kingdom, 48(3): 689–733.

E Contois, B. D. (1959). Kinetics of Bacterial Growth: Relationship between Population Density and Specific Growth Rate of Continuous Cultures. J. gen. Microbial (Vol. 21).

Eastman, J. A., & Ferguson, J. F. (1981). Solubilization of Particulate Organic Carbon during the Acid Phase of Anaerobic Digestion. Journal (Water Pollution Control Federation) (Vol. 53).

Ekama, G. A. (2009b). Using bioprocess stoichiometry to build a plant-wide mass balance based steady-state WWTP model. Water Research, 43(8), 2101–2120. https://doi:10.1016/j.watres.2009.01.036. ISSN:00431354.

Ekinci K., Erdal I, Uysal F.Ö, Tunce H., Doğan A. 2019 Anaerobic digestion of three microalgae biomasses and assessment of digestates as biofertilizer for plant growth. Environmental Progress and Sustainable Energy 38: 1-9 https://doi/org/10.1002/ep

Ellacuriaga, M., Cascallana, J. G., González, R., & Gómez, X. (2021, August 1). High-solid anaerobic digestion: Reviewing strategies for increasing reactor performance. Environments - MDPI. MDPI AG. https://doi:10.3390/environments8080080. ISSN:20763298.

Etsuyankpa, M. B., Augustine, A. U., Musa, S. T., Mathew, J. T., Ismail, H., Salihu, A. M., & Mamman, A. (2024). An Overview of Wastewater Characteristics, Treatment and Disposal: A Review. Journal of Applied Sciences and Environmental Management, 28(5), 1553–1572. https://doi:10.4314/jasem.v28i5.28. ISSN:2659-1502

FAO/WHO Codex Alimentarious Commission 2021 Joint Food and Agriculture Organization of the United Nations and the World Health Organization Codex Committee on Contaminants in Food. Working Document CF/14 INF/1 April 2021.

Gallego, I.; Medic, N.; Pedersen, J. S.; Ramasamy, P. K.; Robbens, J.; Vereecke, E.; *et al.* (2025) The microalgal sector in Europe: Towards a sustainable bioeconomy. New Biotechnology 2025, 86, 1–13. https://doi:10.1016/j.nbt.2025.01.002.

Gao L, Ding W, Xi J, Gao S, Zhou X, Chen Y, Song K, Mao X, Tu R, Jiang G (2023) Effects of different nitrogen/phosphorus ratios on the growth and metabolism of microalgae Scenedesmus obliquus cultured in the mixed wastewater from primary settling. Process Safety and Environmental Protection 170: 824-833 https://doi.org/10.1016/j.psep.2022.12.059

García, J., Green, B.F., Lundquist, T., Mujeriego, R., Hernández-Mariné, M. & Oswald, W.J. 2006. Long term diurnal variations in contaminant removal in high rate ponds treating urban wastewater. Bioresource Technology, 97(14): 1709–1715.

Gargano, M., Bacardit, A., Sannia, G., & Lettera, V. (2023). From Leather Wastes back to Leather Manufacturing: The Development of New Bio-Based Finishing Systems. Coatings, 13(4). https://doi:10.3390/coatings13040775. ISSN:20796412.

Gehring, T., Silva, J.D., Kehl, O., Castilhos, A.B., Costa, R.H.R., Uhlenhut, F., Alex, J., Horn, H. & Wichern, M. 2010. Modelling waste stabilisation ponds with an extended version of ASM3. Water Science and Technology, 61(3): 713–720.

Gnaiger E, Bitterlich G. (1984) Proximate biochemical composition and caloric content calculated from elemental CHN analysis: a stoichiometric concept. Oecologia 62: 289-298 https://doi.org/10.1007/BF00384259

Goldberg, D. E. (2016). The Retreats of Reconstruction. ISBN: 0823272737.

González-Camejo J., Aparicio S, Pcahes M, Borras L, Seco A. (2022) Comprehensive assessment of the microalgae-based wastewater treatment systems: Relevant factors, evaluation methods and control strategies. Algal Research 61: 102563 https://doi.org/10.1016/j.algal.2021.102563

Grau, P., Vanrolleghem, P., & Ayesa, E. (2007). BSM2 Plant-Wide Model construction and comparative analysis with other methodologies for integrated modelling. Water Science and Technology, 56(8), 57–65. https://doi:10.2166/wst.2007.602. ISBN: 1843391481. ISSN:02731223

Grimm Aus Bonn, F. (2012). Regulation of the dsr operon and function of the proteins DsrR and DsrS in the purple sulfur bacterium Allochromatium vinosum.

Gururani, P., Bhatnagar, P., Kumar, V., Vlaskin, M.S., & Grigorenko, A. V. 2022. Algal Consortiums: A Novel and Integrated Approach for Wastewater Treatment. Water (Switzerland), 14(22).

Halfhide, T., Dalrymple, O.K., Wilkie, A.C., Trimmer, J., Gillie, B., Udom, I., Zhang, Q. & Ergas, S.J. 2015. Growth of an Indigenous Algal Consortium on Anaerobically Digested Municipal Sludge Centrate: Photobioreactor Performance and Modeling. Bioenergy Research, 8(1): 249–258.

Harding, T. H. (2020). A Prototype Dynamic model for the Co-Treatment of a High Strength Simple-Organic Industrial Effluent and Coal-mine drainage DOCTOR OF PHILOSOPHY.

Henkel, J. V., Dellwig, O., Pollehne, F., Herlemann, D. P. R., Leipe, T., & Schulz-Vogt, H. N. (2019). A bacterial isolate from the Black Sea oxidizes sulfide with manganese (IV) oxide. Proceedings of the National Academy of Sciences of the United States of America, 116(25), 12153–12155. https://doi:10.1073/pnas.1906000116. ISSN:10916490.

Henze, M., Grady, C. P. L., Gujer, W., Marais, G. V. R., & Matsuo, T. (1987). A general model for single-sludge wastewater treatment systems. Water Research, 21(5), 505–515. https://doi:10.1016/0043-1354(87)90058-3. ISSN:00431354

Henze, M. (2008) *Biological Wastewater Treatment: Principles, Modelling and Design*. IWA Publishing, London.

Hidaka T., Takabe Y., Tsumor, J., Minamiyama M. 2017 Characterization of microalgae cultivated in continuous operation combined with anaerobic co-digestion of sewage sludge and microalgae. Biomass and Bioenergy. 99: 139–146 https://doi.org/10.1016/j.biombioe.2017.02.019

Horn, E. J., Oyekola, O. O., Welz, P. J., & van Hille, R. P. (2022a). Biological desulfurization of tannery effluent using hybrid linear flow channel reactors. Water (Switzerland), 14(1). https://doi:10.3390/w14010032. ISSN:20734441.

Horn, E. J., van Hille, R. P., Oyekola, O. O., & Welz, P. J. (2022b). Functional Microbial Communities in Hybrid Linear Flow Channel Reactors for Desulfurization of Tannery Effluent. Microorganisms, 10(11). https://doi:10.3390/microorganisms10112305. ISSN:20762607.

Horn, E.J., Oyekola, O.O., Welz, P.J. & van Hille, R.P. 2022. Biological desulfurization of tannery effluent using hybrid linear flow channel reactors. Water (Switzerland), 14(1).

Horn EJ, van Hille RP, Oyekola OO, Welz PJ (2022) Functional microbial communities in hybrid linear flow channel reactors for desulfurization of tannery effluent. Microorganisms 10: 2305 https://doi.org/10.3390/microorganisms1011230

Huang, Q., Jiang, F., Wang, L. & Yang, C. 2017. Design of Photobioreactors for Mass Cultivation of Photosynthetic Organisms. Engineering, 3(3): 318–329. http://dx.doi.org/10.1016/J.ENG.2017.03.020.

Huang Y, Luo L, Xu K, Wang XC (2019) Characteristics of external carbon uptake by microalgae: growth-associated effects on algal biomass composition. Bioresource Technology 292: 121887

Iacopozzi, I., Innocenti, V., Marsili-Libelli, S. & Giusti, E. 2007. A modified Activated Sludge Model No. 3 (ASM3) with two-step nitrification-denitrification. Environmental Modelling and Software, 22(6): 847–861.

Ikumi, D. S. (2011). The Development of a Three-Phase Plant-wide Mathematical Model for Sewage Treatment.

Imhoff, J. F., & Thiel, V. (2010, June). Phylogeny and taxonomy of Chlorobiaceae. Photosynthesis Research. https://doi:10.1007/s11120-009-9510-7. ISSN:01668595.

J.W.H., S., Elferink, O., Visser, A., Hulshoff Pol, L. W., & Stams, A. J. M. (1994). Sulfate reduction in methanogenic bioreactors. FEMS Microbiology Reviews, 15(2–3), 119–136. https://doi:10.1111/j.1574-6976.1994.tb00130.x. ISSN:15746976

Jørgensen, B. B., Findlay, A. J., & Pellerin, A. (2019). The biogeochemical sulfur cycle of marine sediments. Frontiers in Microbiology, 10(APR). https://doi:10.3389/fmicb.2019.00849. ISSN:1664302X.

Keller, K. L., & Wall, J. D. (2011). Genetics and molecular biology of the electron flow for sulfate respiration in Desulfovibrio. Frontiers in Microbiology, 2(JUNE). https://doi:10.3389/fmicb.2011.00135. ISSN:1664302X.

Khan N.M., Qadeer A., Khan A., Nasir A., Sikandar A., Muhammad A., Horky P., Weisbauerova P., Kopec T. 2024 Alternative sources of proteins in farm animal feeding. Journal of Microbiology, Biotechnology and Food Science 13: e10605 https://doi.org/10.55251/jmbfs.10605

Khanzada ZT., Övez S. 2018 Growing freshwater microalgae in high ammonium landfill leachate. American Journal of Mechanics and Applications 6: 40-51 https://doi.org/10.11648/j.ajma.20180602.12

Kobayashi, K. (2007). Bacillus subtilis pellicle formation proceeds through genetically defined morphological changes. Journal of Bacteriology, 189(13), 4920–4931. https://doi:10.1128/JB.00157-07. ISSN:00219193.

Kopriva, S., Patron, N. J., Keeling, P., & Leustek, T. (2008). Phylogenetic Analysis of Sulfate Assimilation and Cysteine Biosynthesis in Phototrophic Organisms (pp. 31–58). https://doi:10.1007/978-1-4020-6863-8_3.

Krayzelova, L., Bartacek, J., Díaz, I., Jeison, D., Volcke, E. I. P., & Jenicek, P. (2015, December 1). Microaeration for hydrogen sulfide removal during anaerobic treatment: a review. Reviews in Environmental Science and Biotechnology. Springer Netherlands. https://doi:10.1007/s11157-015-9386-2. ISSN:15729826.

Krishnamoorthy, G., Sadulla, S., Sehgal, P. K., & Mandal, A. B. (2013). Greener approach to leather tanning process: D-Lysine aldehyde as novel tanning agent for chrome-free tanning. Journal of Cleaner Production, 42, 277–286. https://doi:10.1016/j.jclepro.2012.11.004. ISSN:09596526.

Krzemińska I, Pawlik-Skowrońska B, Trzcińska M, Tys J. (2014) Influence of photoperiods on the growth rate and biomass productivity of green microalgae. Bioprocess and Biosystems Engineering 37: 735-741 https://doi.org/10.1007/s00449-013-1044-x

Kushkevych, I., Hýžová, B., Vítězová, M., & Rittmann, S. K. M. R. (2021). Microscopic methods for identification of sulfate-reducing bacteria from various habitats. International Journal of Molecular Sciences, 22(8). https://doi:10.3390/ijms22084007. ISSN:14220067.

Le, Q. H., Carrera, P., van Loosdrecht, M. C. M., & Volcke, E. I. P. (2025). Effective measuring campaigns for reliable and informative full-scale WWTP data. Environmental Science: Water Research and Technology. https://doi:10.1039/d4ew00315b. ISSN:20531419.

Lens, P.N.L. & Khandelwal, A. 2023. Algal Systems for Resource Recovery from Waste and Wastewater.

Leong, Y.K. & Chang, J.S. 2020. Bioremediation of heavy metals using microalgae: Recent advances and mechanisms. Bioresource Technology, 303(December 2019): 122886. https://doi.org/10.1016/j.biortech.2020.122886.

Leung T.L.F, & Poulin, R, 2008. 2008. Mutualism: Exploring The Many Shades Of Symbioses To Cite This Version : Hal Id : Hal-03246057 The Many Shades Of Symbioses. Vie Et Milieu / Life & Environment: 107–115.

Lewis KM, Arntsen AE, Coupel P, Joy-Warren H, Lowry KE, Matsouka A, Mills MM, Dijken GL, Selz V, Arrigo KR (2018) Photoacclimation of Arctic Ocean phytoplankton to shifting light and nutrient limitation. Limnology and Oceanography 64: 284-301 https://doi.org/10.1002/lno.11039

Liamleam, W., & Annachhatre, A. P. (2007, September). Electron donors for biological sulfate reduction. Biotechnology Advances. https://doi:10.1016/j.biotechadv.2007.05.002. ISSN:07349750.

Lin, S., Mackey, H. R., Hao, T., Guo, G., van Loosdrecht, M. C. M., & Chen, G. (2018, October 15). Biological sulfur oxidation in wastewater treatment: A review of emerging opportunities. Water Research. Elsevier Ltd. https://doi:10.1016/j.watres.2018.06.051. ISSN:18792448.

Liu, Y. (2007, January). Overview of some theoretical approaches for derivation of the Monod equation. Applied Microbiology and Biotechnology. https://doi:10.1007/s00253-006-0717-7. ISSN:01757598.

Maina, P., Ollengo, M. A., & Nthiga, E. W. (2019). Trends in leather processing: A Review. International Journal of Scientific and Research Publications (IJSRP), 9(12), p9626. https://doi:10.29322/ijsrp.9.12.2019.p9626.

Marais, T. S. (2020). A novel semi-passive process for sulphate removal and elemental sulphur recovery centred on a hybrid linear flow channel reactor.

Marais, T. S., Huddy, R. J., Harrison, S. T. L., & van Hille, R. P. (2020a). Demonstration of simultaneous biological sulphate reduction and partial sulphide oxidation in a hybrid linear flow channel reactor. Journal of Water Process Engineering, 34. https://doi:10.1016/j.jwpe.2020.101143. ISSN:22147144.

Marais, T. S., Huddy, R. J., Harrison, S. T. L., & van Hille, R. P. (2020b). Effect of hydraulic residence time on biological sulphate reduction and elemental sulphur recovery in a single-stage hybrid linear flow channel reactor. Biochemical Engineering Journal, 162. https://doi:10.1016/j.bej.2020.107717. ISSN:1873295X.

Marais, T., Huddy, R., Harrison, S., & van Hille, R. (2019, March 6). Demonstration of simultaneous biological sulphate reduction and partial sulphide oxidation in a hybrid linear flow channel reactor. https://doi:10.1101/569269. Retrieved from http://biorxiv.org/lookup/doi/10.1101/569269

Marcia, M., Ermler, U., Peng, G., & Michel, H. (2010). A new structure-based classification of sulfide: Quinone oxidoreductases. Proteins: Structure, Function and Bioinformatics. https://doi:10.1002/prot.22665. ISSN:08873585

Mohsenpour, S.F., Hennige, S., Willoughby, N., Adeloye, A. & Gutierrez, T. 2021. Integrating micro-algae into wastewater treatment: A review. Science of the Total Environment, 752(September 2020): 142168. https://doi.org/10.1016/j.scitotenv.2020.142168.

Molwantwa, J. B. (2007). Floating Sulphur Biofilms: Structure, Function And Biotechnology.

Molwantwa, J. B., & Rose, P. D. (2013). Development of a Linear Flow Channel Reactor for sulphur removal in acid mine wastewater treatment operations. Water SA, 39(5), 649–654. https://doi:10.4314/wsa.v39i5.9. ISSN:03784738.

Monzon Martinez L, Duenas RA, Sanchez AG, Andia JM (2025) Study on the growth of a native microalgae–bacteria mixed culture from the Peruvian Andes exposed to different tannery effluent dilutions and photoperiod. Environmental Technology https://doi.org/10.1080/09593330.2025.2485354

Moussa, M.S., Rojas, A.R., Hooijmans, C.M., Gijzen, H.J. & van Loosdrecht, M.C.M. 2004. Model-based evaluation of nitrogen removal in a tannery wastewater treatment plant. Water Science and Technology, 50(6): 251–260.

Mpofu, A. B., & Welz, P. J. (2017). Water And Wastewater Management In The Tanning And Leather Finishing Industry: Natsurv 10 (2 nd EDITION) Report to the Water Research Commission. https://doi:10.13140/RG.2.2.35505.02402. Retrieved from https://www.researchgate.net/publication/327933217

Mpofu AB, Kaira WM, Holtman GA, Oyekola OO, van HIlle RP, Welz PJ (2023) Resource recovery from tannery wastewater using an integrated biological system: towards a circular bioeconomy and net positive tannery operations. Journal of Cleaner Production 387: 135872 https://doi.org/10.1016/j.jclepro.2023.135872

Mpofu AB, Kaira WM, Oyekola OO, Welz PJ (2022) Anaerobic co-digestion of tannery effluent: Process optimisation for resource recovery, recycling and reuse in a circular bioeconomy. Process Safety and Environmental Protection 158: 547-559 https://doi.org/10.1016/j.psep.2021.12.027

Muyzer, G., & Stams, A. J. M. (2008, June). The ecology and biotechnology of sulphate-reducing bacteria. Nature Reviews Microbiology. https://doi:10.1038/nrmicro1892. ISSN:17401526.

Nagabalaji, V., Sivasankari, G., Srinivasan, S. V., Suthanthararajan, R. & Ravindranath, E. 2019. Nutrient removal from synthetic and secondary treated sewage and tannery wastewater through phycoremediation. Environmental Technology (United Kingdom), 40(6): 784–792. https://doi.org/10.1080/09593330.2017.1408689.

Nagabalaji V, Maharaja P, Nishanthi R, Sathish G, Suthanthararanjan R, Srivivasan SV (2023) Effect of co-culturing bacteria and microalgae and influence of inoculum ratio during the biological treatment of tannery wastewater. Journal of Environmental Management 341: 118008 https://doi.org/10.1016/j.jenvman.2023.118008

Nagarajan, D., Lee, D.J., Chen, C.Y. & Chang, J.S. 2020. Resource recovery from wastewaters using microalgae-based approaches: A circular bioeconomy perspective. Bioresource Technology, 302(January): 122817. https://doi.org/10.1016/j.biortech.2020.122817.

Nagi, M., He, M., Li, D., Gebreluel, T., Cheng, B. & Wang, C. 2020. Utilization of tannery wastewater for biofuel production: New insights on microalgae growth and biomass production. Scientific Reports, 10(1): 1–14. http://dx.doi.org/10.1038/s41598-019-57120-4.

Nambukrishnan V, Singaram J (2022) Enhanced biodiesel production by optimizing growth conditions of Chlorella marina in tannery wastewater. Fuel, 316: 123431 https://doi.org/10.1016/j.fuel.2022.123431

Ngobeni PV, Mpofu AB, Ranjan A, Welz PJ (2024) A critical review of systems for bioremediation of tannery effluent with a focus on nitrogenous and sulfurous species removal and resource recovery. Processes, 12: 1527 https://doi.org/10.3390/pr12071527

Nopens, I., Batstone, D. J., Copp, J. B., Jeppsson, U., Volcke, E., Alex, J., & Vanrolleghem, P. A. (2009). An ASM/ADM model interface for dynamic plant-wide simulation. Water Research, 43(7), 1913–1923. https://doi:10.1016/j.watres.2009.01.012. ISSN:00431354.

Okabe, S. (2007). Ecophysiology of sulphate-reducing bacteria in environmental biofilms. In Sulphate-Reducing Bacteria: Environmental and Engineered Systems (pp. 359–382). Cambridge University Press. https://doi:10.1017/CBO9780511541490.013. ISBN: 9780511541490.

Oliveira C.Y.B., Oliveira C.D.L., Prasad R., Ong H.C., Araujo S., Shabnam N., Gálvez A.O. 2021 A multidisciplinary review of Tetradesmus obliquus microalga suitable for large-scale biomass production and emerging environmental applications. Reviews in Aquaculture 1-25 https://doi.org/10.1111/raq.12536

Oruganti, R.K., Katam, K., Show, P.L., Gadhamshetty, V., Upadhyayula, V.K.K. & Bhattacharyya, D. 2022. A comprehensive review on the use of algal-bacterial systems for wastewater treatment with emphasis on nutrient and micropollutant removal. Bioengineered, 13(4): 10412–10453. https://doi.org/10.1080/21655979.2022.2056823.

Paulo, L. M., Stams, A. J. M., & Sousa, D. Z. (2015, December 1). Methanogens, sulphate and heavy metals: a complex system. Reviews in Environmental Science and Biotechnology. Springer Netherlands. https://doi:10.1007/s11157-015-9387-1. ISSN:15729826.

Paytubi, S., Cansado, C., Madrid, C., & Balsalobre, C. (2017). Nutrient composition promotes switching between pellicle and bottom biofilm in Salmonella. Frontiers in Microbiology, 8(NOV). https://doi:10.3389/fmicb.2017.02160. ISSN:1664302X.

Pena A, Agustini CB, Trierweiler LF, Gutterres M (2020) Influence of period light on cultivation of microalgae consortium for the treatment of tannery wastewaters from leather finishing stage. Journal of Cleaner Production, 263: 121618 https://doi.org/10.1016/j.jclepro.2020.121618

Pena A, Bertoldi CF, da Fontoura JT, Trierweiler LF, Gutterres M (2019) Consortium of microalgae for tannery effluent treatment. Brazilian Archives of Biology and Technology, 62: 1–10 https://doi.org/10.1590/1678-4324-2019170518

Pokorna, D., & Zabranska, J. (2015). Sulfur-oxidizing bacteria in environmental technology. Biotechnology Advances. Elsevier Inc. https://doi:10.1016/j.biotechadv.2015.02.007. ISSN:07349750.

Posadas, E., Alcántara, C., García-Encina, P.A., Gouveia, L., Guieysse, B., Norvill, Z., Acién, F.G., Markou, G., Congestri, R., Koreiviene, J. & Muñoz, R. 2017. Microalgae cultivation in wastewater. Microalgae-Based Biofuels and Bioproducts: From Feedstock Cultivation to End-Products: 67–91.

Pudi, A., Rezaei, M., Signorini, V., Andersson, M. P., Baschetti, M. G., & Mansouri, S. S. (2022, October 1). Hydrogen sulfide capture and removal technologies: A comprehensive review of recent developments and emerging trends. Separation and Purification Technology. Elsevier B.V. https://doi:10.1016/j.seppur.2022.121448. ISSN:18733794.

Qian, Z., Tianwei, H., Mackey, H. R., van Loosdrecht, M. C. M., & Guanghao, C. (2019, March 1). Recent advances in dissimilatory sulfate reduction: From metabolic study to application. Water Research. Elsevier Ltd. https://doi:10.1016/j.watres.2018.11.018. ISSN:18792448.

Quijano, G., Arcila, J.S. & Buitrón, G. 2017. Microalgal-bacterial aggregates : Applications and perspectives for wastewater treatment. Biotechnology Advances, 35(6): 772–791. http://dx.doi.org/10.1016/j.biotechadv.2017.07.003

Rabin, N., Zheng, Y., Opoku-Temeng, C., Du, Y., Bonsu, E., & Sintim, H. O. (2015, March 1). Mechanisms of biofilm formation and targets for developing antibiofilm agents. Future Medicinal Chemistry. Future Science Ltd. https://doi:10.4155/fmc.15.6. ISSN:17568927.

Ramanan, R., Kim, B.H., Cho, D.H., Oh, H.M. & Kim, H.S. 2016. Algae-bacteria interactions: Evolution, ecology and emerging applications. Biotechnology Advances, 34(1): 14–29. http://dx.doi.org/10.1016/j.biotechadv.2015.12.003.

Ranieri, E., Giuliano, S., & Ranieri, A. C. (2021). Energy consumption in anaerobic and aerobic based wastewater treatment plants in Italy. Water Practice and Technology, 16(3), 851–863. https://doi:10.2166/wpt.2021.045. ISSN:1751231X.

Ranjan A, Lilly M, Deepnarain N, Welz PJ (2025) Valorization of tannery wastewater with indigenous microalgal strains: Acclimation, identification, biomass characterization and remediation. Algal Research, 86, 103953 https://doi.org/10.1016/j.algal.2025.103953

Ranjan A, Welz P (2025) Influence of season, inoculum density and ammonia concentration on biomass abundance and ammonia utilization of a microalgal consortium for tertiary remediation of tannery wastewater and valorization of biomass. Algal Research Algal Research, 90, 104137 https://doi.org/10.1016/j.algal.2025.104137

Ranjan A, Welz PJ (2022). Concurrent Biodiesel Production and Wastewater Remediation using Microalgae. In M. F. Simpson (Ed.), Series: Energy Science, Engineering and Technology: The Future of Biodiesel (pp. 1–46). Nova Science Publishers, Inc.

Ras, M., Steyer, J.P. & Bernard, O. 2013. Temperature effect on microalgae: A crucial factor for outdoor production. Reviews in Environmental Science and Biotechnology, 12(2): 153–164.

Rather, M. A., Gupta, K., & Mandal, M. (2021, December 1). Microbial biofilm: formation, architecture, antibiotic resistance, and control strategies. Brazilian Journal of Microbiology. Springer Science and Business Media Deutschland GmbH. https://doi:10.1007/s42770-021-00624-x. ISSN:16784405.

Reichert, P., Vanrolleghem, P., Borchardt, D., Henze, M., Rauch, W., Reichert, P., Shanahan, P. & Somlyódy, L. 2001. River Water Quality Model no. 1 (RWQM1): III. Biochemical submodel selection. Water Science and Technology, 43(5): 31–40.

Robles, Á., Vinardell, S., Serralta, J., & Bernet, N. (2020). Anaerobic treatment of sulfate-rich wastewaters: process modeling and control. https://doi:10.2166/9781789060959_0277. Retrieved from http://iwaponline.com/ebooks/book/chapter-pdf/772259/9781789060966_0277.pdf

Rose PD, Maart BA, Dunn KM, Roswell RA, Britz P (1996) High-rate algal oxidation ponding for the treatment of tannery effluents. Water Science and Technology 33: 219-227

Rout, P. R., Shahid, M. K., Dash, R. R., Bhunia, P., Liu, D., Varjani, S., Zhang, T. C., & Surampalli, R. Y. (2021). Nutrient removal from domestic wastewater: A comprehensive review on conventional and advanced technologies. Journal of Environmental Management, 296. https://doi:10.1016/j.jenvman.2021.113246. ISSN:10958630.

Safi, C.; Pollio, A.; Olivieri, G. (2021) Neochloris oleoabundans from nature to industry: a comprehensive review. Reviews in Environmental Science and Bio/Technology 2021, 20(4), 943–958. https://doi:10.1007/s11157-021-09593-x.

Sah, L., Rousseau, D.P.L., Hooijmans, C.M. & Lens, P.N.L. 2011. 3D model for a secondary facultative pond. Ecological Modelling, 222(9): 1592–1603. http://dx.doi.org/10.1016/j.ecolmodel.2011.02.021.

Salbitani G, Carfagna S (2021) Ammonium utlization in microalgae: A sustainable method for wastewater treatment. Sustainability 13: 956 https://doi.org/10.3390/su13020956

Santos A.M., Lamers P.P., Janssen M., Wijffels R.H. 2013 Biomass and lipid productivity of Neochlroris oleoabundans under alkaline-saline conditions. Algal Research 2: 204-211 http://dx.doi.org/10.1016/j.algal.2013.04.007

Saranya, D. & Shanthakumar, S. 2019. Opportunities for phycoremediation approach in tannery effluent: A treatment perspective. Environmental Progress and Sustainable Energy, 38(3): 1–13.

Saranya D, Shanthakumar S (2019) Green microalgae for combined sewage and tannery effluent treatment: Performance and lipid accumulation potential. Journal of Environmental Management, 241: 167–178. https://doi.org/10.1016/j.jenvman.2019.04.031

Saranya D, Shanthakumar S (2020a) An integrated approach for tannery effluent treatment with ozonation and phycoremediation: A feasibility study. Environmental Research, 183: 109163 https://doi.org/10.1016/j.envres.2020.109163

Saranya D, Shanthakumar S (2020b) Effect of culture conditions on biomass yield of acclimatized microalgae in ozone pre-treated tannery effluent: A simultaneous exploration of bioremediation and lipid accumulation potential. Journal of Environmental Management, 273: 111129 https://doi.org/10.1016/j.jenvman.2020.111129

Sarti, A., & Zaiat, M. (2011). Anaerobic treatment of sulfate-rich wastewater in an anaerobic sequential batch reactor (AnSBR) using butanol as the carbon source. Journal of Environmental Management, 92(6), 1537–1541. https://doi:10.1016/j.jenvman.2011.01.009. ISSN:03014797.

Schmidt,'t Boaz Arieli, T. M., Cohen, Y., Padan, E., & Strohll, W. R. (1987). Sulfur Metabolism in Beggiatoa alba. JOURNAL OF BACTERIOLOGY (Vol. 169). Retrieved from https://journals.asm.org/journal/jb

Sehgal A., Goswami K., Pal M., Chikkaputtaiah C., Chetia P., Boruah H.P.D. 2019 Morpho-taxonomic, genetic, and biochemical characterization of freshwater microalgae as potential biodiesel feedstock. 3 Biotech 9: 137 https://doi.org/10.1007/s13205-019-1664-1

Serrano, A., Peces, M., Astals, S., & Villa-Gómez, D. K. (2020). Batch assays for biological sulfate-reduction: a review towards a standardized protocol. Critical Reviews in Environmental Science and Technology, 50(12), 1195–1223. https://doi:10.1080/10643389.2019.1644103. ISSN:15476537.

Shahid A, Malik S, Zhu H, Xu J, Nawaz MZ, Nawaz S, Alam MA, Mehmood MA (2020) Cultivating microalgae in wastewater for biomass production, nutrient removal, and atmospheric carbon mitigation; a review. Science of the Total Environment 704: 135303 https://doi.org/10.1016/j.scitotenv.2019.135303

Shaibur, M. R. (2023). Heavy metals in chrome-tanned shaving of the tannery industry are a potential hazard to the environment of Bangladesh. Case Studies in Chemical and Environmental Engineering, 7. https://doi:10.1016/j.cscee.2022.100281. ISSN:26660164.

Sharmila GS, Banu JR, Kumar MD, Kumar SA, Kumar G (2022) Algal biorefinery towards decarbonization: Economic and environmental consideration. Bioresource Technology 364: 128103 https://doi.org/10.1016/j.biortech.2022.128103

Shen, Y., & Buick, R. (2004). The antiquity of microbial sulfate reduction. Earth-Science Reviews, 64(3–4), 243–272. https://doi:10.1016/S0012-8252(03)00054-0. ISSN:00128252.

Shen X-S, Xu Y-P, Tong X-Q, Huang Q, Zhang S, Gong J, Chu F-F, Zheng RJ (2022) The mechanism of carbon source utilization by microalgae when co-cultivated with photosynthetic bacteria. Bioresource Technology 365: 128152 https://doi.org/10.1016/j.biortech.2022.128152

Solimeno, A., Gómez-Serrano, C. & Acién, F.G. 2019. BIO_ALGAE 2: improved model of microalgae and bacteria consortia for wastewater treatment. Environmental Science and Pollution Research, 26(25): 25855–25868.

Solimeno, A., Parker, L., Lundquist, T. & García, J. 2017. Integral microalgae–bacteria model (BIO_ALGAE): Application to wastewater high rate algal ponds. Science of the Total Environment, 601–602: 646–657. http://dx.doi.org/10.1016/j.scitotenv.2017.05.215.

Solimeno, A., Samsó, R., Uggetti, E., Sialve, B., Steyer, J.P., Gabarró, A. & García, J. 2015. New mechanistic model to simulate microalgae growth. Algal Research, 12: 350–358.

Struk, M., Sepúlveda-Muñoz, C. A., Kushkevych, I., & Muñoz, R. (2023). Photoautotrophic removal of hydrogen sulfide from biogas using purple and green sulfur bacteria. Journal of Hazardous Materials, 443. https://doi:10.1016/j.jhazmat.2022.130337. ISSN:18733336.

Sun, J., Dai, X., Liu, Y., Peng, L., & Ni, B. J. (2017). Sulfide removal and sulfur production in a membrane aerated biofilm reactor: Model evaluation. Chemical Engineering Journal, 309, 454–462. https://doi:10.1016/j.cej.2016.09.146. ISSN:13858947.

Sutherland DL, Ralph PJ. (2021) Differing growth responses in four related microalgal genera grown under autotrophic, mixotrophic and heterotrophic conditions. Journal of Applied Phycology 33: 3359-3553 https://doi.org/10.1007/s10811-021-02593-y

Swartz, C. D., Jackson-Moss, C., Rowswell, R. A., Mpofu, A. B., & Welz, P. (2017). Water and waste-water management in the tanning and leather finishing industry : report to the Water Research Commission. Water Research Commission. ISBN: 9781431208814.

Tang, K., Baskaran, V., & Nemati, M. (2009, April 15). Bacteria of the sulphur cycle: An overview of microbiology, biokinetics and their role in petroleum and mining industries. Biochemical Engineering Journal. https://doi:10.1016/j.bej.2008.12.011. ISSN:1369703X.

Tariq, S. R., Shah, M. H., & Shaheen, N. (2009). Comparative statistical analysis of chrome and vegetable tanning effluents and their effects on related soil. Journal of Hazardous Materials, 169(1–3), 285–290. https://doi:10.1016/j.jhazmat.2009.03.093. ISSN:03043894.

Urbina-Saurez NA, Salcedo-Pabon CJ, Contreras-Ropero JE, Lopez-Barrera GL, Garcia-Martinez JB, Barajas-Solano AF, Machuca-Martinez F (2025) Biotechnological strategy for TWW treatment: Bicarbonate/H2O2 oxidation integrated with microalgae cultivation. Case Studies in Chemical and Environmental Engineering 11: 101060 https://doi.org/10.1016/j.cscee.2024.101060

Urbina-Suarez NA, Ayala-González DD, Rivera-Amaya JD, Barajas-Solano AF, Machuca-Martínez F. (2022). Evaluation of the Light/Dark Cycle and Concentration of TWW in the Production of Biomass and Metabolites of Industrial Interest from Microalgae and Cyanobacteria. Water, 14: 3. https://doi.org/10.3390/w14030346

Van Den Bosch, P. L. F., Van Beusekom, O. C., Buisman, C. J. N., & Janssen, A. J. H. (2007). Sulfide oxidation at halo-alkaline conditions in a fed-batch bioreactor. Biotechnology and Bioengineering, 97(5), 1053–1063. https://doi:10.1002/bit.21326. ISSN:00063592.

Van Der Steen, P., Rahsilawati, K., Rada-Ariza, A.M., Lopez-Vazquez, C.M. & Lens, P.N.L. 2015. A new photo-activated sludge system for nitrification by an algal-bacterial consortium in a photo-bioreactor with biomass recycle. Water Science and Technology, 72(3): 443–450.

Van Hille, R. P., Van Wyk, N., Motleleng, L., & Mooruth, N. (2011). Lessons in passive treatment: Towards efficient operation of a sulphate reduction-sulphide oxidation system.

Van Loosdrecht, M. C. M., Lopez-Vazquez, C. M., Meijer, S. C. F., Hooijmans, C. M., & Brdjanovic, D. (2015). Twenty-five years of ASM1: Past, present and future of wastewater treatment modelling. Journal of Hydroinformatics, 17(5), 697–718. https://doi:10.2166/hydro.2015.006. ISSN:14647141.

Vanrolleghem, P. A., Insel, G., Petersen, B., Sin, G., De Pauw, D., Nopens, I., Dovermann, H., Weijers, S., & Gernaey, K. (2012). A COMPREHENSIVE MODEL CALIBRATION PROCEDURE FOR ACTIVATED SLUDGE MODELS. Proceedings of the Water Environment Federation, 2003(9), 210–237. https://doi:10.2175/193864703784639615. ISSN:1938-6478.

Velasquez-Orta SB, Yanez-Noguez I, Ramírez IM, Ledesma MTO. (2024) Pilot-scale microalgae cultivation and wastewater treatment using high-rate ponds: a meta-analysis. Environmental Science and Pollution Research 31: 46994–47021 https://doi.org/10.1007/s11356-024-34000-7

Volcke, E. I. P., van Loosdrecht, M. C. M., & Vanrolleghem, P. A. (2006). Continuity-based model interfacing for plant-wide simulation: A general approach. Water Research, 40(15), 2817–2828. https://doi:10.1016/j.watres.2006.05.011. ISSN:00431354.

Vu, H. P., Nguyen, L. N., Wang, Q., Ngo, H. H., Liu, Q., Zhang, X., & Nghiem, L. D. (2022, February 1). Hydrogen sulphide management in anaerobic digestion: A critical review on input control, process regulation, and post-treatment. Bioresource Technology. Elsevier Ltd. https://doi:10.1016/j.biortech.2021.126634. ISSN:18732976.

Wágner, D.S., Valverde-Pérez, B., Sæbø, M., Bregua de la Sotilla, M., Van Wagenen, J., Smets, B.F. & Plósz, B.G. 2016. Towards a consensus-based biokinetic model for green microalgae – The ASM-A. Water Research, 103: 485–499.

Wang, R., Lin, J. Q., Liu, X. M., Pang, X., Zhang, C. J., Yang, C. L., Gao, X. Y., Lin, C. M., Li, Y. Q., Li, Y., Lin, J. Q., & Chen, L. X. (2019). Sulfur oxidation in the acidophilic autotrophic Acidithiobacillus spp. Frontiers in Microbiology. Frontiers Media S.A. https://doi:10.3389/fmicb.2018.03290. ISSN:1664302X.

Wang, Y., Ho, S.H., Cheng, C.L., Guo, W.Q., Nagarajan, D., Ren, N.Q., Lee, D.J. & Chang, J.S. 2016. Perspectives on the feasibility of using microalgae for industrial wastewater treatment. Bioresource Technology, 222: 485–497. http://dx.doi.org/10.1016/j.biortech.2016.09.106.

Wang, Y.-N., & Zeng, Y. (2012). Ammonia nitrogen in tannery wastewater: Distribution, origin and prevention. Article in Journal of the American Leather Chemists Association. Retrieved from https://www.researchgate.net/publication/262715453

Wasmund, K., Mußmann, M., & Loy, A. (2017, August 1). The life sulfuric: microbial ecology of sulfur cycling in marine sediments. Environmental Microbiology Reports. Wiley-Blackwell. https://doi:10.1111/1758-2229.12538. ISSN:17582229.

Watanabe MW, Isdepsky A (2021) Biocrude oil production by integrating microalgae polyculture and wastewater treatment: novel proposal on the use of deep water-depth polyculture of mixotrophic microalgae. Energies 14: 6992 https://doi.org/10.3390/en14216992

Welz, P.J., De Jonge, N., Lilly, M., Kaira, W. & Mpofu, A.B. 2024. Integrated biological system for remediation and valorization of tannery wastewater: Focus on microbial communities responsible for methanogenesis and sulfidogenesis. Bioresource Technology, 395(November 2023): 130411. https://doi.org/10.1016/j.biortech.2024.130411.

Welz PJ, Ranjan A, Ngobeni PV, Mpofu AB, Ikumi D (2025) Towards microalgal biorefineries: a review of biomass valorisation opportunities and remediation studies. Submitted Bioresource Technology Research August 2025.

Welz PJ, Thobejane MP, van Blerk GN (2023) Ammonium oxidizing bacterial population in South African activated sludge wastewater treatment plants. Water Environment Research 95: 10945 https://doi.org/10.1002/wer.10945

Woertz, I., Feffer, A., Lundquist, T. & Nelson, Y. 2009. Algae Grown on Dairy and Municipal Wastewater for Simultaneous Nutrient Removal and Lipid Production for Biofuel Feedstock. Journal of Environmental Engineering, 135(11): 1115–1122.

Wu, J., Niu, Q., Li, L., Hu, Y., Mribet, C., Hojo, T., & Li, Y. Y. (2018). A gradual change between methanogenesis and sulfidogenesis during a long-term UASB treatment of sulfate-rich chemical wastewater. Science of the Total Environment, 636, 168–176. https://doi:10.1016/j.scitotenv.2018.04.172. ISSN:18791026.

Yen, H.W., Hu, I.C., Chen, C.Y., Nagarajan, D. & Chang, J.S. 2018. Design of photobioreactors for algal cultivation. Second Edition. Elsevier B.V. https://doi.org/10.1016/B978-0-444-64192-2.00010-X.

Zambrano, J., Krustok, I., Nehrenheim, E. & Carlsson, B. 2016. A simple model for algae-bacteria interaction in photo-bioreactors. Algal Research, 19: 155–161.

Zengh H., Wu X., Zou G., Zhou T, Liu Y Ruan R. (2019) Cultivation of Chlorella vulgaris in manure-free piggery wastewater with high-strength ammonium for nutrients removal and biomass production: Effect of ammonium concentration, carbon / nitrogen ratio and pH. Bioresource Technology 273: 203-211 https://doi.org/10.1016/j.biortech.2018.11.019

Zerveas S, Mente MS, Tsakiri D, Kotzabasis K. (2021) Microalgal photosynthesis induces alkalanization of aquatic environent as a result of H+ uptake independently from CO_2 concentration – New perspectives for environmental applications. Journal of Environmental Management 289: 112546 https://doi.org/10.1016/j.jenvman.2021.112546

Zhang, Z., Zhang, C., Yang, Y., Zhang, Z., Tang, Y., Su, P., & Lin, Z. (2022a), November 20). A review of sulfate-reducing bacteria: Metabolism, influencing factors and application in

wastewater treatment. Journal of Cleaner Production. Elsevier Ltd. https://doi:10.1016/j.jclepro.2022.134109. ISSN:09596526.

Zhao, C. & Chen, W. 2019. A review for tannery wastewater treatment: some thoughts under stricter discharge requirements. Environmental Science and Pollution Research, 26(25): 26102–26111.

Zhao, X., Zhao, F., Wang, J., & Zhong, N. (2017). Biofilm formation and control strategies of foodborne pathogens: Food safety perspectives. RSC Advances. Royal Society of Chemistry. https://doi:10.1039/c7ra02497e. ISSN:20462069.